MODELING PRECIPITATION-RUNOFF RELATIONSHIPS TO DETERMINE WATER YIELD FROM A PONDEROSA PINE FOREST WATERSHED

By Assefa S. Desta

A Thesis

Submitted in Partial Fulfillment

of the Requirements for the Degree of

Master of Science

in Forestry

Northern Arizona University

August 2006

Approved:

____

Aregai Tecle, PhD., Chair

____

Daniel Neary, Ph.D.,

____

Alex Finkral, Ph.D.

ABSTRACT

MODELING PRECIPITATION-RUNOFF RELATIONSHIPS TO DETERMINE WATER YIELD FROM ARIZONA'S PONDEROSA PINE FORESTS

ASSEFA S. DESTA

A stochastic precipitation-runoff modeling is used to estimate a cold and warm-seasons water yield from a ponderosa pine forested watershed in the north-central Arizona. The model consists of two parts namely, simulation of the temporal and spatial distribution of precipitation using a stochastic, event-based approach and estimation of water yield from the watershed using deterministic and spatially varied water balance technique. In the first part, a selected group of theoretical probability distribution functions are used to describe the probability distribution of the various precipitation characteristics, such as storm depth, storm duration, and interarrival time between events. Then, a synthetic data of each precipitation characteristic are generated using the best distribution function that fit the observed data. The other precipitation characteristics evaluated in this part is the spatial distribution of precipitation. The distribution of storm depth and duration across the watershed with respect to the landscape characteristics such as latitude, longitude, elevation and aspect is studied. In addition, the form of precipitation, snow or snow during the cold-season is analyzed by simulating temperature. Overall the models for two seasons work well except that the cold-season model overestimate precipitation events of small depth and duration while, the warm-season model overestimate the total seasonal amount.

The generated precipitation events in the first part are used as an input in precipitation-runoff relationship model, discussed in the second part of this study.

Geographical information system (GIS) is used to describe the spatial characteristics and subdivided the watershed into cells of 90m by 90m size assumed to be homogeneous with respect to elevation, aspect, slope, overstory density and soil type. Water yield is estimated at a cell level using a water balance approach that incorporates the hydrologic processes such as canopy interception, evaporation, transpiration, infiltration, snow accumulation and melt. The estimated runoff from the cells, is, then routed from cell to cell in a cascading fashion in the direction of flow. The total water yield is the accumulated surface runoff generated at the watershed outlet. Finally the estimated water yield is compared with the observed stream flow data to test the reliability of the model. The results showed that the simulated water yield is similar to the water yield of previous research but lower that the observed data.

Acknowledgments

This research is partially funded by the state of Arizona prop 301 funding

I would like to thank Dr. Aregai Tecle, my committee chair, for giving me endless hours of support and guidance. I want to give thank to my other committee members, Dr. Daniel Neary and Dr. Alex Finkral for their valuable time in reading my thesis and providing important suggestions. This research would have not been possible with out a valuable help from the Statistical Consulting Lab (Dr. Roy St. Laurent) of the Department of Mathematics and Statistics. Thanks to all graduate students of School of Forestry, Boris Poff, Gustavo Perez, and Andrew Sanchez Meador for their help in various aspect. Great thanks to Mario Motese for providing me important climatological and soil moisture data. Last but not least, thank to all my families and friends for their prayer and encouragement.

Table of Contents

List of Tables

List of Figures

Chapter 1

General Introduction

The mixed conifer forests located in the higher-elevation watersheds of north central Arizona have been recognized as important sources of water for the fast growing population in the Phoenix metropolitan area and the other communities in the Salt and Verde River Valley of Arizona (Baker and Ffolliott, 1999). The area has four seasons consisting of wet winter and summer and relatively dry fall and spring. Winter precipitation often comes in the form of snow resulting from frontal storms moving to the region from the Pacific Northwest. Summer storms are primarily of convective type produced from moistures that originate in the Gulf of Mexico (Sellers et al., 1985).

Snowmelt from winter precipitation has been considered as the primary source of the annual water yield in the area. Because of this, previous research efforts in north central Arizona had focused only on winter precipitation to estimate annual water yield without any consideration to contribution from summer thunderstorms (Fogel et al., 1971). This is in spite of the fact that intensive thunderstorms occasionally generating significantly large downstream flows.

Accurate precipitation data only exist at point locations, where the gauging stations are located. Hence, precipitation data measured at one gauging station in the watershed may not represent the precipitation falling on the entire watershed because the distributions of depth and duration of precipitation vary with space along the watershed landscape (Marquinez et al., 2003). This variation in spatial distribution of precipitation affects the total amount of water yield from the watershed. The proposed conceptual models are a stochastic, event-based, and spatially varied precipitation model and a deterministic water yield model. In the stochastic event-based model of precipitation, synthetic precipitation data are generated and used as an input in the water yield model.

Objectives

This research focuses on developing an appropriate conceptual model to estimate the amounts of cold and warm-seasons water yields from the ponderosa pine watersheds of Arizona.

There are three main objectives of this study:

1. To develop conceptual event-based, stochastic models to describe and simulate temporal distribution of cold and warm-seasons precipitation falling in the ponderosa pine forested watersheds in north central Arizona.
2. To study the spatial distribution of precipitation along the ponderosa pine watershed
3. To develop conceptual cold and warm-seasons precipitation-runoff algorithms that take into account the temporal and spatial distribution of precipitation and other important watershed characteristics, such as elevation, slope, aspect, soil structure and texture, overstory vegetation cover and various climatic data.

Temporal Distribution of Precipitation

A stochastic approach is used to estimate the occurrence likelihood of a random phenomenon such as a hydrological event (Bonta, 2004). The stochastic approach is selected to account for the inherently uncertain characteristics of precipitation and its ability to provide a better forecast of future scenarios. Knowledge of the probability of the occurrence of a certain precipitation or hydrologic magnitude is useful in water resource management decision making (Tecle and Rupp, 2002).

The reason for developing event-based models is that, cold and warm-seasons water yields are hypothesized to be dependent on inter-arrival time, depth and duration of precipitation events. Cold-season precipitation, in addition to the above factors, depends on the form in which precipitation comes, and the characteristics of snowpack. For example, a spring rainfall storm falling on an existing snowpack is expected to produce more runoff than an early winter snowfall even though the amounts of water equivalents of the two events are similar. This occurs due to higher amounts of water losses from evaporation and sublimation occurring during the early cold season snowpack period. An event-based model can account for variations in water yield caused by different combinations of storm interarrival time, depths and durations, as well as the form of precipitation, and evaporation and snowmelt.

The temporal component is a stochastic simulator of storm event depth, duration and inter-arrival time between events. In the case of winter precipitation, events occurring within a few days of each other are said to be part of the same storm sequence, as they are related to a large-scale weather system. Under this condition, two additional variables are needed to adequately describe the precipitation characteristics in the area: inter-arrival time between sequences and the number of events occurring in a sequence. Univariate distribution functions are fit to the frequency distributions of the interarrival time between events, number of events per sequence and interarrival time between sequences. However, a bivariate probability density function is fit to the depth-duration data to reflect their interdependence. A random number generator is used to aid the synthetic generation of future events on the basis of the selected theoretical distributions.

Spatial Distribution of Precipitation

The spatial component of the precipitation model estimates the precipitation amount at any point on the watershed. Data from the network of precipitation gauges in the Beaver Creek watershed are used to create a regression equation that allow predicting the precipitation amount at any point given the location's elevation, latitude, longitude and aspect. A GIS software is used to generate raster, or grid, surfaces of both depth and duration of a precipitation event. And a third grid of average event intensity is created from a combination of the depth and duration surfaces. The information generated in the precipitation model is then used as one of the inputs into the deterministic water yield model.

To better estimate the water yield from the watershed, the effects of spatial distribution of watershed characteristics on runoff are analyzed using Geographical Information Systems (GIS). This makes it possible to describe the spatial data in a high-resolution. Variables important to determine runoff such as precipitation, temperature, elevation, slope, aspect, vegetation cover, and soil type will not be averaged over a watershed area has been done in many studies.

Water Yield

The watershed is sub-divided into cells of 90 by 90 m size using GIS. The various watershed characteristics that affect the amount of runoff, for each cell, including elevation, aspect, slope, vegetation cover and soil type as well as the dynamic climatic variables of solar radiation, relative humidity were studied. A water balance that consists of hydrologic inputs and outputs is constructed to estimate the runoff existing in each cell. The inputs and outputs are computed using a selected set of mathematical equations. The runoff from each cell is routed downstream from one cell to another in a cascading fashion to determine the total amount of water yield at the outlet of the watershed. The individual cold and warm-seasons runoff events are then temporally and spatially cumulated to determine the seasonal amount of water yield from the entire watershed. In the end, the annual water yield will be determined by summing up the seasonal water yields.

Study Area

This study uses Bar M watershed as a case study for developing a water yield model. With an area of 6,678 ha, the watershed is the largest of the Beaver Creek experimental watersheds. The Beaver Creek experimental watersheds, which encompass 111,289 ha, are a group of watersheds located within the Coconino National Forest in central Arizona. This project was one of Arizona's watershed programs, initiated by the USDA Forest Service as pilot study in 1957. The Beaver Creek watersheds were selected for research because they contain extensive areas of ponderosa pine and pinyon-juniper woodlands. The main objective of the project was to test the effects of vegetation management practices on water yield and forage production. Later in 1971, the objectives of the project shifted towards developing and testing the responses of natural resources from disturbances and developing a multiple use management models (Baker Jr. and Brown, 1974).

Based on different research and practical experiences heavy vegetation are generally associated with relatively comparatively low water yields. On the other hand, practices which reduce vegetation density tend to increase water yields, and practices which favor heavy vegetation density tend to minimize water yield (Barr, 1956). In the Beaver Creek watersheds, various vegetation manipulation treatments including clear cutting, uniform strip cutting, irregular strip cutting, and thinning. Similarly, the effects of these vegetation treatments on water yield, sediment, forage production, timber production, wildlife, and recreation values were studied (Baker, 1999).

The study consisted of 20 watersheds in which 14 of them were experimental watersheds, treated with different levels of vegetation treatments while the other six were designed as control watersheds and left untreated. The Bar M watershed was one of the control watersheds covered by ponderosa pine forest (See Figure 1-1). The outlet of the Bar M watershed lies at 111^{o} 36' 19" W longitude and 34^{o} 51' 40" N latitude and has an elevation of 1,930 m. The highest point of the watershed rises to an elevation of 2,324 m. The watershed is generally inclined to the southwest and has an average slope of 12 degrees. Eighty percent of the watershed is covered by ponderosa pine (*Pinus ponderosa*). The remaining 12 and 3 percent of the watershed are covered by gambel oak (*Quercus gambelii*) and aspen (*Populus tremuloides*), respectively. The main grass species in the watershed are: Arizona fescue (*Festuca arizonica*), mountain muhly (*Muhlenbergia palmeri*), blue grama (*Bouteloua gracilis*), and squirrel tail (*Elymus elymoides*) (Anderson et al., 1960)

Volcanic parent material covers the Beaver Creek area with thickness that start at zero in the lower elevations to an estimated 305 m thickness near some of the cinder cones in the area. The average thickness is believed to be approximately 152 m based on the projected position of the erosion surface of the Kaibab formation on which the volcanic material was deposited (Baker, 1982). The sedimentary rocks below the volcanic cover are porous and permeable because of their origin and the abundant fracture systems developed in them (Baker, 1982). The volcanic material resulted from a serious of lava flow deposits. Each deposit has its own distinct set of vertical contraction joints, which do not penetrate from one layer of deposit to the next (Rupp, 1995). These joints are the primary passage ways for the downward movement transport of surface water that enters into the relatively impervious lava rock formation. Since the vertical fractures do not extend to the adjacent deposits, the entry of large amounts of water to the sedimentary rock below is generally inhibited (Rush, 1965). Only two percent of the total precipitation that falls on the Mogollon Rim, which cuts through the Beaver Creek watershed, reaches the aquifers in the sedimentary rock formation (Rupp, 1995). Baker (1982) found that, in the Beaver Creek area, water passes to the sedimentary layer only in two out of the twenty experimental watersheds.

The predominant soils in the ponderosa pine forested watersheds are Eutroboralfs and Argiborolls of the Brollier (loam to fine clay), Siesta (silt loam), and Sponseller series (stony silt loam), and are developed on basalt and Cinders (Williams and Anderson, 1967; Campbell and Ryan, 1982). The average depth of these soils is less than one meter and predominantly the soils have low permeability. For over 90 percent of the soils in the ponderosa pine type, the infiltration rate ranges from 20 to 64 mm/hr, the permeability rate varies from one to five mm/hr and the soil water storage capacity is between 152 to 457 mm. The other ten percent of the soils in the ponderosa pine type have similar permeability and infiltration rates, but have water storage capacities greater than 457 mm (Williams and Anderson, 1967).

The Beaver Creek area receives precipitation during two periods of the year namely the cold season, which runs roughly from October to April and the warm season from May to September. The frontal cold season precipitation results from large cyclonic storms that originate in the northern Pacific Ocean while the convective, short lived summer precipitation comes from the Gulf of Mexico (Bescheta, 1976). On average the area receives 431 mm of precipitation during the cold season in the form of snow whereas 216 mm of precipitation falls during summer season. Baker (1982) found that 22 percent of the annual precipitation converts to surface runoff. Ninety seven percent of the annual runoff produced from snow melts during the cold season. The underlayng rock formation allows very little water to seep down and reach the regional water table, which lies 305 to 610 m below the surface (Rush , 1965). Estimate of the evapotranspiration value for the area have been made by subtracting the measured runoff from the precipitation. According to Baker (1982), on the average about 500 mm of water is lost to the atmosphere through evapotranspiration annually.

Cold-season temperature in the ponderosa pine forest part of the Beaver Creek averages 1.3 ^{0}C, with a low monthly mean of -2.2 ^{0}C in January to 7.2^0 C (Campbell and Ryan, 1982). The diurnal temperature fluctuation, or the difference between the daily maximum and daily minimum temperatures average about 17^0 C during the cold season (Beschta, 1976; Campbell and Ryan, 1982).

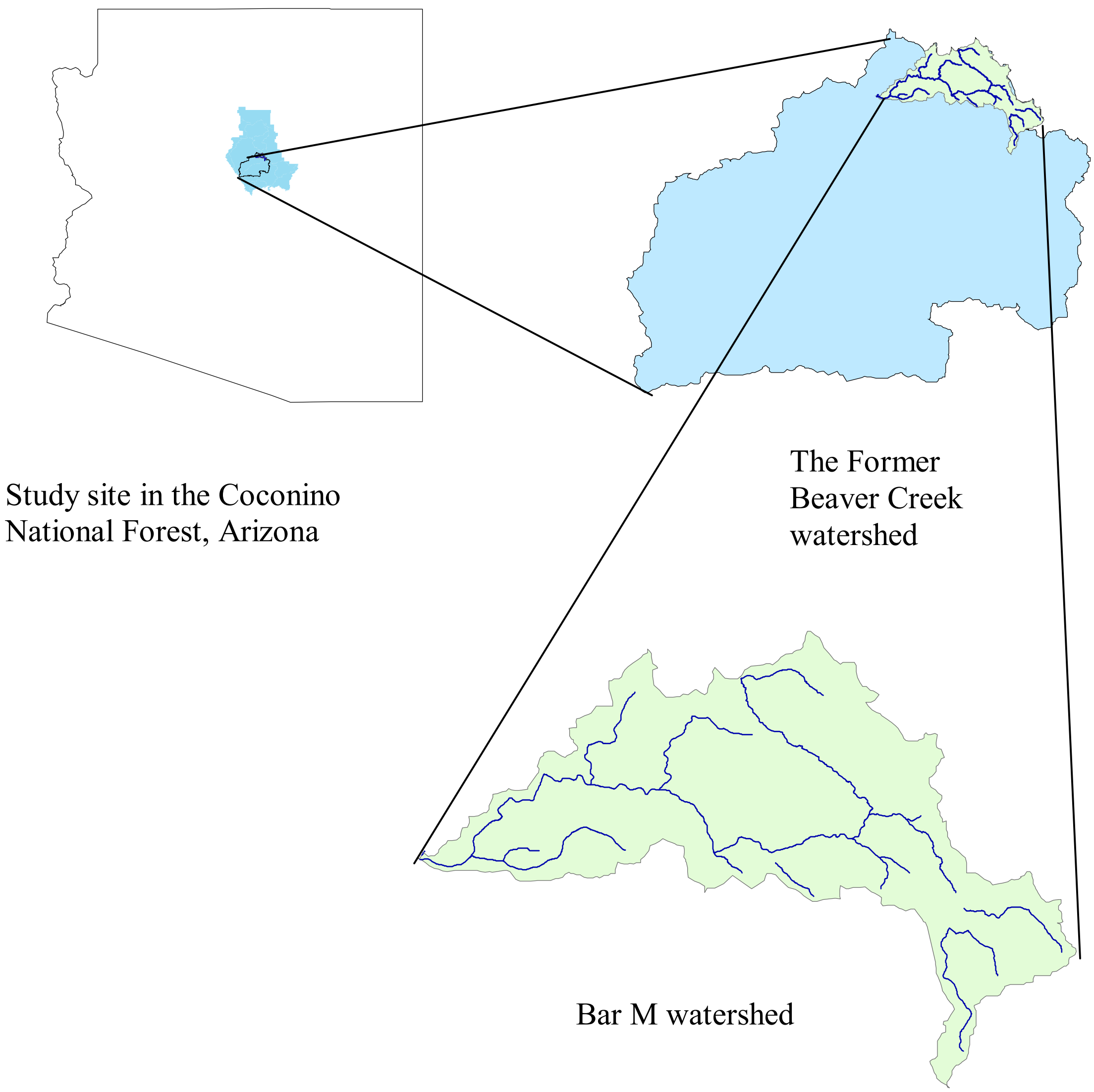

Figure 1-1. Location of Mar M watershed in the former Beaver Creek experimental watershed.

Literature cited

Anderson, T.C. Jr., J.A. Williams, and D.B. Crezee, 1960. Soil management report for Beaver Creek Watershed of Coconino National Forest Region 3, Forest Service, Department of Agriculture.

Baker, M.B. Jr., 1982. Hydrologic regimes of forested areas in the Beaver Creek Watershed, USDA Forest Service General Technical Report Rm-90, Rocky Mountain Forest and Range Experiment Station , Fort Collins, Colorado.

Baker, M.B. Jr., and H.E. Brown, 1974. Multiple use evaluations on ponderosa pine forest land, 18th Arizona Watershed Symposium, Report No 6.

Baker, M.B. Jr., and P.F. Ffolliott, 1999. Interdisciplinary land use along the Mogollon Rim, Chapter 5. In: Malchus B. Baker,. Jr., compiler, History of watershed research in the central Arizona highlands. USDA Forest Service, Research paper RMRS-GTR-29. pp. 27-33.

Barr, G.W., 1956. Recovering rainfall, Department of Agricultural Economics, University of Arizona, Tucson, Arizona.

Beschta, R.L., 1976. Climatology of the ponderosa pine type in central Arizona, Technical Bulletin 228, Agricultural Experimental Station, College of Agriculture, University of Arizona, Tucson, Arizona.

Bonta, J.V., 2004. Stochastic simulation of storm occurrence, depth duration, and with in storm intensities. American Society of Agricultural Engineers ISSN 0001-2351. 47(5), pp. 1573-1584

Campbell, R.E., and M.G. Ryan, 1982. Precipitation and temperature characteristics of forested watershed in central Arizona, USDA Forest Service General Technical Report Rm-93, Rocky Mountain Forest and Range Experiment Station , Fort Collins, Colorado.

Fogel, M.M., L. Duckstein, and C.C. Kisiel, 1971. Space- time validation of a thunderstorm rainfall model, Water Resources Bulletin 7(2) pp 309-315.

Marquinez, J., J. Lastra, and P. Garcia, 2003. Estimation models for precipitation in mountainous regions: The use of GIS and multivariate analysis. Journal of Hydrology, 270(2), pp.1-11.

Rupp, D.E., 1995. Stochastic, event-based modeling of upland watershed precipitation-runoff relationships, master's thesis, Northern Arizona University, Flagstaff, Arizona.

Rush, R.W., 1965. Report of geological investigation of six experimental drainage basin, unpublished report, Rocky Mountain Forest and Range Experiment Station, Flagstaff, Arizona.

Sellers, W. D., R.H. Hill, and M.S. Rae, 1985. Arizona Climate: The Hundred years, The University of Arizona Press, Tuccson.

Tecle. A, and D.E. Rupp, 2002. Stochastic precipitation-runoff modeling for water yield from a semi-arid forested watershed. In: Risk, Reliability, Uncertainty, and Robustness of Water Resources Systems. Cambridge University press: London. Pp. 56-63.

Williams, J.A., and T.C. Anderson, Jr., 1967. Soil Survey of Beaver Creek area, USDA Forest Service and Soil Conservation Service, and Arizona Agricultural Experiment Station, U.S. government printing office, Washington, D.C.

Chapter 2

Stochastic Event-based and Spatial Modeling of Precipitation

Abstract

The temporal and spatial distributions of precipitation for cold and warm-seasons are studied in a particular watershed in the ponderosa pine forest type located in Beaver Creek area in north-central Arizona 42 km South of Flagstaff. A stochastic, event-base technique is used to simulate the temporal pattern of precipitation. The technique, first, requires selecting appropriate theoretical distribution functions to describe the probability distribution of precipitation characteristics such as storm event depth, event duration and inter-arrival time between events. Then, it involves generation of random numbers using the selected theoretical distribution functions to synthetically simulate each precipitation characteristic. Weibull and gamma probability distribution functions are the best models used to describe the variables for both seasons. The results indicate that the cold-season precipitation model over-estimates the small-depth precipitation events while the warm-season precipitation model over-estimates the total average seasonal amount of precipitation. The spatial distribution of precipitation in the area is highly influenced by orographic, and seasonal and local climatic conditions. The results are displayed using a geographical information system (GIS) format. Some landscape characteristics such as elevation, latitude, longitude, and aspect are also considered to have important effects on the spatial distribution of precipitation. The cold-season precipitation events are highly influenced by latitude while warm-season precipitation events are mostly affected by the longitude and elevation of the areas. Therefore, more northerly (higher latitude) areas receive larger amounts of cold-season precipitation while, more easterly located areas (higher longitude) with higher elevation receive larger amounts of warm-season

precipitation. In addition, the form of cold-season precipitation, rain or snow, is dependent upon ambient temperature, which varies with time and space.

Introduction

Precipitation is governed by physical laws and complex atmospheric processes. Atmospheric processes that generate precipitation systems are complex and spatially and temporally varying, making accurate prediction of precipitation practically difficult. Therefore, precipitation is often evaluated statistically as a random process, in which its future temporal distribution is studied based on its historical distribution pattern (Viessman, Jr. and Lewis, 2003; Rupp, 1995). A stochastic, event based precipitation modeling that takes the advantage of GIS technology is developed for both cold and warm-seasons precipitation in a ponderosa pine forested watersheds in north-central Arizona. This chapter focuses on developing a model to generate synthetic precipitation data, to be used as an input into the water yield model developed in the next chapter. To be realistic the model developed considers both the temporal and spatial characteristics of the precipitation events in the study area.

The temporal component of this model uses a stochastic process to describe the distribution of precipitation characteristics such as inter-arrival time between events, and the depth and duration of the individual storm. The procedure uses appropriate theoretical probability distribution functions and a random number generator to describe and simulate the various precipitation characteristics. The frequency distribution of the inter-arrival time between events is modeled using a univariate Weibull probability distribution function. Depth and duration are modeled using a joint bivariate distribution function to account for their dependency on each other. Using the selected theoretical distribution functions, random numbers are generated for each precipitation characteristic to simulate a synthetic time series of precipitation events.

The types of models used depend on the characteristics of the precipitation patterns in the cold and warm-seasons in north central Arizona. The cold-season precipitation events are typically the result of frontal storms (Sellers et al., 1985) while warm-season precipitation events are generally monsoonal type convective storms that tend to be highly localized and intensive but short lived lasting from several minutes to a few hours (Fogel and Duckstein,1969; Fogel et al., 1971). The cold-season precipitation, however, can have duration of more than one day and individual storms may be related to each other by large-scale weather systems. An independent model is used to describe warm-season precipitation events, while cold-season precipitation events are described using a dependent model with additional parameters to adequately describe their characteristics (Duckstein et al., 1975). A test of precipitation models shows that they produce the cold and warm-seasons precipitation patterns in the study area reasonably well. The relative frequency distribution of twenty-year simulated total seasonal amount are compared with the frequency distribution of twenty-year of measured cold and warm-seasons precipitation events resulting in reasonable correlation.

The spatial analysis is used to define the areal distribution of precipitation event depth and duration, as well as the form of precipitation, rain or snow, over the watershed. The event depth and duration at any point on the watershed is described as a function of the point's location in terms of its elevation, aspect, latitude and longitude as well as a function of the storm depth and duration simulated at the outlet of the watershed.

A GIS is used with the above functions to generate raster, or grid, surfaces of event depth and duration. The two grids are combined to form a third surface of precipitation intensity. Because the difference in elevation over the watershed ranges over 421 m, it is possible for storm precipitation to take the form of rain at the lower elevation while falling as snow at the higher elevations. Therefore, the daily maximum and minimum temperatures, which are used to determine the form of precipitation, are described as functions of elevation. A GIS is employed to describe the spatial variability of elevation, and thus temperature, across the watershed. In this manner, the form of precipitation for any storm event is determined at any point on the watershed.

Literature Review

Temporal Distribution of Precipitation

Precipitation is governed by physical laws and complex atmospheric processes. The fact that these processes are complex and spatially and temporally dependent on each other, make accurate prediction of precipitation practically difficult (Viessman Jr. and Lewis, 2003). The complexity of the processes, however, allows a probabilistic description of variables such as rainfall depth, intensity of an event, interarrival time between events and statistical analyses of these random variables provide simulation of future properties of rainfall events (Smith and Schreiber, 1973). These probabilistic models of precipitation consist of a combination of theoretical probability distributions of the above mentioned variables and a random number generation to simulate the precipitation events (Tecle et al., 1988).

There are two types of models used to simulate random processes depending on the type of relationship that exist between two sequential events: dependent or independent models. Dependent models are used to characterize and simulate random processes when the events are related to each other while independent models are used if the events are not related to each other. An independent model is used to describe the convective, highly intensive, short duration and widely scattered summer thunderstorms that show relative independence between any two consecutive rain events. The dependent model, on the other hand, is used to describe the frontal-type storms which exhibit strong relationship between consecutive rain events (Fogel and Duckstein, 1969; Fogel et al., 1971; Duckstein et al., 1975; Tecle et al., 1988).

Stochastic, Event-based Modeling of Cold-season Precipitation

Generally, synoptic weather systems determine the amount and frequency of the storms occurring during the cold-season in Arizona (Sellers and Hill, 1974). The frontal storms associated with these systems tend to result in the occurrence of more than one precipitation events in a period of more than one day. The consecutive precipitation events resulting from the same synoptic system are not independent from one another, on the other hand, the arrivals of the synoptic systems themselves are considered to be independent of one another (Duckstein et al., 1975; Hanes et al., 1977; Baker, 1982).

A stochastic, event-based model that accounts for the independence of synoptic systems and the persistence of events within a system was developed by Duckstein et al. (1975) and Rupp (1995). Ducksten et al. (1975), in their model, categorized precipitation events into “groups” and “sequences” in order to address the persistence of events. They defined an event as an individual wet day in which precipitation amount of 0.25mm or more was recorded. Groups were defined as a number of one or more consecutive rain events separated by less than three days while sequences are one or more group of events separated by more than three days (Rupp, 1995).

In the modeling process, data on the various variables describing the different precipitation characteristics are generated. The first three variables, which deal with the persistence of events, are: the number of groups per sequence, the number of dry days between two consecutive groups, and duration of groups. The other two independent variables are sequence interarrival time, the time interval between the beginnings of two consecutive storm sequences; and the amount of precipitation in each group. Figure 2-1 shows the five precipitation model variables used by Duckstein et al. (1975).

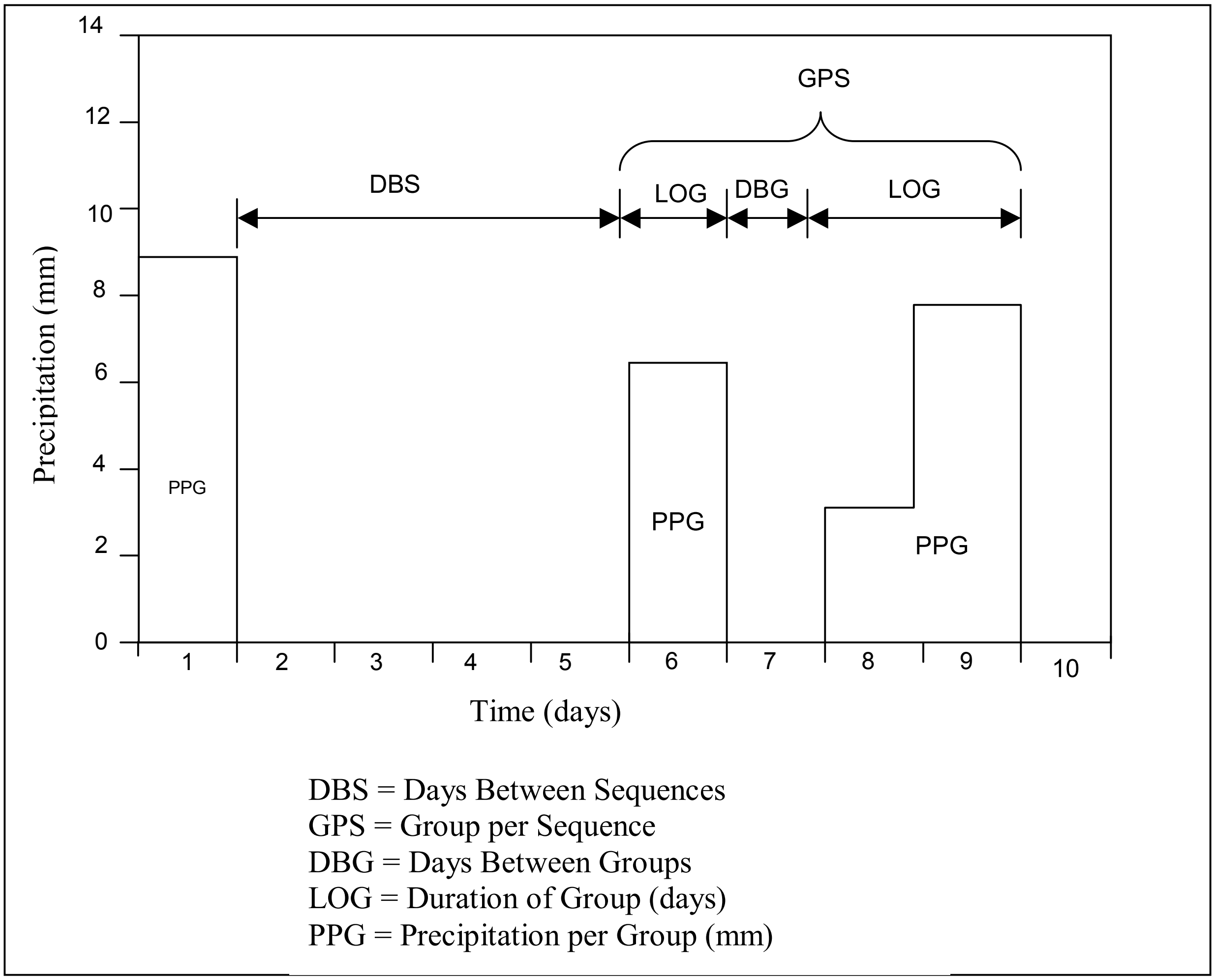

Figure 2-1. Winter precipitation model variables as described in Duckstein et al., (1975).

Rupp (1995) modified the model that was developed by Duckstein et al. (1975) in order to allow for the simulation of precipitation intensity by considering the amount and duration of individual precipitation events. He defined an event as an uninterrupted rainfall or snowfall of any duration. He removed “group” from his model but used the same definition for a storm sequence except changing the one day time resolution that separates two consecutive precipitation events to as little as five minutes. Rupp (1995) used 3.5 days as the minimum inter-arrival time between two consecutive storm sequences. The five variables used by Rupp (1995) to simulate a sequence-based model are:1) time between sequences (days), 2) number of events per sequence, 3) time between events (hours), 4) precipitation amount per event (mm) 5) duration of event (hours).

In both studies (Duckstein et al., 1975 and Rupp, 1995) appropriate theoretical distribution functions were selected that fit best the distributions of the observed precipitation characteristics or model variables. Random numbers were generated in each model to simulate the precipitation data. Duckstein et al. (1975) made two important assumptions regarding the operation of their model. The first is the independence between the amount of precipitation received in a group and the duration of the group. Hanse et al. (1977) conducted a test to check this assumption and they found that the two variables are not correlated. The second assumption is that precipitation depths are uniformly distributed over the duration of the storm group. Hanes et al. (1977) accepted this assumption on the basis of “the majority of the winter precipitation that falls as snow and rarely melting immediately.” However, due to two reasons, the justification for the second assumption is questionable. First, in their study site, the White Mountains of Arizona, where the elevations range from 2318 to 2684 m, though most of the winter precipitation falls as a snow, there is a significant amount that falls as rain. Second, due to the rapid warming of the ambient air, there are occasions in which the snow melts soon after it falls on the ground (Rupp, 1995).

Modeling of interdependent variables such as depth and duration, or intensity and duration, of storms using a bivariate distribution was developed in different areas. Bacchi et al. (1994) described the joint frequency distribution of the intensities and durations of extreme rainfall events in terms of a bivariate distribution function with exponential marginals derived by Gumbel (1960). This bivariate distribution function is applicable for a negative correlation coefficient ranging from 0 - 0.404 between the two dependent variables. Singh K. and Singh V., (1991) also used a bivariate distribution function with exponential marginal to describe a joint frequency distribution of storm intensity and duration. Etoh and Murota (1986) developed a general gamma-type bivariate distribution function to describe the joint distribution of duration and depth.

Schmeiser and Lal (1981) reviewed several methods for generating bivariate distributions using gamma marginal distributions. Each method has different limits imposed on the correlation. They also developed a new method suitable for the entire range of possible correlation coefficients. They supplied algorithms that produce a family of bivariate gamma distributions from any gamma marginal distributions, correlation coefficient, and regression curves describing the conditional expectations E{X1/X2} and E{X2/X1}. In addition, Kottas and Lau (1978) discussed a method of simulating with bivariate distributions by describing the first random variable in terms of its marginal distribution, then defining the conditional distribution of the second variable explicitly. Rupp (1995) used a bivariate distribution to describe the precipitation depth and duration on a watershed close to our study area. He used two different procedures for generating two dependent random variables with gamma marginal distributions. The first procedure was trivariate reduction (TVR) method with Cherian's bivariate gamma distribution function (Cherian, 1941). This method first generates three independent random variables with gamma distributions, which are then combined and reduced down to two independent variables with gamma distributions in this case, duration and depth.

Rupp (1995) referred to the second method as "explicit conditional distribution (ECD)." The ECD method, unlike other methods where the conditional distributions arise implicitly from bivariate probability distribution function (*pdf*), the conditional distribution is modeled directly. To develop a bivariate model using the ECD method to simulate storm depth and duration, one has to first find the marginal distribution of duration. Then the conditional distribution of depth will be determined based on the marginal distribution of duration. Both the marginal and conditional distributions are assumed to be gamma with the shape and scale parameters of depth that are dependent on the shape and scale parameters of duration.

Stochastic, Event-based Modeling of Warm-season Precipitation

Unlike cold-season precipitation, warm-season precipitation is caused by convective-type systems. Thunderstorm rainfall is recognized to be more variable in time and space than other storm types (Fogel et al., 1971). Nearly 36% percent of the annual precipitation in north central Arizona occurs as thunderstorms during the summer. Although these storms occur frequently, individual storm usually covers relatively small areas and have short-duration (Baker, 1982). The spatial and temporal variability of summer thunderstorm precipitation events in other parts of Arizona, where summer precipitation is dominant, has been simulated using a stochastic event-based approach (Fogel and Duckstein, 1969; Fogel et al., 1971; Duckstein. et al., 1972). The same method has also been employed in other semi-arid part of the world (Fogel and Duckstein, 1981; Bogardi et al., 1988). Bogardi et al. (1988) have developed an event-based approach to semi-arid climatic conditions in Central Tanzania. In their model, Bogardi et al. (1988) defined a rainfall event as an uninterrupted sequence of rainy days with an amount of above a certain threshold value, 5mm d^{-1}, and a dry event as a sequence of dry days as observed at a given rain gage. The threshold value is approximately equivalent to the expected daily evaporation rate. Precipitation events below this threshold value do not produce utilizable surface runoff and were not considered in the model. The variables used by Bogardi et al. (1988) to describe this precipitation model were: depth of event, duration of events, interarrival time and number of events per season (see Figure 2-2). Though the recording of data on a daily basis is, believed to indicate the occurrence and amount of total rainfall depth of events adequately, it does not reveal the characteristics of individual storms of short duration.

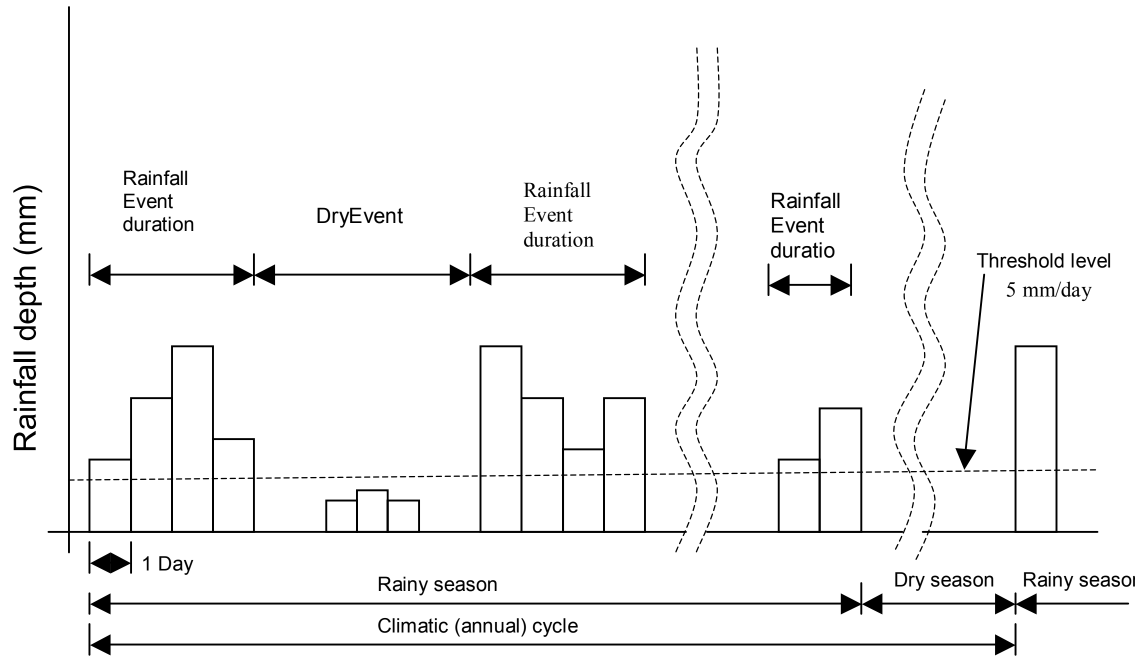

Figure 2-2. Summer precipitation model variables (Bogardi et al., 1988).

Duckstein et al. (1972) developed a stochastic model of runoff-producing rainfall for summer type storms. In their work, they reviewed two definitions of an event used by various researchers. The first definition, as used in the Atterbury Experimental watershed near Tucson, Arizona, is the occurrence of at least one storm center (point of maximum rainfall) over the 52 km^2 watershed. The second definition, on the other hand, is an event when the mean precipitation of the rain gages is greater than 12.5 mm and one gage records more than 25.4 mm. The second definition is used by most urban areas, which have a sufficient number of gages. The primary objective of the model was to simulate seasonal summer storms in order to simulate seasonal runoff. In their model they first simulated two variables: number of events per season and depth of point rainfall and then they simulated the total depth of precipitation per season by multiplying the two variables.

Various theoretical distribution functions have been used to describe the model variables. Precipitation events during the summer months are generally of the convective storm type such that the events appear to occur in an independent manner in time and space. Hence the variable for the number of events per season has been described using a Poisson distribution. Further, geometric distribution is used to describe precipitation depth (Fogel and Duckstein, 1969; Duckstein et al., 1972; Fogel and Duckstein, 1981; Bogardi et al., 1988)

Spatial Modeling of Precipitation

Cold-season Precipitation

Topographic features in Central Arizona, such as the San Francisco Mountains, the Mogollon Rim and the White Mountains play an important role in the spatial distribution of precipitation in these areas. These topographic features cause orographic lifting of air masses and accentuate the frontal and convection activity during precipitation period (Beschta, 1976). Some studies have been conducted to characterize the spatial distribution of precipitation in central-Arizona at a large-scale level (Beschta, 1976; Baker 1982; Campbell and Ryan, 1982) and at a watershed level (Rupp, 1995).

Beschta, (1976) developed isohyets of mean annual precipitation of 127 mm interval for the pine and spruce-fir forest type for a large area that stretches about 170 kilometers eastward. Based on over 22 year data, Baker (1982) found that precipitation on Beaver Creek increased with elevation at a rate of 85 mm for every 300 m. Campbell and Ryan, (1982) determined the average areal precipitation over the Beaver Creek watershed using Theissen polygon method. Even though the Theissen Polygon is an acceptable method to find the average precipitation for a watershed, other methods such as the isohyetal method would be appropriate for this kind of situation. The isohytal method, which uses a computer to generate contours (isohyets) of equal precipitation depth, makes a better representation of the precipitation distribution than Theissen polygon when orographic influence on precipitation is significant (Dingman, 1994; Ward and William, 1995).

Campbell and Ryan, (1982) indicated that precipitation increases with elevation on the southwestern slopes of Arizona. On the other hand, areas of the same elevation further north and east receive less amount of precipitation due to rain shadow effect. This is because the predominately southwesterly wind lifts up the air masses along southwestern slopes. The air masses rise and cool and result in condensation and precipitation. After the air masses lose their moisture during the orographic process in the windward direction, they become drier as they move to the leeward directions that cause the leeward slope to be warmer and drier. Due to the fact that spatial distribution of precipitation is affected by different factors, a simple regression between elevation and precipitation may not be a reliable model that can be used widely. This problem is illustrated in the work of Beschta (1976), which showed that a 35 cm precipitation depth variation occurs between two points of equal elevation but at different locations within the pine and the mixed-conifer forest types of central Arizona.

Rupp (1995) analyzed the spatial distribution of the wet season precipitation in one of the experimental watersheds, Woods Canyon, in the Beaver Creek area. The watershed is located in the Mogollon Rim where major orographic features have been identified as having an important influence on the spatial distribution of precipitation. He examined how precipitation depth and duration of precipitation vary with topographic characteristics of the area such as elevation, geographic location in terms of Universal Transverse Mercator (UTM) coordinates, and aspect in relation to the prevailing wind. He finally produced a multvariate regression equation relating precipitation depth and duration with those variables. Elevation shows strong correlation with precipitation depth next to UTM-Y coordinate, on the other hand, duration of precipitation in the area is highly influenced by elevation, which supports the previous studies in central Arizona. Aspect plays little role in spatial distribution of both depth and duration of precipitation in the area as compared with elevation. According to Rupp (1995) the reason for the small role of aspect played in the spatial distribution of precipitation may be that the topographic features in the study area, such as hills and ridges, are not large enough to cause rain shadow effect.

Warm-season Precipitation

Court (1961) proposed a bivariate Gaussian distribution approach that would give elliptical isohyets to describe the spatial distribution of convective storms in the southwestern United States. In his model, rainfall depths decrease exponentially away from the point of maximum rainfall or storm center within a roughly circular shape of diameter between 6.4-9.6 km (Fogel and Duckstein, 1969; Duckstein et al., 1973). Duckstein et al., 1973 suggested that dense and evenly distributed rain gauges are needed to obtain sufficient information about the spatial distribution of summer precipitation because of its scattered nature.

In general, the spatial distribution of summer precipitation shows the same pattern as winter precipitation in Arizona. Precipitation is highest in the summer at about the same location as it is in winter on the central Mogollon Rim (Jameson, 1969). Duckstein et al. (1973) have found similar result that summer thunderstorm precipitation increases with elevation in southern Arizona.

Methods

Temporal Analysis of Precipitation Pattern

Cold-season Precipitation

The cold-season precipitation model used in this study follows the one used by Rupp (1995), which is a modified version of the model used in Duckstein et al. (1975). The modified stochastic model developed in Rupp (1995) and adopted in this study allows the simulation of precipitation intensity, the most important variable input used to determine the amount of surface runoff and sediment yield. The previous models focused only on simulation of total daily rainfall, while this model includes storm duration, which allows a determination of individual storm intensity.

The first modification of the model is redefinition of an event. An event is defined as uninterrupted rainfall or snowfall of any duration which can last minutes to many hours. If it stops raining then starts again after five minutes, the second period rainfall is considered a separate event. The second modification is the removal of the variable "group". The definition of storm sequence, however, remains the same except for one difference. Duckstein et.al (1975) defined storm sequence as three consecutive days of dry weather that separates two successive storm events. Their time resolution was one day. However, this research deals with time period of as little as five minutes. To deal with the interval of storm events, Duckstein et.al (1975) equated an inter-arrival time of events between 1.5 and 2.5 days to two days, and 2.5 to 3.5 days to three days and so on. Therefore, in this study the minimum time between consecutive storm sequences is changed to 3.5 days.

The new model, which is the modified of Duckstein et al. (1975) and used by Rupp (1995), is described as follows in terms of five variables:

1. Time between sequences (days),
2. Number of events per sequence,
3. Time between events (hours),
4. Precipitation amount per event (mm), and
5. Duration of events (hours)

Figures 2-3a and 2-3b illustrate the relationship of these variables to each other.

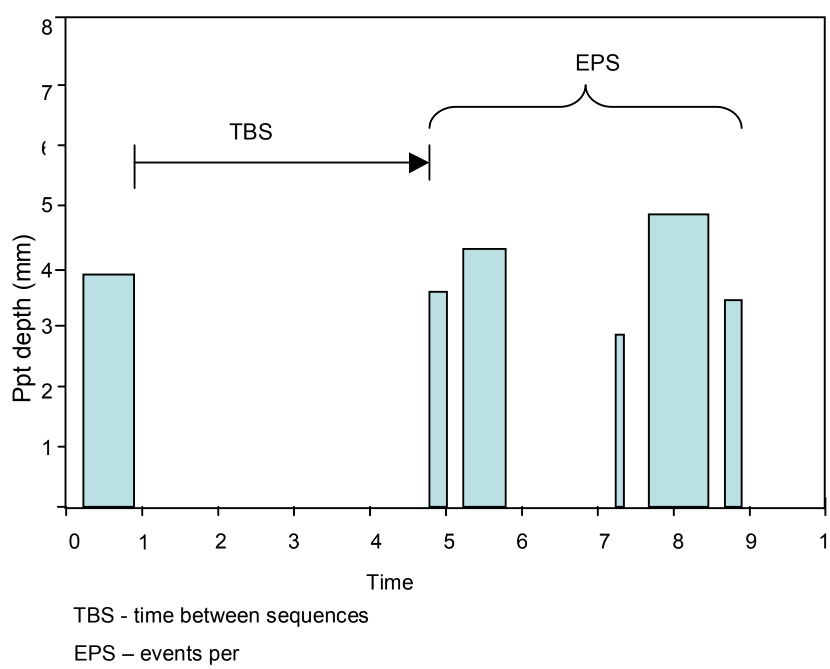

Figure 2-3a. Cold-season model variables for storm sequences.

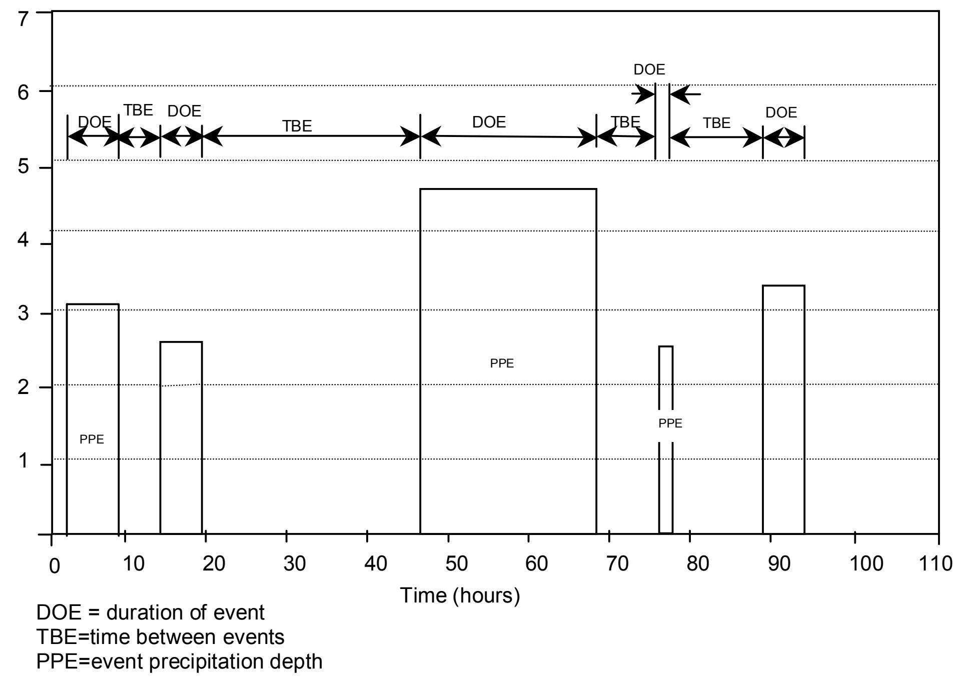

Figure 2-3b. Cold and warm-seasons precipitation model variables for storm events.

Warm-season Precipitation

Because consecutive rain events of the convective thunderstorm type are relatively independent from each other, we use an independent event-based model to simulate their temporal distribution (Tecle et al., 1988). The model used in this study is the modification of that developed by Bogardi et al. (1988). The work of Bogardi et al. (1988) dealt with the total rainfall depths and durations that occurred in consecutive rainy days. This doesn't allow for describing the intensity of individual storms. Hence, the modification is needed to allow for the simulation of individual storm event intensities.

The most important change in the model is a redefinition of an event, which is the same as that used for cold-season precipitation model, uninterrupted rainfall of any duration. The second modification is the removal of number of events per season, because this study attempts to describe the general pattern of individual warm-season precipitation events instead of a pattern of storms in a season. The new warm-season precipitation model, similar to Bogardi et al (1988) is described using three variables:

1. Precipitation amount per event (mm)
2. Duration of events (hours)
3. Time between events (hours)

Various theoretical distribution functions have been used in past studies to describe the probability distribution of precipitation characteristics (Eagleson, 1972; Duckstein et..al, 1973; Duckstein et al., 1975; Hanes et al., 1977; Rupp, 1995). Likewise the statistical simulation method used in this study involves the fitting of known theoretical probability distribution functions, such as Weibull, gamma and exponential to describe the above variables. One way of fitting these models to the observed data is using the method of moments. The method requires estimating the parameters of the various distribution functions (Barndorff-Nielsen et al., 1996). Some distributions require multiple parameters while others use only one parameter. The exponential probability distribution function, for example, uses only the mean of the population as its parameter the only parameter (see equation 2-1):

$$f(x) = \left(\frac{1}{\beta}\right)e^{-x/\beta} \tag{2-1}$$

where: $f(x)$ is the probability distribution function (pdf), β is the population mean and x is a random variable.

For example, to fit this exponential distribution function to the time between storm sequences, the mean of the sample data becomes the parameter β.

Actual simulation of synthetic data from a probability distribution function *(pdf)* requires deriving its cumulative distribution function *(cdf)*. The *cdf* is calculated by integrating the *pdf* over the desired range of variable values. For instance, to find the probability of occurrence, $F(x)$, of the time between storm sequences that are less than or equal to x days, the *pdf* is integrated from 0 to x:

$$F(x) = \int_0^x f(x)dx \tag{2-2}$$

For example, the *cdf* of the exponential function in equation (2-1) can be expressed as:

$$F(x) = 1/\beta \int_0^x e^{-x/\beta} dx \tag{2-3}$$

Solving the integration in equation (2-3) gives:

$$F(x) = 1 - e^{-x/\beta} \tag{2-4}$$

Next, to determine the time between two storm sequences for a given frequency, equation (2-4) is solved for the time as follows:

$$x = -\beta \ln(1 - F) \tag{2-5}$$

where F is the cumulative frequency distribution function, and β and x are as described above. The value of F is obtained using a random number generator which gives values that lie in the interval between zero and one.

In the case of other probability distribution functions, such as the gamma distribution function, analytical integration of their pdf's is not possible; therefore, approximations to the integral solution must be determined instead. The pdf of the gamma distribution function takes the following form:

$$f(x) = \frac{\beta^{-\alpha} x^{\alpha-1} e^{-x/\beta}}{\Gamma(\alpha)} \tag{2-6}$$

where α is the shape parameter and equals $\frac{\mu^2}{\sigma^2}$, β is the scale parameter and equals $\frac{\sigma^2}{\mu}$, and $\Gamma(\alpha)$ is the gamma function defined by

$$\Gamma(\alpha) = \int_0^\infty \theta^{\alpha-1} e^{-\theta} d\theta \tag{2-7}$$

and μ and σ^2 are the population mean and variance, respectively.

After the distributions were hypothesized for the data and their parameters were estimated, it is necessary to examine whether the fitted distribution is in agreement with the observed data.

The test used in this study for assessing goodness-of-fit of the theoretical *pdf's* to the observed data is the Kolomogorov-Smirnov test, or K-S test. The test compares an empirical distribution function, $F_e(x)$, with the distribution function of the hypothesized distribution or theoretical distribution, $F_t(x)$ (Law and Kelton, 1982). The null hypothesis of the K-S test is that the empirical *pdf* and the theoretical *pdf* are equivalent. If the test does not prove that the two distributions are statistically different, then the fit is assumed to be good.

When the observed data are sorted in ascending order, the empirical distribution function becomes:

$$F_e(x) = i/n; \qquad i = 1,2,\ldots.. n \tag{2-8}$$

where i is a specific observation in the samples.

The K-S test evaluates the difference between the empirical and the theoretical distribution function for each data point, X. The test statistic is the maximum of these differences, D. This statistic is the largest (vertical) distance between $F_e(x)$ and $F_i(x)$ and is determined using equation (2-9).

$$D = \max\{|F_e(x) - F_t(x_i)|\} \tag{2-9}$$

for every x. D can be computed by substituting $\frac{i}{n}$ for $F_e(x)$ as shown in equation (2-10)

$$D^+ = \max\left\{\frac{i}{n} - F_t(x_i)\right\} \tag{2-10}$$

$$D^- = \max\left\{F_t(x_i) - \frac{(i-1)}{n}\right\} \tag{2-11}$$

then

$$D = \max\{D^+, D^-\} \tag{2-12}$$

If the value of D exceeds some critical value, d, the null hypothesis is rejected. The critical value, d, depends on the sample size, n, the level of significance of the test, α, and on the hypothesized distribution function when the distribution parameters are estimated from the observed data. Law and Kelton (1982) reviewed the procedures for the normal, exponential, and Weibull distributions.

The "goodness of fit" is checked using two other tests in addition to the K-S test, called the Anderson-Darling test and the Cramer-Smirnov-Von-Mises test. Both tests are modifications of the Kolmogorov-Smirnov test. The Anderson-Darling test gives more weight to the tails than does the K-S test. The K-S test is distribution free in the sense that the critical values do not depend on the specific distribution being tested. The Anderson-Darling test makes use of the specific distribution in calculating critical values. This has the advantage of allowing a more sensitive test and it has the disadvantage of requiring that critical values must be calculated for each distribution. The Cramer-Simirnov-von Mises test is similar to the Kolmogorov test, but somewhat more complex computationally (Stephens, 1977; Law and Kelton, 1982).

Three of the precipitation model variables (time between sequences, number of events per sequence, time between events) can be described using a univariate probability distribution functions described above. The modeling of depth and duration, however, is more complex because these two variables are not independent of each other. Therefore, a different method suitable for simulating two dependent random variables is used.

Rupp (1995) used two different methods to generate the joint probability distribution function for duration and depth with a marginal gamma distributions. One of them is the trivariate reduction (TVR) method. The second procedure involves explicitly describing the conditional probability distribution of depth given the duration of the event. He found out that this method produced the best fitting *pdf* for simulation and it is used in this study to describe and simulate the joint distributions of duration and depth of precipitation events for both cold and warm-seasons. This method of simulation using such a bivariate distribution function is described by Kottas and Lau (1978), and Schmeiser and Lal (1981) consider it an “excellent approach” especially when the dependency structure between the random variables is well understood.

To develop the bivariate model for simulating storm depth and duration, the marginal distribution (the distribution of a univariate random variable) for duration is first found. Assuming the marginal distribution function to be gamma, the *pdf* for the duration, τ_I is:

$$f_1(x_1) = \frac{(\beta_1^{-\alpha_1} x_1^{\alpha_1 - 1} e^{-x_1/\beta_1})}{\Gamma(\alpha_1)} \tag{2-13}$$

In this equation the α_1 and β_1 are respectively the shape and scale parameters of the gamma distribution for duration.

A conditional distribution is then determined for depth. In this study, the conditional distribution for depth is assumed to be gamma with its shape and scale parameters being dependent on the duration. A visual examination of a plot of observed depth and duration hints that the gamma function is appropriate. Grayman and Eagelson (1969) made the same observation to describe storm data taken in Boston, Massachusetts. Letting x_2 equal the depth, the conditional pdf of depth given duration is expressed as

$$f_2(x_2) = \frac{(\beta_2^{-\alpha_2} x_2^{\alpha_2 - 1} e^{-x_2/\beta_2})}{\Gamma(\alpha_2)} \tag{2-14}$$

where α_2 and β_2 are respectively the shape and scale parameters of the gamma distribution for depth given duration.

As described previously, the shape and scale parameters are both calculated from the mean and variance such that $\alpha_2 = \mu_2^2 / \sigma_2^2$ and $\beta_2 = \mu_2 / \sigma_2^2$. To implement equation (2-14), it is necessary to know how the distribution of depth varies with duration. To gain an understanding of the structural dependency between duration and depth, a simple linear regression of depth versus duration is developed. The regression model is:

$$\delta_i = b_0 + b_1 x_i + \varepsilon_i; \qquad i = 1,2,\ldots\ldots\ldots\ldots\ldots n \qquad (2\text{-}15)$$

where δ_i is the depth, x_i is the duration, b_0 and b_1 are regression coefficients, and ε_i is the error of the regression. Such a regression model gives an estimate of the mean depth conditional upon duration.

The next step describes how the variance of the conditional distribution of depth varies with duration. To accomplish this task, the duration is first divided into intervals so that each interval contains approximately the same number of data points and that each interval has enough points to estimate a variance for that interval. The sample variance of depth for each duration interval is then calculated. The depth variances of each interval are regressed against the mean of the durations of the interval data to obtain a function that estimates the variance of depth conditioned upon duration. The regression model has the form:

$$v_i^2 = c_0 + c_1 \tau_i^{\gamma} + \varepsilon_1; \qquad i = 1,2,\ldots\ldots\ldots\ldots\ldots m \qquad (2\text{-}16)$$

where v_i^2 is the variance of depth in the i^{th} interval, τ_1 is the mean of the duration data in the i^{th} interval, γ is a constant, c_0 and c_1 are regression coefficients, ε_i is the error of the regression, and m is the number of intervals.

The above two regressions provide the expressions for estimating the mean and the variance of the depth conditional up on the duration. These functions are respectively,

$$x_2(x_1) = b_0 + b_1 x_1 \tag{2-17}$$

and

$$v_2^2(\tau_1) = c_0 + c_1 \tau_i^{\gamma} \tag{2-18}$$

Substituting μ_2 for $x_2(x_1)$ and σ_2^2 for $v_2^2(x_1)$ into equations (2-17) and (2-18), respectively, gives:

$$\mu_2 = b_0 + b_1 x_1 \tag{2-19}$$

and

$$\sigma_2^2 = c_0 + c_1 x_1^{\gamma} \tag{2-20}$$

Knowledge of the conditional mean and variance of depth allows estimation of the shape and scale parameters for the conditional gamma *pdf* (equation 2-14). The shape and scale parameters for the conditional distribution of depth given duration are calculated using the following equations:

$$\alpha_2 = \mu_2^{\,2} / \sigma_2^{\,2} = (b_0 + b_1 x_1)^2 / (c_0 + c_1 x_1^{\gamma}) \qquad (2\text{-}21)$$

and

$$\beta_2 = \sigma_2^{\,2} / \mu_2 = (c_0 + c_1 x_1^{\gamma}) / (b_0 + b_1 x_1) \qquad (2\text{-}22)$$

The probability density functions for each one of the five cold-season and the three warm-season precipitation events characteristics are determined for one gauge (#38) in the study area. The data from the remaining gauges are used to analyze the spatial distribution of precipitation on the watershed. Statistical software known as SAS were used to develop the frequency distribution for each variable, to fit a theoretical probability distribution function *(pdf)* to the data of each variable, and generate random numbers to synthetically construct future scenarios of the two seasonal precipitation event types.

Spatial Analysis of Precipitation Events

The spatial distribution of the precipitation in the ponderosa pine forested area of north central Arizona is affected by the major orographic features such as the Mogollon Rim, the White Mountains and the San Francisco Peaks that dominate the landscape in the area (Beschta, 1976; Campbell and Ryan, 1982). The study watershed is situated along one of these physiographic features, the Mogollon Rim. Hence, studying the spatial distribution of precipitation across the watershed requires describing of the topographic and climatic characteristics of the study area. In general, those areas with highest elevation and where air masses rise the fastest are likely to receive the highest amount of precipitation. In mountainous regions, this rapid ascent takes place on the windward side of the topography (Barros and Lettenmaier, 1994). For these reasons, an analysis of the areal distribution of precipitation needs to look at both wind direction during storm events and the areas where ascent occurs (Oki and Musiake, 1991).

Actual precipitation data are available only for point locations where the gauging stations are in the watershed. Therefore, the precipitation events data measured at the gauging stations do not accurately represent the precipitation condition over the entire watershed because the depths and durations of the precipitation events vary with space over watershed landscape (Marquinez et al., 2003). The spatial distribution analysis of precipitation events, therefore, enables estimation of precipitation event depths and durations across the entire study watershed.

This study examined the spatial distributions of cold and warm-seasons precipitation events and then used this spatial variation of total precipitation for each season to estimate the spatial distribution of individual events. The effects of the various landscape characteristics on the spatial distribution of precipitation depth and duration on the watershed were studied. The variables examined are gauge elevation, geographic location in terms of Universal Transverse Mercator (UTM) and aspect. Gauge elevation was selected because previous studies showed precipitation in the region generally increases with elevation (Beschta, 1976; Campbell and Ryan, 1982). Similarly, the UTM coordinates of the gauges were examined because they represent the general trend of the Beaver Creek watersheds rising northeastward. Finally, the aspects of the gauges were analyzed to see if differences in precipitation exist between windward and leeward sites.

In the temporal analysis of the precipitation part of the study, precipitation for only one gauge, gauge #38, located at the outlet of the watershed was simulated. The spatial analysis of precipitation across the watershed will be used to estimate the simulated amount of precipitation in the entire watershed given the simulated precipitation at gauge #38. The precipitation events depths and durations at any point in the watershed are assumed to be related to the depth and duration values determined at gauge #38. Therefore, this analysis examined the relationship between the ratio of the precipitation depth and duration at any point to the precipitation depth and duration at gauge #38 to determine the spatial distribution of precipitation events. The relationships are described in the form of regression equations.

In the case of precipitation depth, the dependent variable in the regression equation is the ratio of precipitation falling at gauge i to that falling at gauge #38, while in the case of precipitation duration, the dependent variable is the ratio of the duration of precipitation at gauge i to that at gauge #38. In both cases, the independent variables are gauge elevation, UTM x-coordinate, UTM y-coordinate and aspect, and the analysis is made to determine the level of influence these variables have on the amount and duration of the precipitation at the different locations in the watershed.

Once the prediction equations for precipitation depth and duration are determined, a GIS is implemented along with the equations to map the spatial distribution of event depth and duration. The use of GIS enables efficient determination of storm depth and duration at any location in the watershed. In this study, the watershed is divided into 90 by 90 m cells and the elevation, position, and aspect for each one of these cells are determined. Once the storm depth and duration is simulated at gauge #38, then both the depth and duration at each cell are estimated using the respective prediction equation. Two grids are created in the process: one for the spatial distribution of storm depth and the other for the spatial distribution of storm duration. These two grids are combined to form a third grid to describe the spatial distribution of storm intensity across the watershed.

Analysis of Temperature and Form of Precipitation

In addition to a storm's depth, duration and intensity, the form of its occurrence as rain, snow or a mixture of rain and snow, is also determined. Daily maximum and minimum temperatures are used to determine the form of precipitation in the cold-season and to calculate the average daily temperatures used in the various water balance equations of the next chapter. This study uses the same criteria used in Solomon et al. (1976) to determine the form of precipitation. Precipitation is considered rain when the minimum temperature exceeds 1.7^{o} C (35^{o} F). Precipitation takes the form of snow when the maximum temperature is below 4.4^{o} C (40^{o} F) and the minimum temperature is less than 1.7^{o} C (35^{o} F). The third condition which is a mix of rain and snow occurs when the maximum temperature exceeds 4.4^{o} C (40^{o} F) and the minimum temperature drops below 1.7^{o} C (35^{o} F). When the precipitation is mixed, Solomon et al. (1976) used the following equation developed by Leaf and Brink (1973) to determine the amount of snow precipitation:

$$P_S = P_T\,[1 - (T_{max} - 1.7) / (T_{max} - T_{min})] \qquad (2\text{-}23)$$

where P_S is the amount of precipitation that comes as snow in water equivalent, P_T is the total event precipitation, and T_{max} and T_{min} are the maximum and minimum temperatures, respectively.

The amount of precipitation that takes the form of rain is simply P_T minus P_S. Cold and warm-seasons temperature data taken at the outlet of the watershed are analyzed to estimate the daily maximum and minimum temperatures. Using the maximum and minimum temperatures, a data set of varying diurnal temperature is created. The sets of the daily maximum temperature and the varying diurnal temperatures are then divided into those days in which precipitation occurred and those days in which it did not. Best fit models are developed to the wet and dry day data to describe the change in the mean daily maximum temperature and the varying diurnal temperature throughout the seasons.

During the simulation process, the daily maximum temperature and the diurnal temperature variation are generated independently. The daily minimum temperature is then calculated by subtracting the diurnal variation from the daily maximum temperature. The maximum and diurnal temperature variations are simulated using the lag-one Markov model (Fiering and Jackson, 1971) as adopted by Rupp (1995). This model is used to provide the correlation between subsequent data that occur on a daily basis. The lag-one, multi-period Markov model for temperature takes the general form:

$$T_{i,j} = T_{ave,j} + r_j \frac{S_j}{S_{j-1}} \left(T_{i,j-1} - T_{ave,j-1}\right) + t_{i,j} S_j \left(1 - r_j^{\,2}\right)^{1/2} \qquad \text{(2-24)}$$

where $T_{i,j}$ is the temperature generated on day j in season i, $T_{i,j-1}$ is the previous day's temperature in season i, $T_{ave,j}$ is the mean temperature for day j, $T_{ave,j-1}$ is the mean temperature for day $j-1$, r_j is the lag-one autocorrelation coefficient for day j and $j-1$, $t_{i,j}$ is the normally distributed random variable with zero mean and unit variance for day j in season i, and S_i and S_j are the standard deviations of temperatures of days j and $j-1$, respectively.

In this study, two separate forms of equation (2-24) are used for each season: one for dry days when there was no precipitation and the other for wet days when there is precipitation. One autocorrelation coefficient is used for the dry days and the wet days, and both are assumed constant throughout the seasons. The mean maximum temperatures for both dry and wet days vary with time in accordance with relationships described using equations functions that fit the data. For example, the following parabolic equations are used to describe the change in daily maximum temperature with time for both dry and wet days, respectively:

$$T_{dry,i} = b_0 + b_1 x + b_2 x^2 \tag{2-25}$$

$$T_{wet,i} = b_3 + b_4 x + b_5 x^2 \tag{2-26}$$

where $T_{dry,i}$ and $T_{wet,i}$ are the average maximum daily temperatures for dry and wet days for season i, respectively, x is the time in days since the beginning of the season, and b_0 through b_5 are regression coefficients.

A least-square regression procedure is used to determine the best fit to the data. The standard deviations for the dry and wet day temperatures used are the root mean square errors of the dry and wet day regression equations, respectively.

To simulate the maximum temperature for consecutive dry days, the following equation is used:

$$T_{i,j} = T_{dry,j} + r_{dry}\left(T_{i,j-1} - T_{dry,j-1}\right) + t_{i,j} S_{dry}\left(1 - r_{dry}{}^{2}\right)^{1/2} \tag{2-27}$$

where $T_{dry,j}$ is the temperature calculated using equation (2-25) for day j , $T_{i,j-1}$ is the simulated temperature for day $j-1$ and season i , $T_{dry,j-1}$ is the temperature calculated using equation (2-25) for day $j-1$ and season i , r_{dry} is the autocorrelation coefficient for dry days, and S_{dry} is root mean square error (RMSE) of equation (2-25).

The equation can be simplified by assuming that the standard deviations for temperature do not vary from day to day, thus S_j / S_{j-1} equals one.

When simulating the maximum temperatures for consecutive wet days, the following equation is used

$$T_{i,j} = T_{wet,j} + r_{wet}\left(T_{i,j-1} - T_{wet,j-1}\right) + t_{i,j} S_{wet}\left(1 - r_{wet}{}^{2}\right)^{1/2} \tag{2-28}$$

where $T_{wet,j}$ is the temperature calculated using equation (2-26) for day j, $T_{i,j-1}$ is the simulated temperature for day $j-1$ and season i, $T_{wet,j-1}$ is the temperature calculated from equation (2-26) for day $j-1$ and season i, r_{wet} is the autocorrelation coefficient for wet days, and S_{wet} is the root mean square error (RMSE) of equation (2-26).

The same assumptions that were made in equation (2-27) are also made here. When a wet day follows a dry day, or a dry day follows a wet day, a special case of equation (2-24) for r_j equals zero is used. In other words, the model assumes no persistence for these two cases. This is equivalent to saying that the arrival or departure of a storm system interrupts the prevailing temperature pattern completely, and the new day's temperature will be unaffected by the previous day's temperature. When the autocorrelation is set to zero, equations (2-27) and (2-28) reduce to, respectively,

$$T_{i,j} = T_{dry,j} + t_{i,j}S_{dry} \tag{2-29}$$

and

$$T_{i,j} = T_{wet,j} + t_{i,j}S_{wet} \tag{2-30}$$

Finally, to simulate the minimum daily temperature, its diurnal variation is generated in the same manner as that for maximum temperature. The first step is to describe any trend in the diurnal variation with time throughout each season. As with the maximum temperature, the parabolic functions may be used to model the change in diurnal variation with time for dry and wet days. The functions for dry days and wet days are, respectively:

$$DV_{dry,i} = b_6 + b_7 x + b_8 x^2 \tag{2-31}$$

$$DV_{wet,i} = b_9 + b_{10} x + b_{11} x^2 \tag{2-32}$$

where $DV_{dry,i}$ and $DV_{wet,i}$ are the diurnal variations for dry and wet days for season i, respectively, x is the time in days since the beginning of the season, and b_6 through b_{11} are regression coefficients.

Simulation of the diurnal variation uses the same procedure as that for maximum temperature. The lag-one Markov equations for the dry diurnal variation and the wet day diurnal variation are, respectively,

$$DV_{i,j} = DV_{dry,j} + r_{dvdry}\left(DV_{i,j-1} - DV_{dry,j-1}\right) + t_{i,j} S_{dvdry}\left(1 - r_{dvdry}{}^2\right)^{1/2} \tag{2-33}$$

$$DV_{i,j} = DV_{wet,j} + r_{dvwet}\left(DV_{i,j-1} - DV_{wet,j-1}\right) + t_{i,j} S_{dvwet}\left(1 - r_{dvwet}{}^2\right)^{1/2} \tag{2-34}$$

where the diurnal variation (DV) has simply replaced the maximum temperature (T) in equations (2-27) and (2-28) and the subscript $dvday$ and $dvwet$ stands for the diurnal variation for dry and wet days, respectively.

When a dry day follows a wet day, or a wet day follows a dry day, the diurnal variation is simulated by the special case of equation (2-33) and (2-34) for *r* equals zero. The equations for a dry day following a wet day and a wet day following a dry day are respectively,

$$DV_{i,j} = DV_{dry,j} + t_{i,j} S_{dvdry} \tag{2-35}$$

and

$$DV_{i,j} = DV_{wet,j} + t_{i,j} S_{dvwet} \tag{2-36}$$

where the diurnal variation (DV) has simply replaced the maximum temperature (T) in equations (2-29) and (2-30).

Calculation of the daily minimum temperature is made by subtracting the simulated diurnal variation, DV_j, from the simulated daily maximum temperature, T_j. Once the daily maximum and minimum temperatures are determined for one site in the study area, the temperatures across the entire watershed are estimated by adjusting the site temperature for changes in elevation. Mean monthly environmental lapse rates for daily maximum and daily minimum temperatures for the ponderosa pine type of central Arizona are used to model the change in temperature with elevation. The lapse rates (see Table 2-1) are calculated from data in Beschta (1976).

Table 2-1 Mean monthly lapse rates for daily maximum and minimum temperatures (Beschta, 1976).

Month	Lapse rate of maximum temperature (^{o}C/km)	Lapse rate of minimum temperature (^{o}C/km)
January	2.4	9.3
February	4.6	10
March	6.0	8.9
April	6.2	10
May	7.3	13.12
June	8.02	13.12
July	8.75	12.4
August	8.02	11.67
September	6.92	13.85
October	5.6	10.8
November	3.1	8.0
December	0.5	8.5

Results

Temporal Analysis of Precipitation Events

The temporal behavior of the precipitation data from gauge #38, which is located at the outlet of Bar M watershed, was analyzed. The reasons why gauge #38 was selected were because: it is a recording gauge, which was equipped with a hygrothermograph for the twenty years of study, and it is the only gauge that is still in operation. During the twenty years of precipitation record used in this study, the gauge recorded precipitation on average 15 percent of the days in the cold-seasons and 20 percent of the days in the warm-seasons. Figure 2-4 shows the locations of the precipitation gauges in the Beaver Creek watershed area.

We used SAS statistical software to analyze the observed frequency distribution of the precipitation characteristics and fitting of the various known theoretical probability distribution functions and identifying the best fitted model using four goodness-of-fit tests (SAS. institute, 2004). Four theoretical probability distribution functions including lognormal, gamma, Weibull and exponential distributions were fitted to the frequency distribution of the observed data. Kolmogorov smirinov, Cramer-Von Mises, Anderson-Darling and Chi- square tests were used for the goodness-of-fit test to determine appropriate models for the data distributions. According to these tests, a model with *p*-value of greater than or equal to 0.05 was selected as best model to describe the observed distribution data at 5% significant level which indicated that the data came from the fitted distribution.

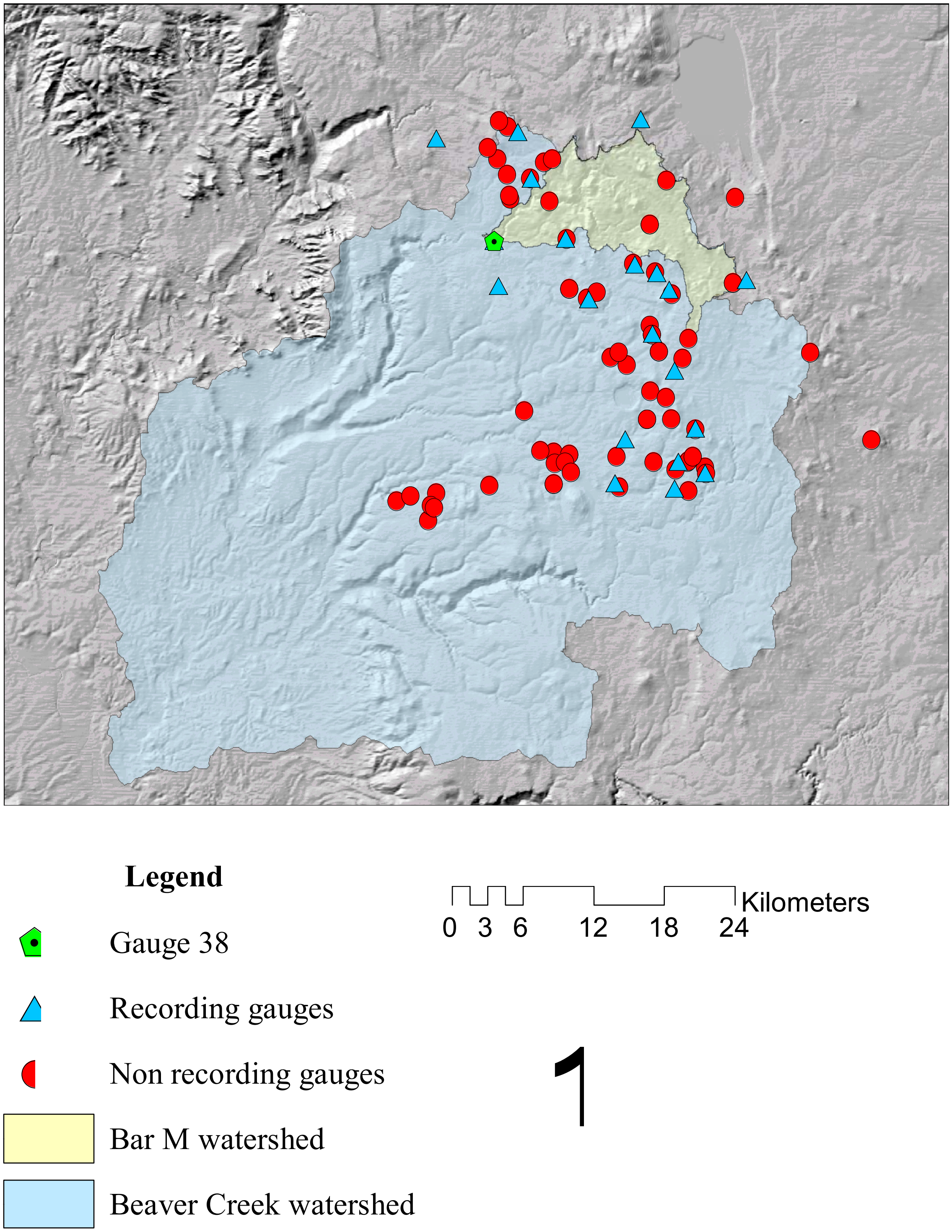

Figure 2-4. Bar M watershed and the precipitation gauge network in the former Beaver Creek experimental pilot project.

Cold-season Precipitation

The inter-arrival time between cold-season precipitation events in a sequence were truncated at 3.5 days, in order to re-normalize the data so that their cumulative distribution function *(cdf)* becomes one when the inter-arrival time is 3.5 days. The purpose for the truncation was to avoid simulation of a time between events greater than 3.5 days, by definition, if the inter-arrival time between two events is more than 3.5 days, it is considered to belong to a different sequence. Of the four models fitted to the time between events data, the Weibull distribution function seems to fit better than the others (Figure 2-5).

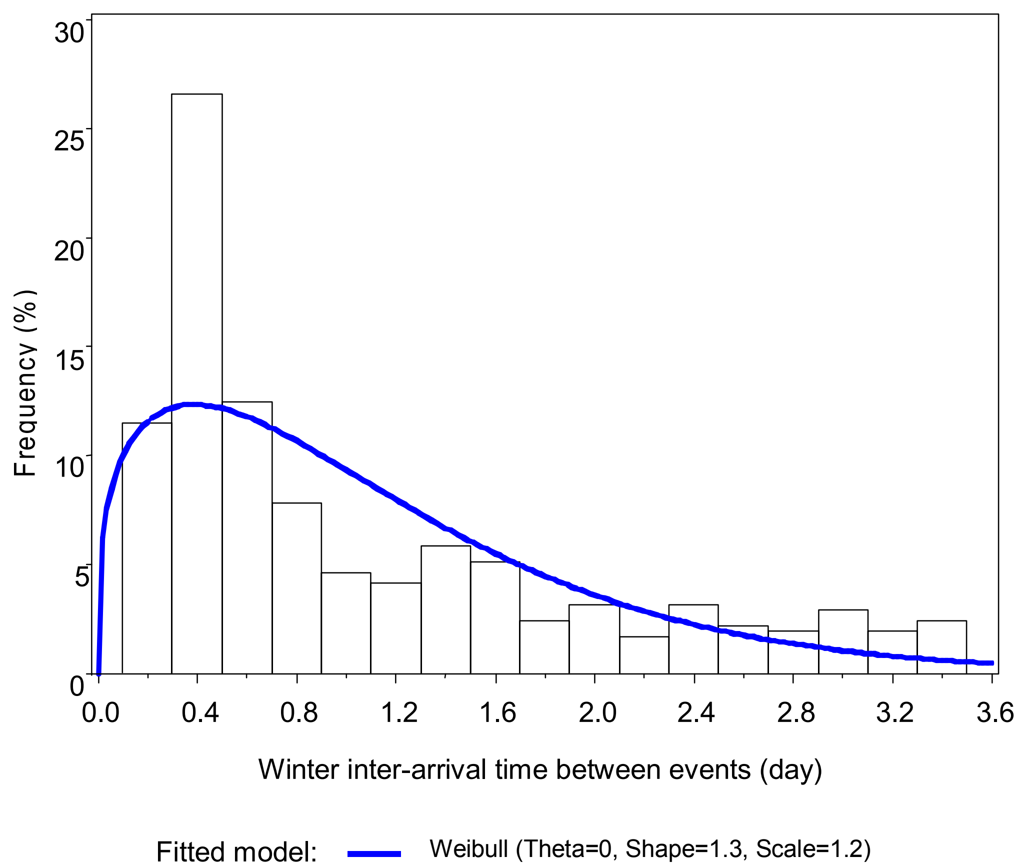

Figure 2-5. Frequency distribution of interarrival time between cold-season events fitted with Weibull probability distribution function (*p*-value = 0.01).

The distribution of the number of events per sequence was also best described using the Weibull distribution function while the time between sequences was described using gamma distribution. However, one adjustment is made to the time between sequences of cold-season precipitation to improve the fit. Because the lower limit of the time between sequences was 3.5 days, the distribution is shifted so that 3.5 days become the zero point. In practice, 3.5 days is subtracted from all the data prior to constructing the frequency distribution. This shifting of the distributions downward is easily corrected during simulation by adding 3.5 days to each value of the generated time between sequences. The frequency distribution of the number of events per sequences and the time between sequences with their respective best fitted theoretical frequency distribution functions are shown in Figures 2-6 and 2-7, respectively.

The distribution of time between sequences was not significantly different from the gamma distribution at the 5% level of significance with a p-value of 0.5. However, all the four models fail to fit the time between events and number of events per sequence data at 5% level of significance. However, Weibull distribution performs well for both as compared with other models.

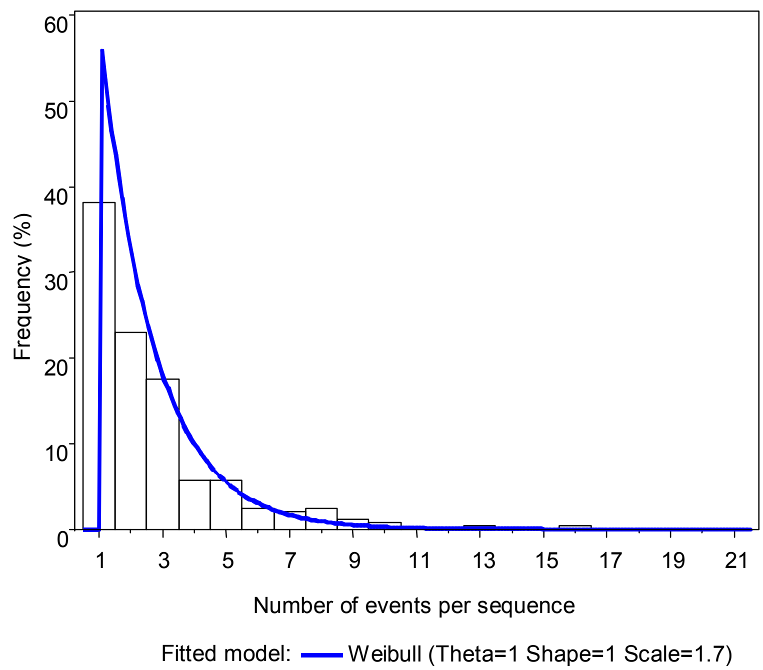

Figure 2-6. Frequency distribution of number of events per sequence fitted with Weibull probability distribution function (p-value = 0.01).

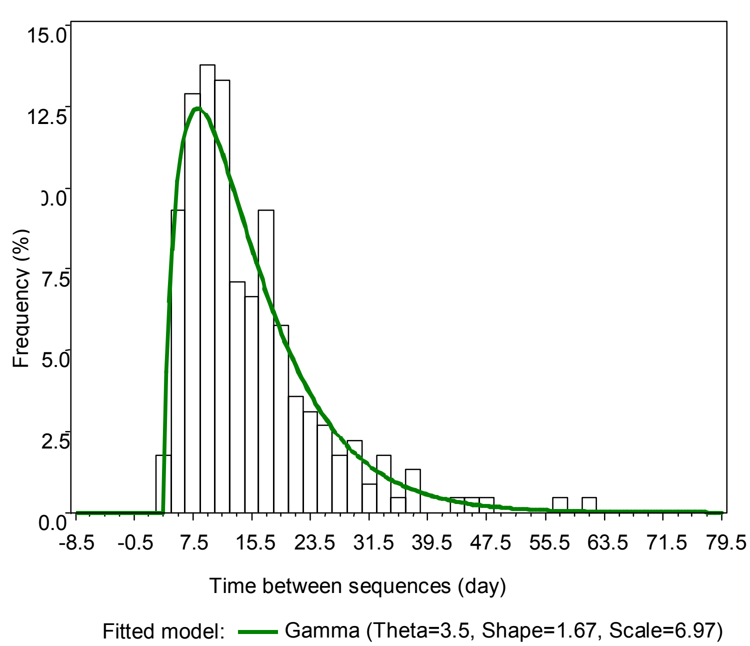

Figure 2-7. Frequency distribution of time between sequences fitted with gamma probability distribution function (p-value = 0.5).

In the case of the joint distributions of depth and duration, the gamma distribution performed best in describing their marginal distribution functions than other distributions (see Figures 2-8 and 2-9). However, the model failed all the tests at the 5% level. As with sequence inter-arrival time, both the distributions of event depth and duration needed shifting before fitting. Because of the precision of the gauge charts upon which precipitation was recorded, event duration was measured at five minutes intervals. Any duration less than 2.5 minutes was assumed to be zero, while any event lasting between 2.5 and 7.5 minutes was assumed to have a duration of five minutes. For this reason, the distribution was shifted downward so that a duration of 2.5 minutes, or 0.014667 hours, became zero. Similarly, since the precipitation depth value from gauge the charts began at 0.254 mm, a value of 0.127 mm was subtracted from the data before fitting. Once the values of duration and depth were generated using the shifted distributions, the simulated values were shifted back upward by adding 0.014667 hours and 0.127 mm, respectively. The model goodness-of-fit tests for the different precipitation event characteristics are shown in Table 2-2.

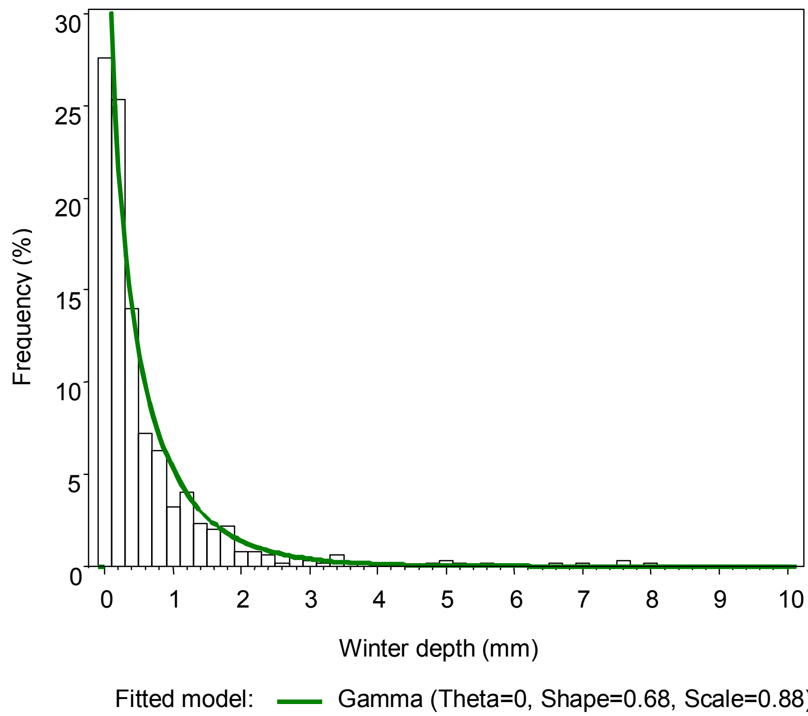

Figure 2-8. Frequency distribution of cold-season event depth fitted with gamma probability distribution function (*p*-value =0.04).

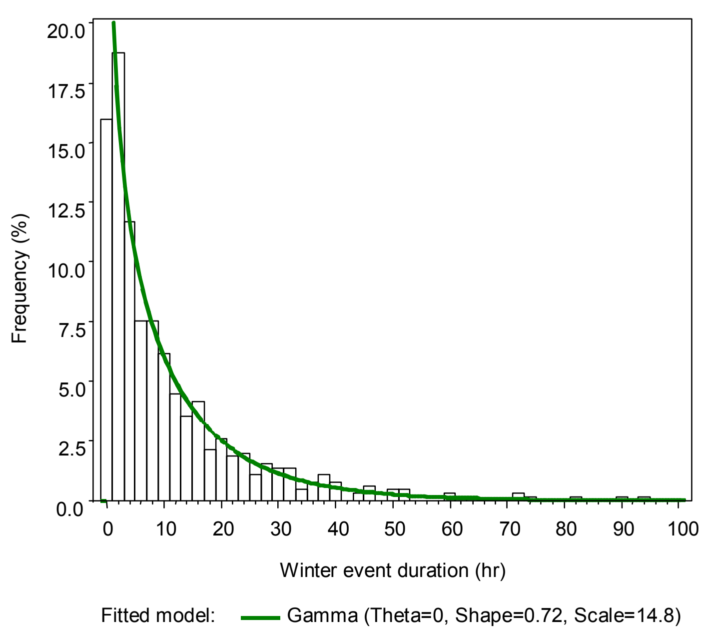

Figure 2-9. Frequency distribution of cold-season event duration fitted with gamma probability distribution function (*p*-value = 0.035).

Table 2-2. p-values for the best fitted models of cold-season precipitation characteristics

Variables	Best fitted probability distribution functions	Tests: Kolmogorov-Smirnov	Cramer-Von Mises	Anderson-Darling	Chi-Square	Level of significance
Time between sequences	Gamma	0.5	0.5	0.5	0.184	5%
Number of event per sequence	Weibull		0.01	0.01	0.001	5%
Time between events	Weibull		0.01	0.01	0.001	5%
Duration of events	Gamma				0.035	5%
Depth of events	Gamma				0.04	5%

Because of the dependency between duration and depth, we used explicit conditional bivariate distribution (ECD) to simulate the joint distribution of both precipitation characteristics. The regression equation of event depth (d) in terms of event duration (t) is:

$$d = 1.522\,t - 0.9923; \qquad r^2 = .68 \qquad (2\text{-}37)$$

and the regression equation for the variance of event depth with respect to its duration is

$$S_d^2 = 0.0462\,t^{2.7919} + 1.004; \qquad r^2 = .988 \qquad (2\text{-}38)$$

The value, 2.7919, of the exponent in equation (2-38) was arrived at by trial and error to meet two criteria: a maximum r^2 value and a y-intercept that approaches a value of one to be consistent with the data. The bivariate distribution generated using the ECD method provided good fit to the observed data, except for short duration and low depths (see Figures 2-10 and 2-11).

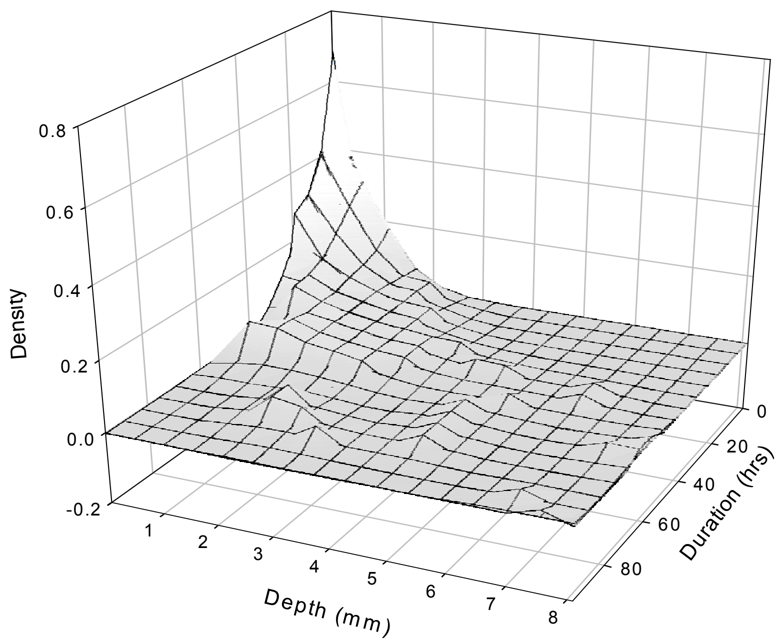

Figure 2-10. Bivariate probability density of observed cold-season precipitation depth.

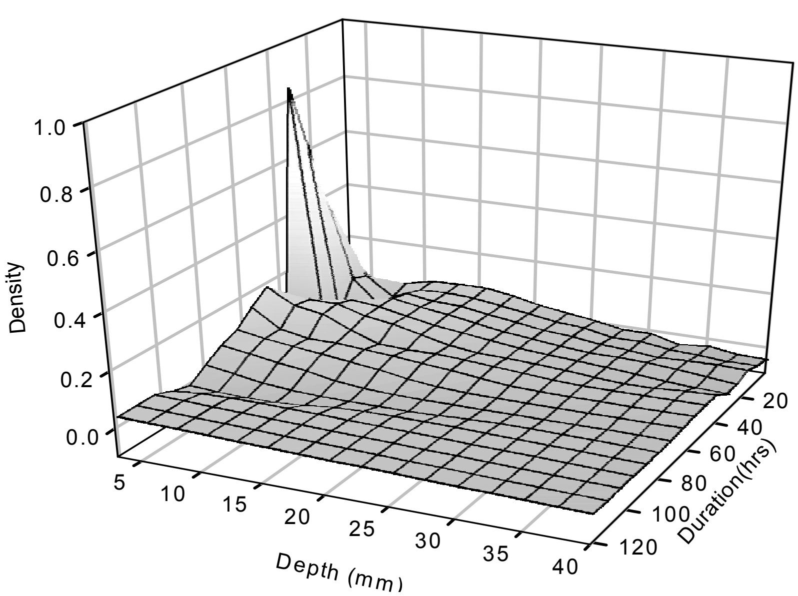

Figure 2-11. Bivariate probability density of simulated cold-season precipitation depth.

To examine the performance of the cold-season precipitation model, twenty cold-seasons total precipitation depths are simulated, amounting to approximately 780 precipitation events. We compared the relative frequency distributions of the twenty years measured total cold-season precipitation data with twenty years of simulated data. Based on the relative frequency histograms of the measured and simulated data shown in Figures 2-12 and 2-13 respectively, there was a significant difference in the mean and range values. The mean and the range of the observed data are 423 mm and 300 mm, respectively, while the simulated data has a mean of 482 mm and a range of 312 mm. However, there was only a small difference between the two data types in the most often occurring (mode) total cold-season precipitation depth. The measured data showed a mode between 400 to 450 mm, while the mode of the generated data was between 450 and 500 mm.

As a result, care must be taken in interpreting the actual and simulated cold-season total precipitation event depths due to small number of sampling years (twenty years). Overall the results showed that the winter season point precipitation model performed well.

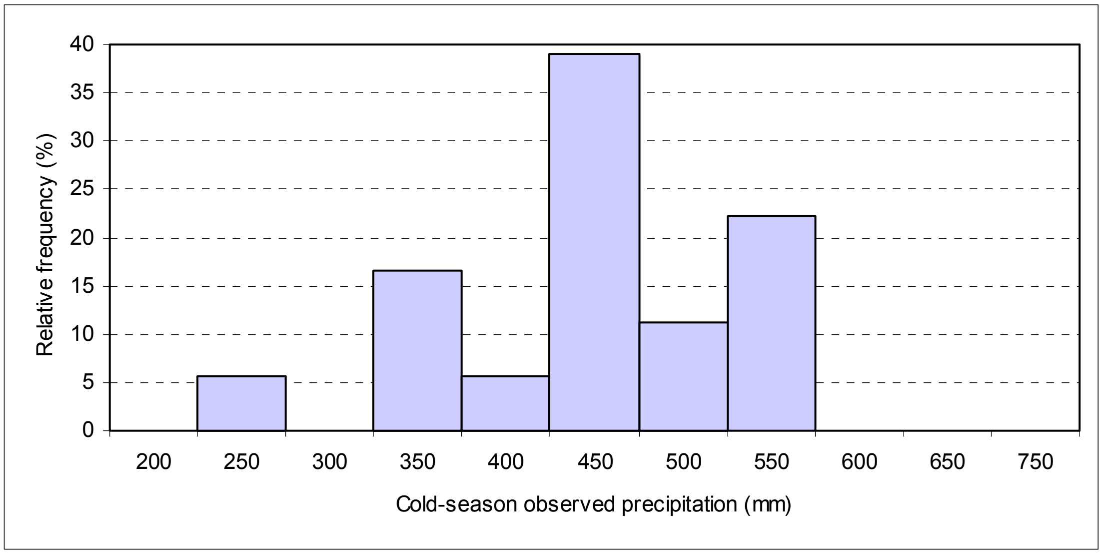

Figure 2-12. Relative frequency of measured cold-season precipitation. N = 20 years.

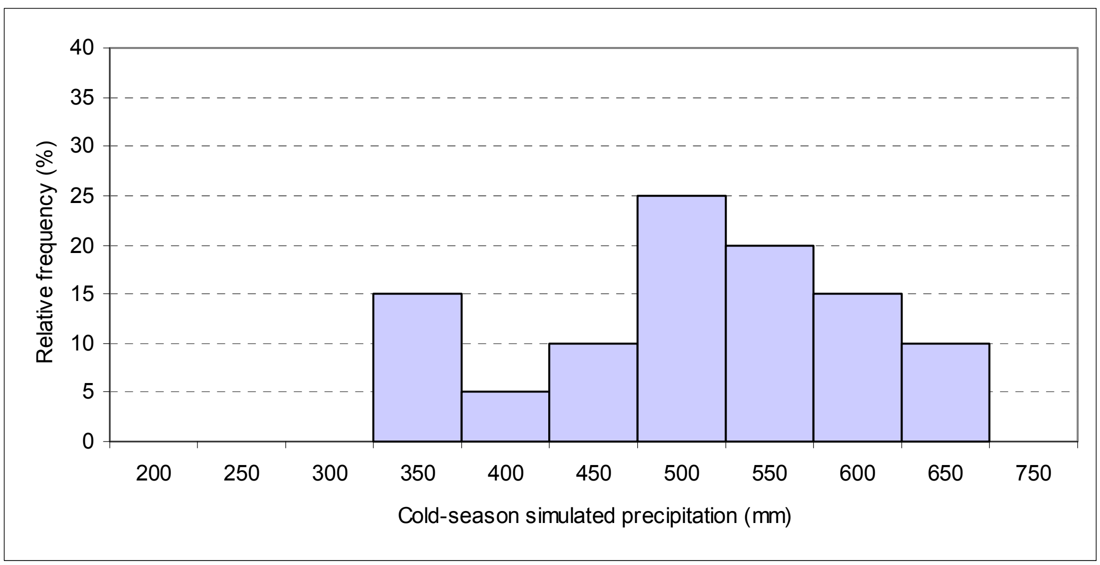

Figure 2-13. Relative frequency of simulated cold-season precipitation. N = 20 years.

Warm-season Precipitation

Unlike cold-season precipitation, warm-season precipitation events are independent from each other hence we used an independent model to describe them. Inter-arrival time between events, event depth, and event duration were the variables we considered to simulate the warm-season precipitation. As in the case of cold-season precipitation, the four theoretical probability distribution functions were unable to describe the distribution of the variables well enough. However, the Weibull distribution performed better than the others to describe inter-arrival time between events (Figure 2-14). On the other hand, the marginal distribution of both duration and depth of events are described using the gamma distribution (Figures 2-15 and 2-16).

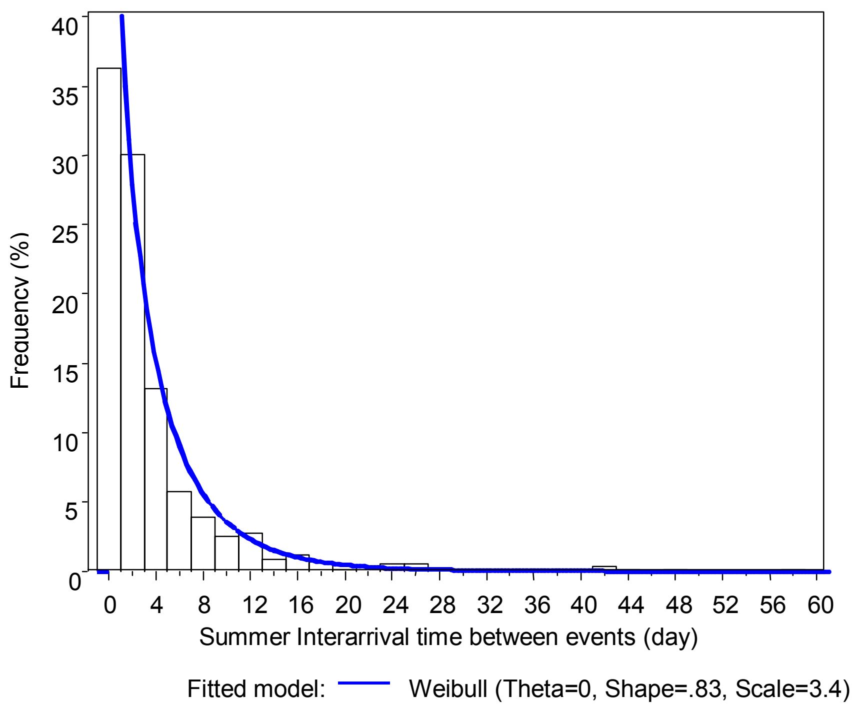

Figure 2-14. Frequency distribution of interarrival time between warm-season events fitted with Weibull probability distribution function (p-value =0.01).

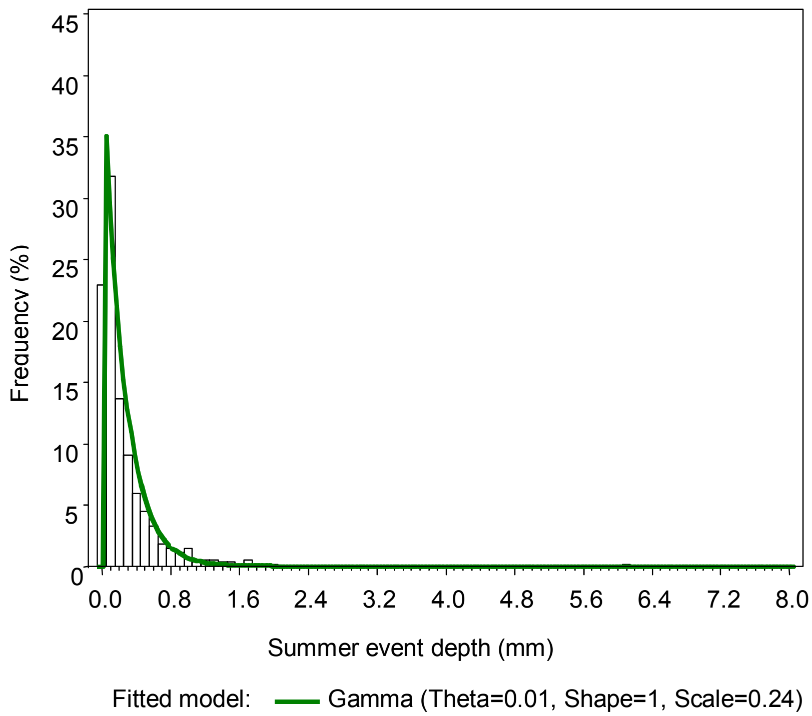

Figure 2-15. Frequency distribution of warm-season event depth fitted with gamma probability distribution function (*p*-value =0.042).

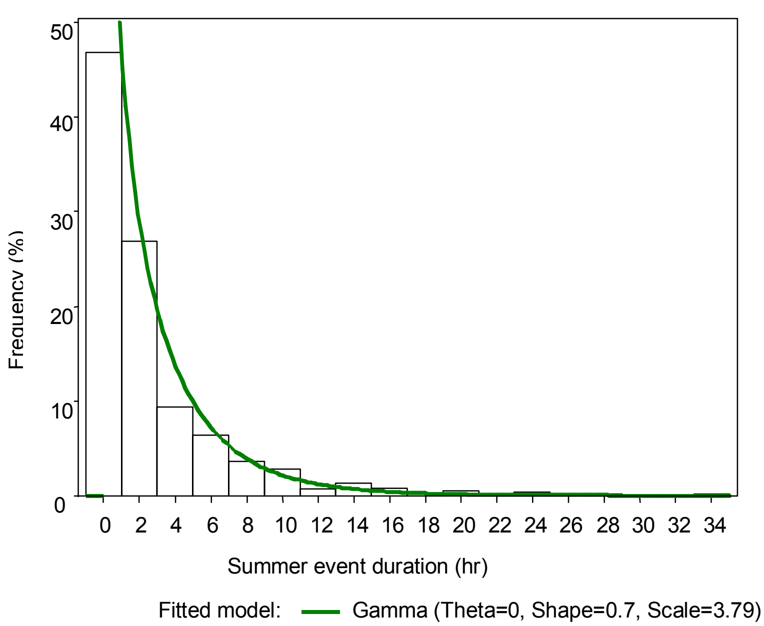

Figure 2-16. Frequency distribution of warm-season event duration fitted with gamma probability distribution function (*p*-value =0.032).

The explicit conditional bivariate distribution (ECD) was also used to simulate the summer precipitation event depth and duration. A regression equations were developed that relate depth of precipitation event (d) and duration (t) as well as variance of event depth and variance of event duration (equations 2-39, and 2-40). The regression equation of event depth in terms of event duration is

$$d = 1.298\ t + 2.8964; \qquad r^2 = .562 \qquad (2\text{-}39)$$

$$S_d^2 = 10.299\ t^{1.4979} + 1.002; \qquad r^2 = .88 \qquad (2\text{-}40)$$

The same trial and error procedure was applied to determine the 1.4979 exponent in equation (2-40) to attain a maximum r^2 value and a y-intercept close to one. The bivariate distribution generated using the ECD method provided good fit to the observed data, except for low depth and small durations (see Figures 2-17 and 2-18).

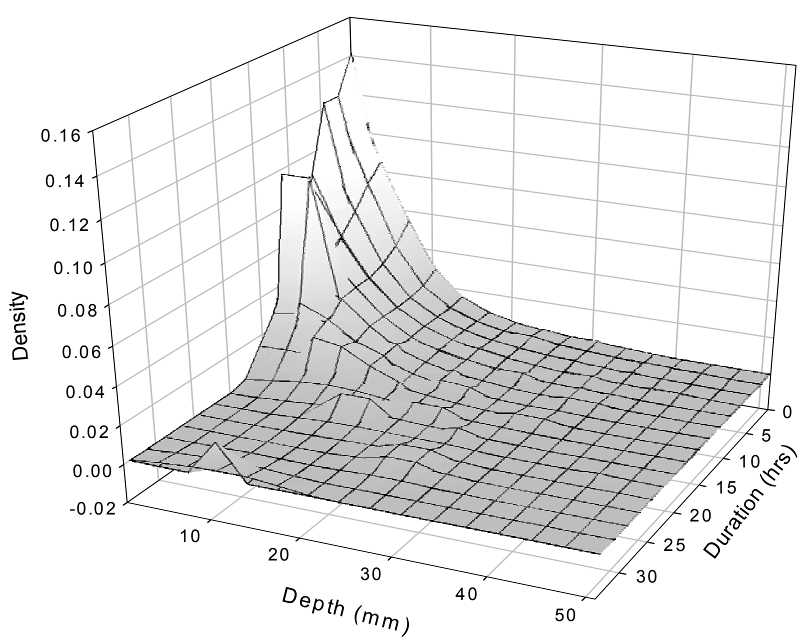

Figure 2-17. Bivariate probability density of observed warm-season precipitation depth.

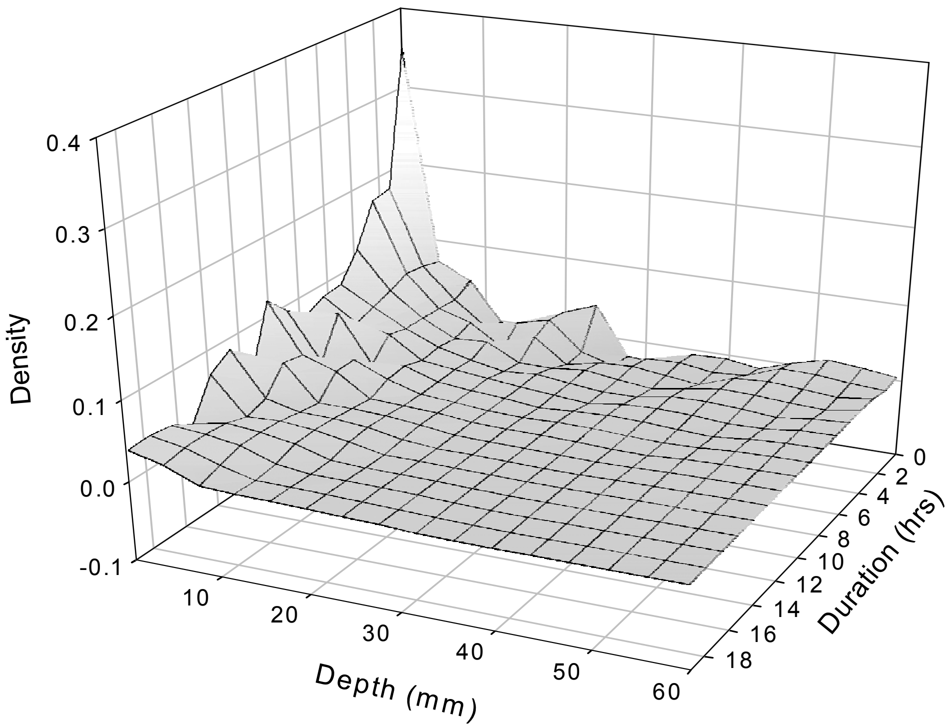

Figure 2-18. Bivariate probability density of simulated warm-season precipitation depth.

The performance of the warm-season precipitation model was examined by comparing the recorded twenty year total warm-season precipitation depth with the simulated twenty year seasonal precipitation depth (Figures 2-19 and 2-20). As shown in the relative frequency histogram, there was a discrepancy in the range values. The range of the actual measured warm-season total precipitation is 219 mm, while the generated precipitation data has a range of 286 mm. In addition, there was a small difference between the mean values of the observed and simulated data. The average observed precipitation amount was 203 mm, where as the average simulated amount was 215 mm. However, the modes in both cases were similar (200-250 mm). Due to short data collection period and best models inadequacy, there was a slight difference between the actual and simulated precipitation amounts, but in general the warm-season precipitation simulation model performed better than that of the cold-season.

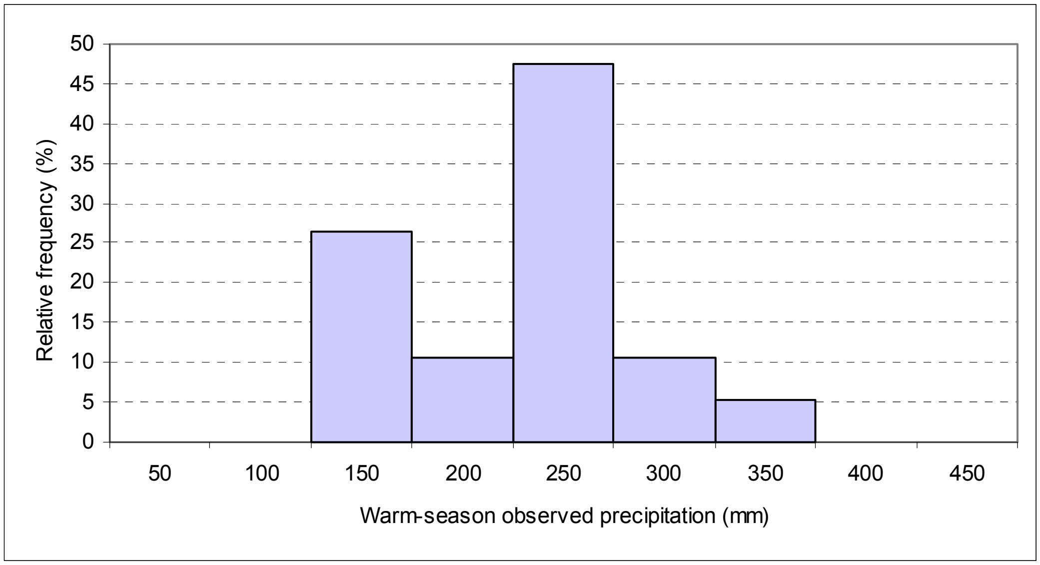

Figure 2-19. Relative frequency of the actual warm-season precipitation. (N = 20 years).

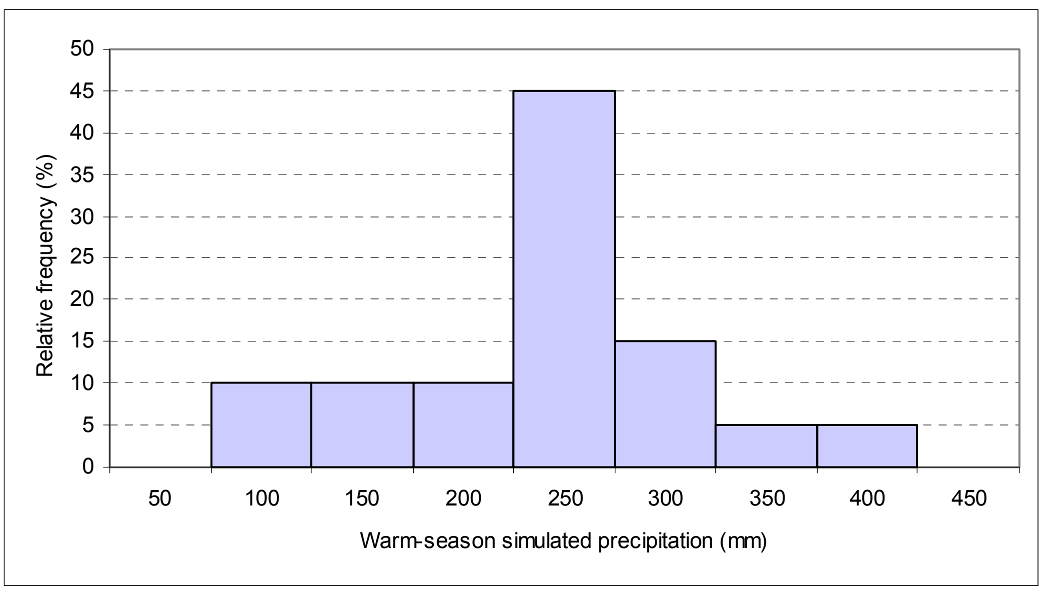

Figure 2-20. Relative frequency of simulated warm-season precipitation. (N = 20 years).

Spatial Analysis of Precipitation

The spatial variability of precipitation in the Bar M watershed was analyzed using a subset of the gauges in the Beaver Creek precipitation gauge network. In selecting gauges we considered all gauges that were operational at the same period of time, as well as being within and nearby the Bar M watershed. However, gauges with elevations much lower than that of the Bar M watershed and located in other forest type were excluded. An additional restriction necessary for the storm duration analysis is gauges to be recording ones.

Twenty out of 89 gauges fulfilled the above criteria and had at least with six years of precipitation data. The depth and duration of all the individual storms used were separately summed over the six year period to obtain a six-year total of storm depth and a six-year total of storm duration. The ratio of the six-year total precipitation depth in gauge i (P_i) to the six-year total depth in gauge #38 (P_{38}) and the ratio the six-year total precipitation duration in gauge i (D_i) to that of gauge (D_{38}) were used as dependent variables, (P_i/P_{38}) and (D_i/D_{38}) respectively. The ratio was used to determine the spatial distribution of precipitation depth and duration across the watershed given any simulated storm depth and duration at gauge #38.

Latitude, longitude, elevation, and aspect were chosen as independent variables in the regression equation. The correlations between (P_i/P_{38}) and (D_i/D_{38}) and any of the four dependent variables were examined to determine the likely candidates for developing a best regression equation. A high correlation coefficient between the predictor variables and the predicted ones indicates a preferred regression equation.

Cold-season Precipitation

The correlation coefficients between the linear regression equations of (P_i/P_{38}) and (D_i/D_{38}) and the four independent variables for cold-season precipitation are shown in Table 2-3.

Table 2-3. Correlation coefficients for precipitation depth and duration for cold-season

Dependent variable	Independent variable			
	Latitude	Longitude	Elevation	Aspect
(P_i/P_{38})	0.748	-0.045	0.183	-0.16
(D_i/D_{38})	0.438	0.106	0.516	-0.142

In addition, Figures 2-21a through 2-21d show the scatter plot and the best fit regression line of each predictor variable versus the ratio of precipitation depth, P_i to P_{38}. Latitude (UTM-Y) seems to have the strongest effect on the distribution of precipitation depth with more northerly precipitation gauges (higher UTM-Y values) receiving more precipitation amount. Elevation and aspect show respectively positively and negatively weak relationships with depth. The correlation between longitude (UTM-X) and precipitation depth is even weaker and negative.

A stepwise forward ranking procedure was applied to select the best predictor among the four variables to create the best fit regression equation for the change in precipitation depth with space. The best fit regression equation was created with UTM-Y but addition of any one of the three variables: UTM-X, elevation, aspect have little or no effect on the regression equation (see equation 2-41). Since the relationship between UTM-Y and the precipitation depth appear nonlinear, a second degree polynomial regression equation represents the relationship better. The non linear model has a value of

r^2 that is eight percent higher than the r^2 for a linear regression representation of the problem. These shows that gauges located on a more northerly position receive large amounts of precipitation. (Figures 2-21b and 2-23).

$$P_i/P_{38} = 2x10^{-13}(\text{UTM-Y})^3 - 2x10^{-6}(\text{UTM-Y})^2 + 7.827(\text{UTM-Y}) - 1x10^7 \qquad (2\text{-}41)$$

$$r^2 = 0.748$$

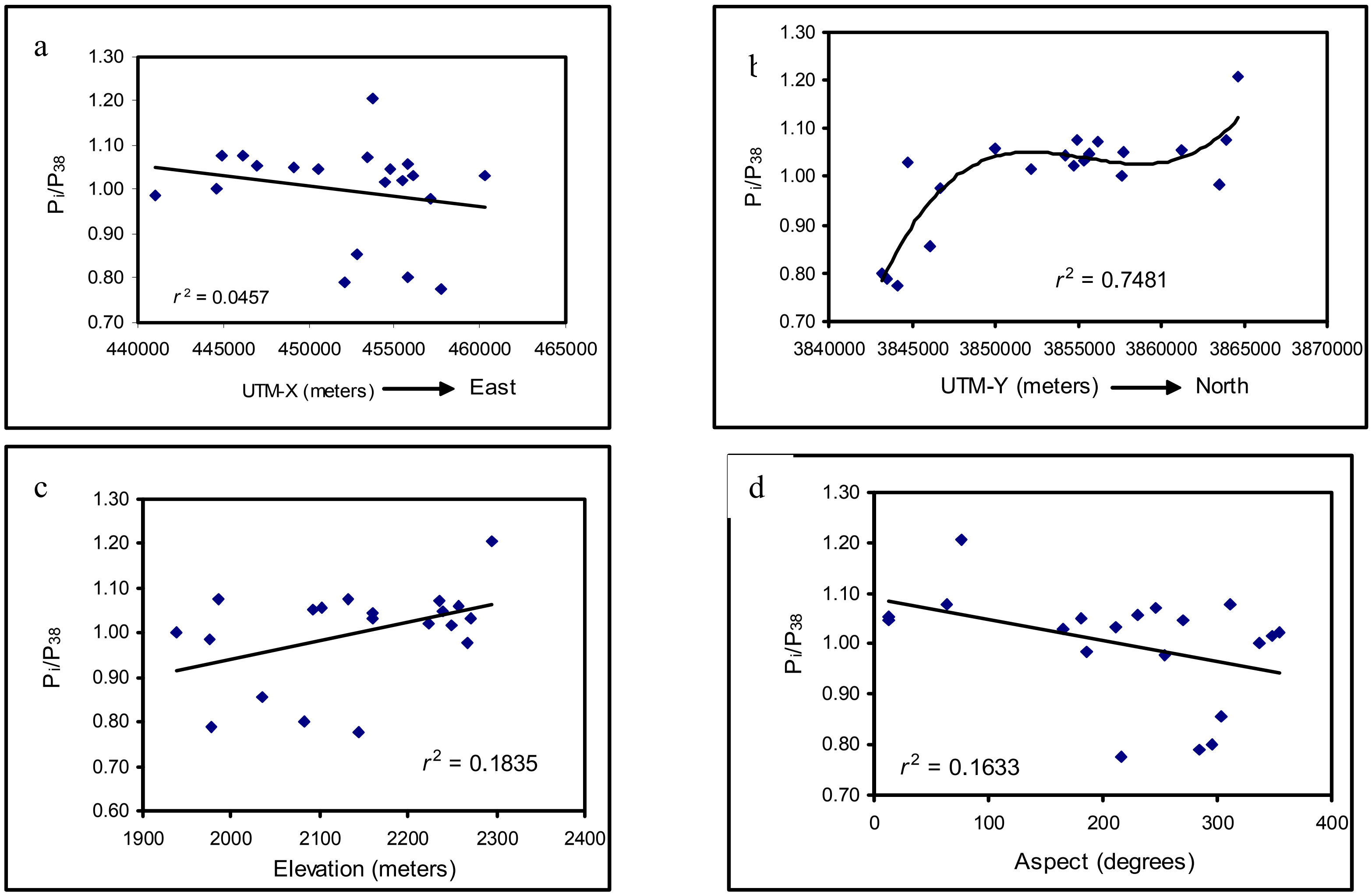

Figures 2-21. Scatter plots of cold-season precipitation depth ratio vs. predictors (a: UTM-X, b: UTM-Y, c: elevation, d: aspect).

The landscape parameters such as longitude and elevation may have little effect on the spatial distribution of precipitation may be due to the relatively small areal extent of the study area. In addition, aspect does not play a large role because the topographic features within and around the study area, such as hills and ridges are not large enough to cause any rain shadow effect. Another reason may be that storms were not analyzed on an individual basis. Instead they were all assumed to come from the same direction, which, though generally the case, is not always true.

As with depth, the spatial distribution of storm duration was analyzed by looking at the effects of each of the spatial variables (latitude, longitude, elevation and aspect) on the response function (duration) using a linear regression. The r^2 values of the regression equations of duration versus each spatial variable and their respective scatter plot are shown in Table 2-3 and Figures 2-22a through 2-22d. The highest correlation coefficients are between duration and elevation, and duration and latitude. These means gauges located at higher elevation and on a more northerly position receive precipitation that last longer (Figures 2-22b, 2-22c, and 2-24). Hence, the best fit regression model includes elevation and latitude and has the form shown in equation 2-42.

$$D_i/D_{38} = 3.148 \times 10^{-4}(\mathrm{ELEV}) + 3.3 \times 10^{-6}(\mathrm{UTM\text{-}Y}) - 12.37 \qquad (2\text{-}42)$$

$$r^2 = 0.66$$

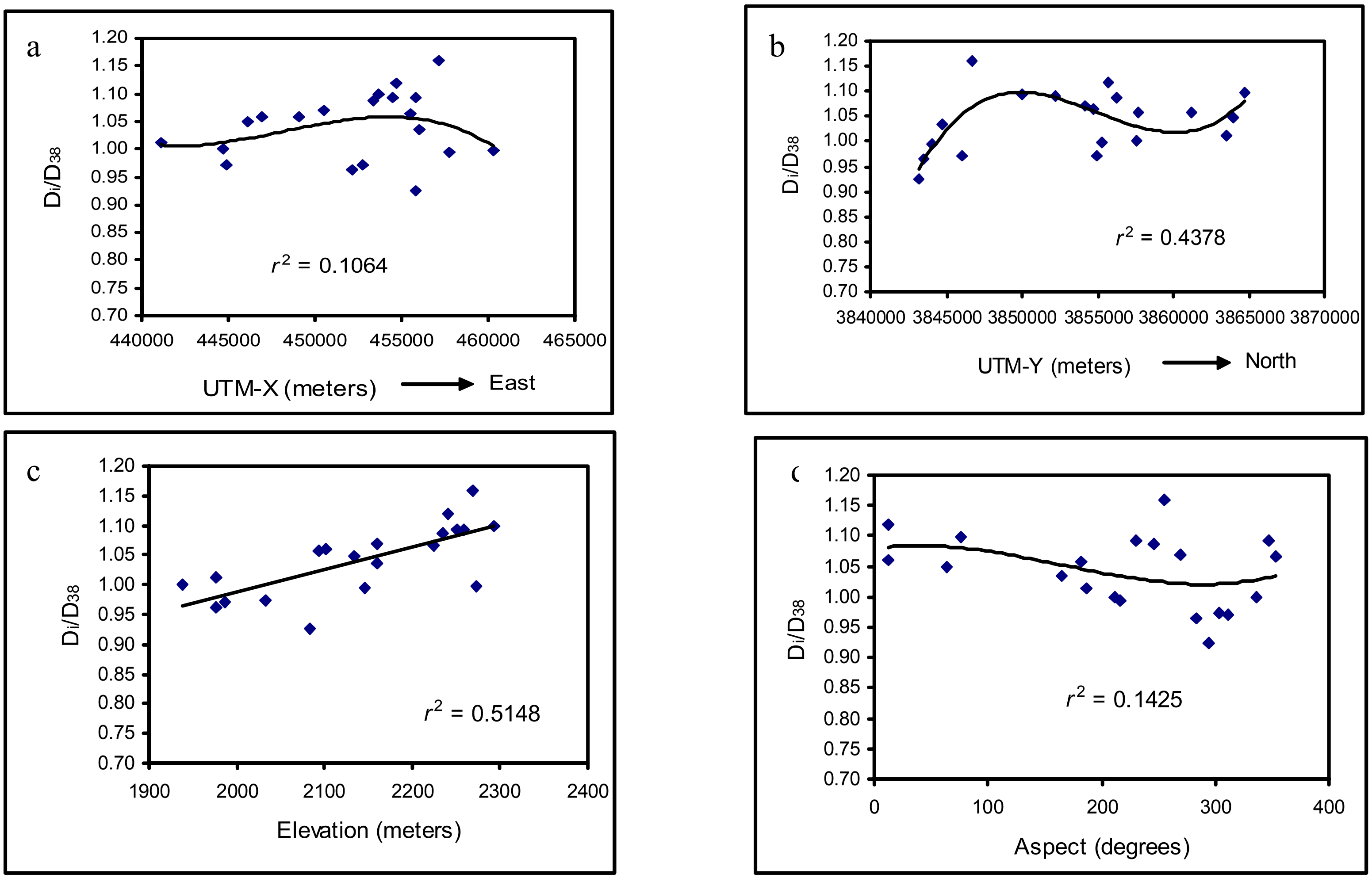

Figures 2-22. Scatter plot of cold-season precipitation duration ratio vs. predictors (a: UTM-X, b: UTM-Y, c: elevation, d: aspect).

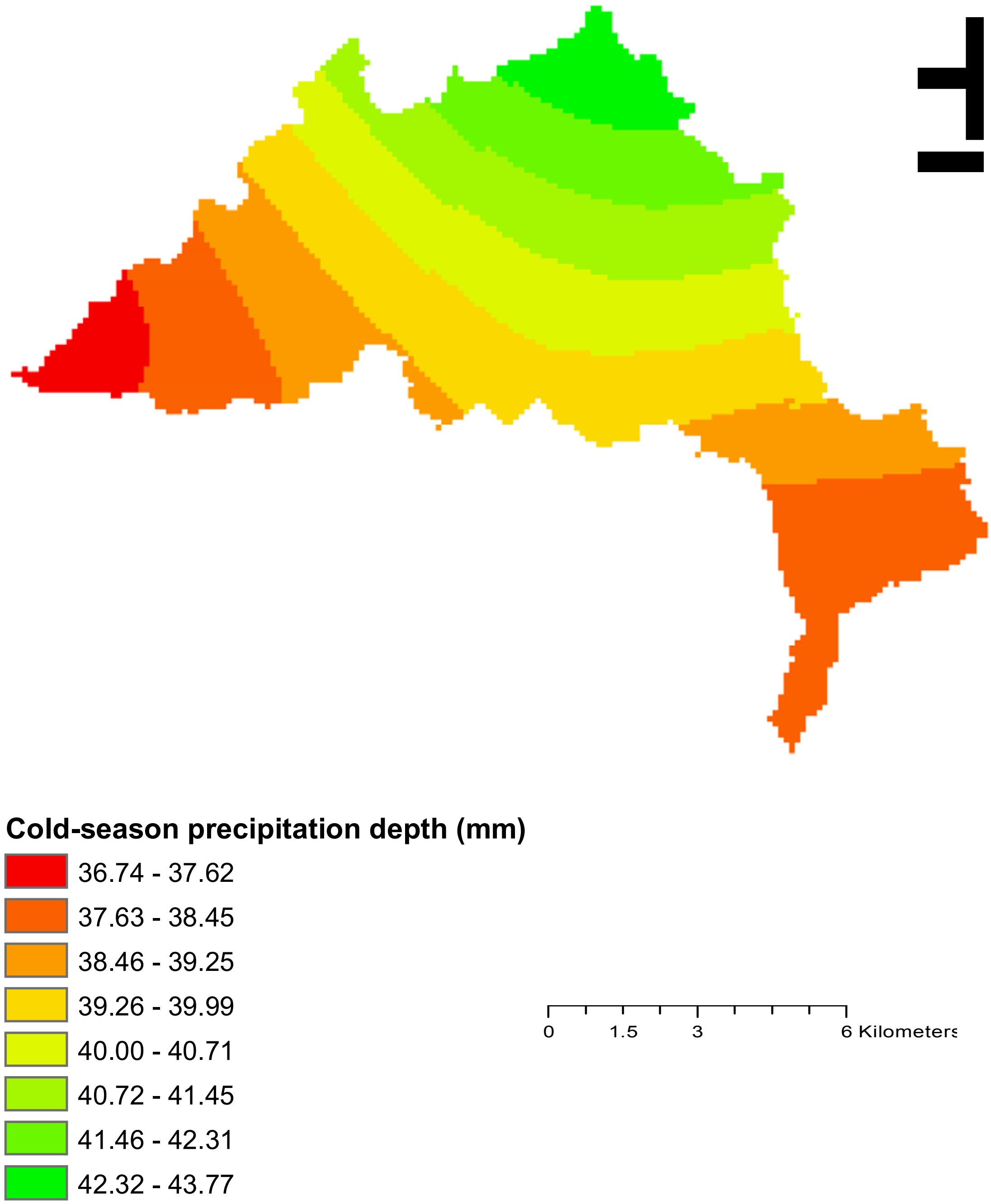

Figure 2-23. A simulated spatial distribution of a sample cold-season precipitation depth.

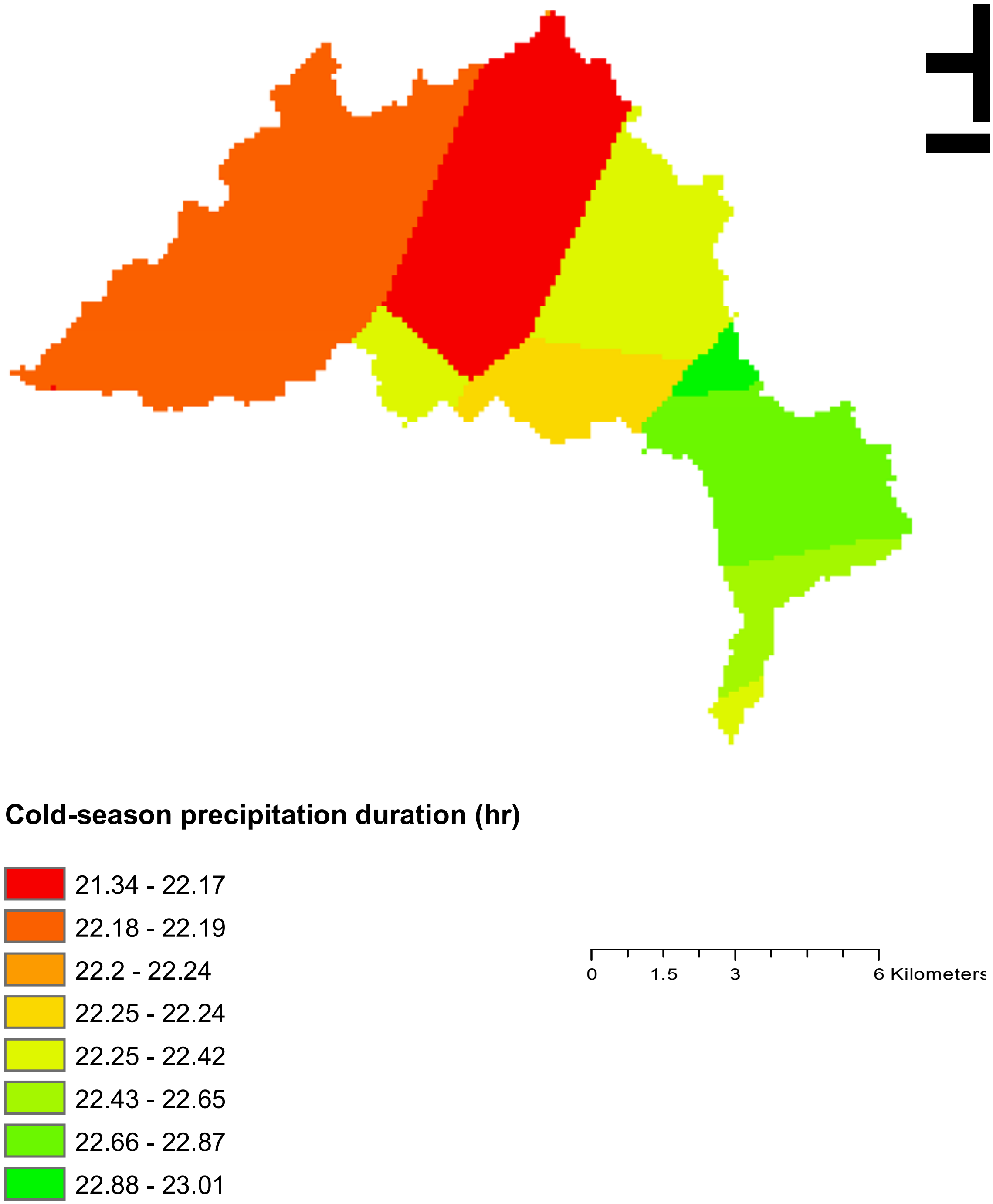

Figure 2-24. A simulated spatial distribution of sample cold-season precipitation duration.

Warm-season Precipitation

As for the cold-season precipitation depths and durations the spatial distribution of warm-season precipitation depths and durations are described in terms of the four independent spatial variables of latitude, longitude, elevation, and aspect. The correlation coefficients between the linear regression of precipitation storm depth ratio (P_i/P_{38}) and storm duration ratio (D_i/D_{38}) in any location *i* with respect to the four independent landscape variables are shown in Table 2-4.

Table 2-4. Correlation coefficients between warm-season precipitation depth and duration and the four spatial variables.

Dependent	Independent variables			
variables	Latitude	Longitude	Elevation	Aspect
(P_i/P_{38})	-0.32	0.57	0.297	0.092
(D_i/D_{38})	-0.11	0.51	0.46	-0.0002

Figures 2-26a through 2-26d show the scatter plots and the best fit regression lines of each spatial variable versus the precipitation depth ratio. The correlation coefficients between the precipitation ratio and the variables, longitude (UTM-X), latitude (UTM-Y), and elevation were significant at the 5% level, while that between the variable, aspect and the precipitation depth ratio was weak. More northerly and easterly precipitation gauges and those located at higher elevations received larger amounts of precipitation.

A stepwise forward ranking procedure was applied to select the best predictor from among the four variables to create the best fit regression equation starting with the variable that has the highest correlation coefficient, in this case, is longitude. The best regression equation was created with UTM-X, UTM-Y and elevation and addition of aspect did not improve the r^2 value of the regression equation (equation 2-43). This indicates that gauges located in the southeast and at higher elevation, more southerly, and more easterly position receive higher amount of precipitation (Figures 2-25a, 2-25b, and 2-27).

$$P_i/P_{38} = 1.04\text{x}10^{-7}(\text{UTM-X}) - 4\text{x}10^{-6}(\text{UTM-Y}) + 3.77\text{x}10^{-4}(\text{ELEV}) + 16.88 \qquad (2\text{-}43)$$

$$r^2 = 0.45$$

In the case of summer precipitation duration, there was a better relationship between duration and the variables longitude and elevation. Hence, gauges located at higher elevation and on a more easterly location received precipitation of longer duration (Figures 2-26a, 2-26c, and 2-28)

For this reason, the best regression model includes longitude and elevation and has the form

$$D_i/D_{38} = 1.19\text{x}10^{-5}(\text{UTM-X}) + 2.68\text{x}10^{-4}(\text{ELEV}) - 4.79 \qquad (2\text{-}44)$$

$$r^2 = 0.55$$

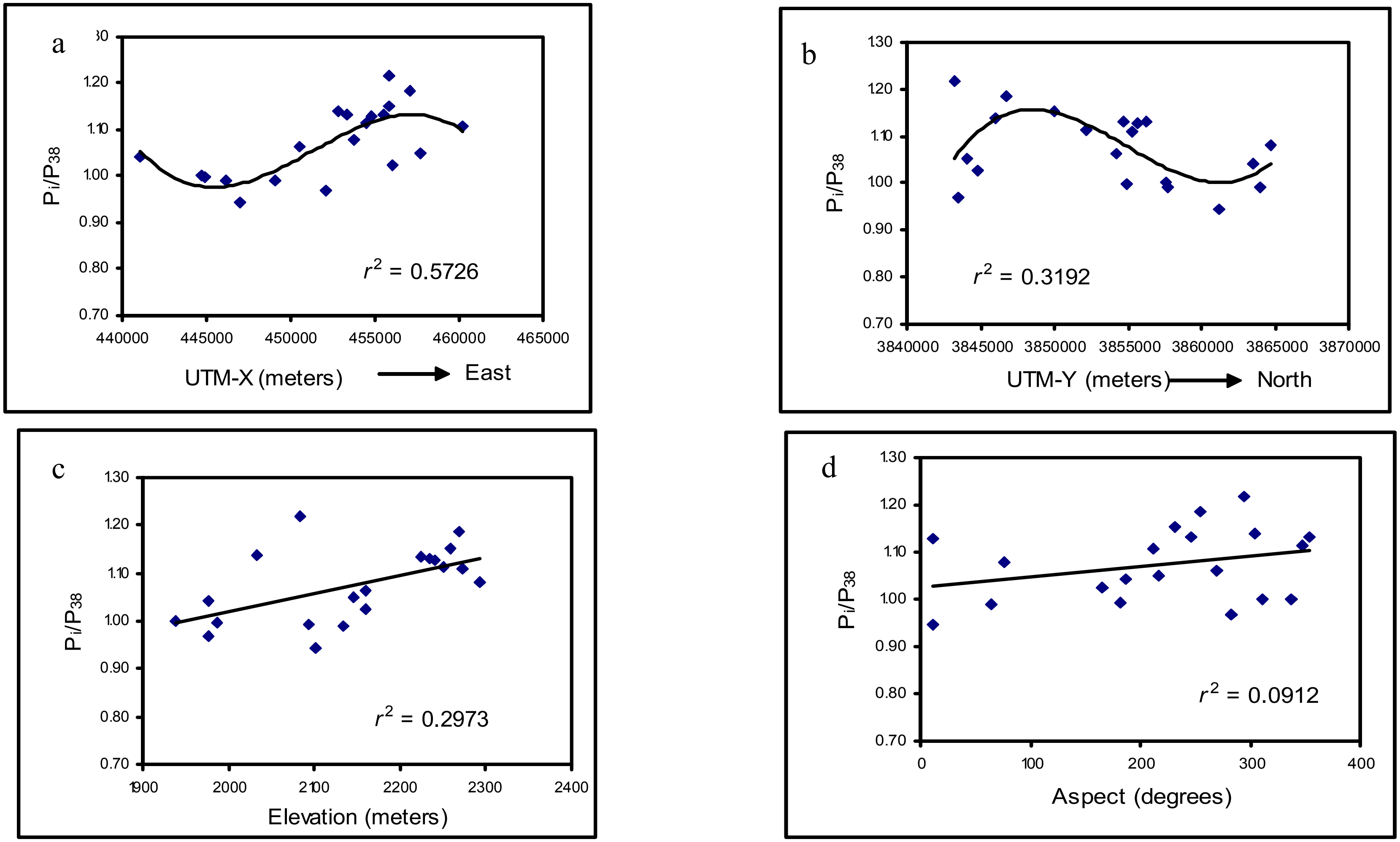

Figures 2-25. Scatter plots of warm-season precipitation depth ratio vs. predictors (a: UTM-X, b: UTM-Y, c: elevation, d: aspect).

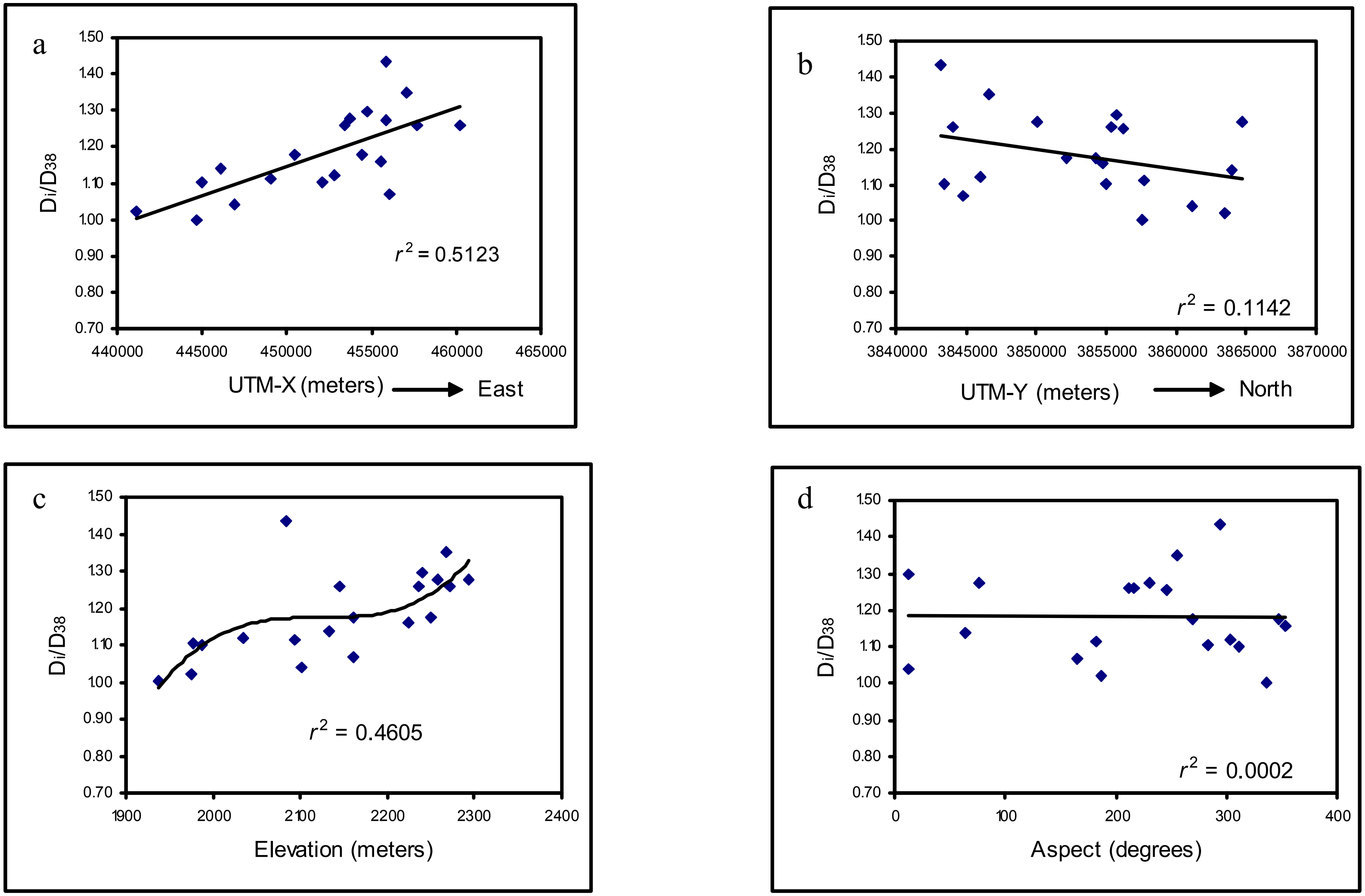

Figures 2-26. Scatter plots of warm-season precipitation duration ratio vs. predictors (a: UTM-X, b: UTM-Y, c: elevation, d: aspect).

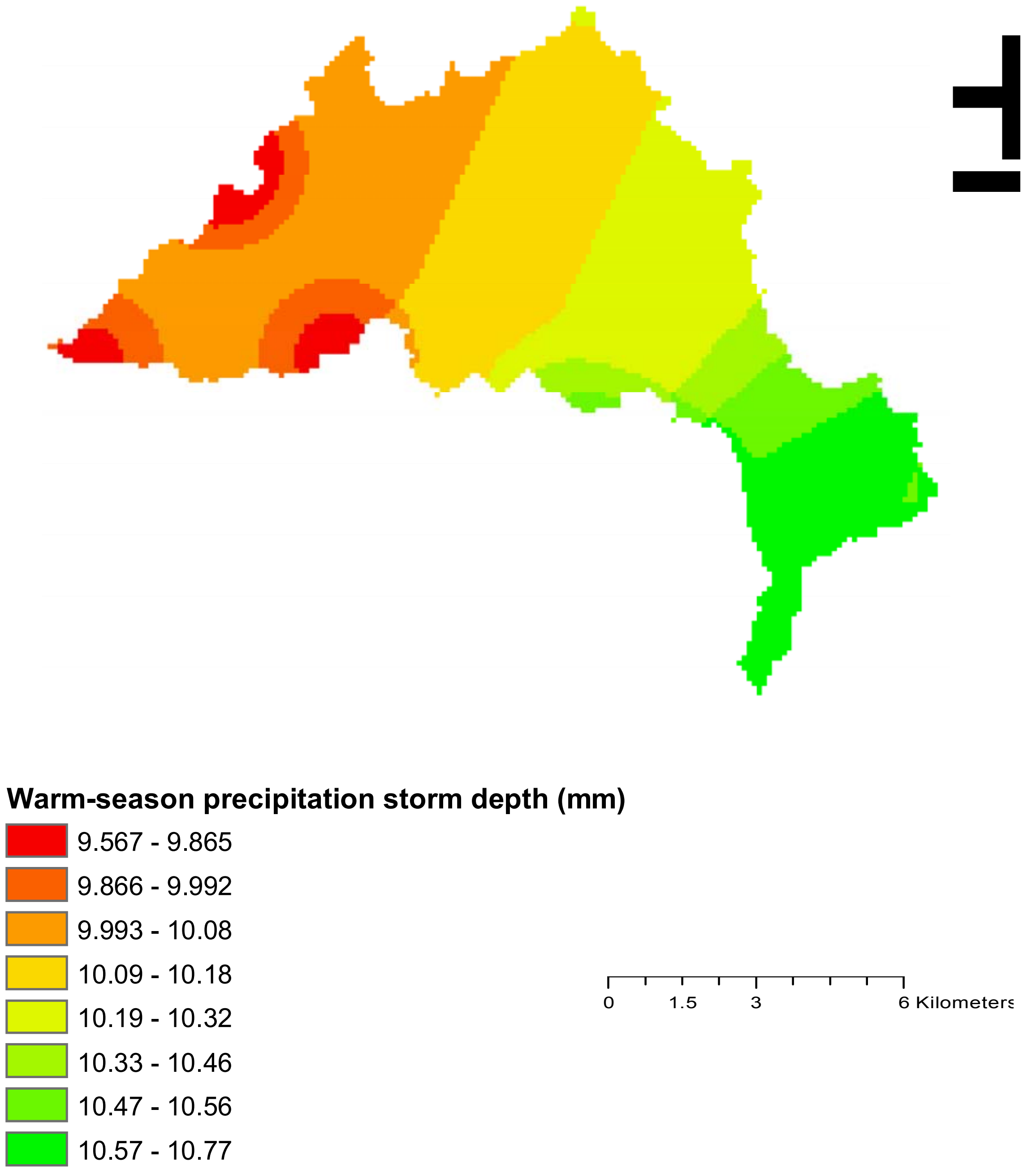

Figure 2-27. A simulated spatial distribution of a sample warm-season precipitation storm depth

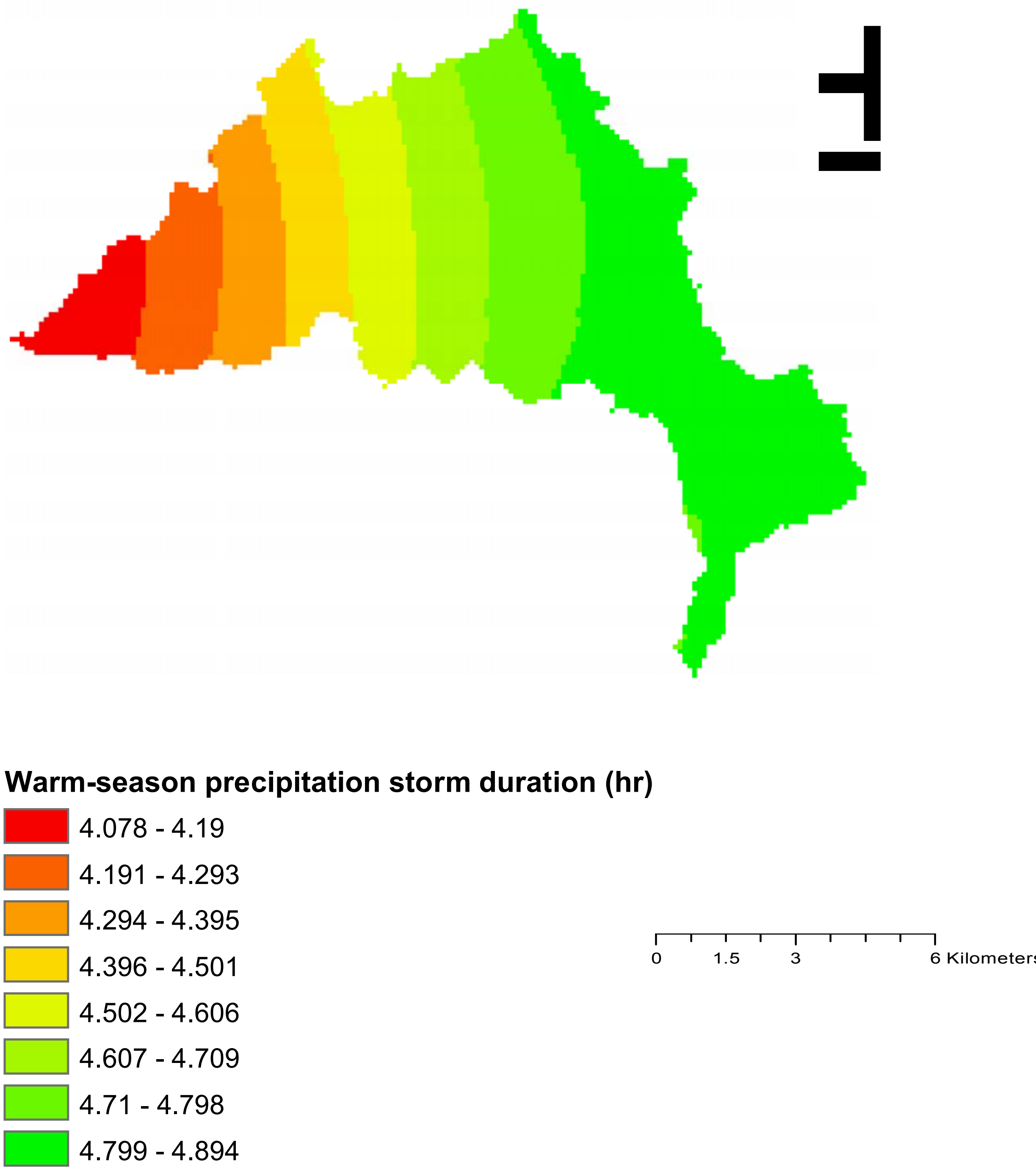

Figure 2-28. A simulated spatial distribution of sample warm-season precipitation storm duration

Analysis of Temperature

Analyzing the temperature of the study area is important for a number of reasons. It helps to determine the type of precipitation during the cold-season, and it is one of the main factors contributing to evapotranspiration, snowmelt, and sublimation. Usually daily temeratures vary with the number of days of the year. Hence, temperature equations are developed for wet and dry days usng the lag-one Markov model.

Cold-Season Temperature

Cold-season season daily maximum temperatures for dry and wet days are described using parabolic functions. This is done by regressing temperature against day of the year to determine the equation that best fit the data. In constructing the regression equations, October 1st was set as day 1and April 30th, the end of the winter season, as day 212. The regression equation for the maximum temperature during a dry day with respect to the sequential number of day from the beginning is

$$T_{dry} = 23.391 - 0.278(DAY) + 0.0012(DAY)^2 \qquad (2\text{-}45)$$

$$r^2 = 0.89$$

Where T_{dry} (^{o}C) is the predicted daily maximum temperature in a dry (or non rainy) day and DAY is the number of days since the beginning of the cold-season. The root mean square error (RMSE) of the regression equation is 1.48, the value of its r^2 is 0.89, and it is significant with *p*-value of less than 0.0001. Similarly, the regression equation for the maximum temperature during a wet day in terms of the day number from the beginning of the cold-season is

$$T_{wet} = 15.846 - 0.217(DAY) + 0.0009(DAY)^2 \quad (2\text{-}46)$$

$$r^2 = 0.48$$

Where T_{wet} (^{o} C) is the predicted daily maximum temperature in a wet day. The RMSE for the regression is 3.468, while its r^2 value is 0.48, and, similar to that of maximum temperature, the equation is significant at the 0.0001 level. The twenty years average maximum daily temperatures for both dry and wet days and their best fit to parabolic functions are shown in Figure 2-29.

We also developed equations to express the diurnal variation of temperatures for dry and wet days. As shown in Figure 2-30, the same procedure as with the maximum temperature is used to show the trends of the average diurnal temperature variations. Equation 2-47 is a parabolic expression that best represents the diurnal temperature variation in dry days.

$$DV_{dry} = 21.84 - 0.0711(DAY) + 0.0003(DAY)^2 \quad (2\text{-}47)$$

$$r^2=0.41$$

where DV_{dry} (^{o} C) is the predicted diurnal variation in temperature during dry days.

The RMSE of the regression for the diurnal temperature variation is 1.33, its r^2 value is 0.41 and is significant at the 0.0001 level.

For the wet days data the best fit regression equation for the diurnal temperature variation with respect to days since the beginning of the winter season is:

$$DV_{wet} = 16.22 - 0.0977(DAY) + 0.0005(DAY)^2 \tag{2-48}$$

$$r^2=0.42$$

where DV_{wet} (^{o}C) is the diurnal variation in temperature when precipitation occurs. The RMSE for such data is 2.1 and the equation has an r^2 value of 0.4 with significant level of 0.0001.

Simulation of the daily maximum temperatures for consecutive dry and wet days was done using the Markov equations of (2-25) and (2-26), respectively. These equations require determining the lag-one autocorrelation coefficients for each day type. The autocorrelation coefficients for both dry and wet days are found to be high: 0.839 and 0.892 respectively. This indicates that daily maximum temperatures do not vary greatly from one day to the next day.

Similarly, simulation of the daily minimum temperature using the Markov equations of (2-33) and (2-34) needs the use of the lag-one autocorrelation coefficients for diurnal temperature variation for both consecutive dry and wet days, respectively. The autocorrelation coefficient for consecutive dry days equals 0.456, while that for consecutive wet days is equal to 0.281. Then, the simulated maximum and minimum temperature for cold-season were used to determine the form of the precipitation falling in the wet days. Eventually, the simulated results are used to determine the average day time and night time temperatures used to calculate the various output components of the water balance in the next chapter.

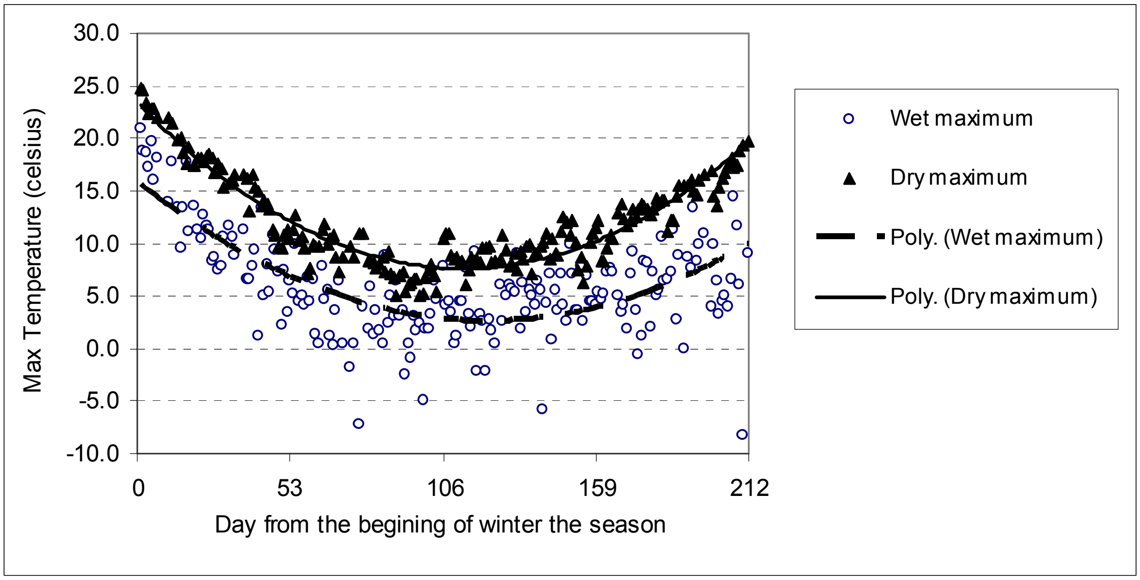

Figure 2-29. Graph of average cold-season daily maximum temperatures for dry and wet days fit the second degree parabolic functions.

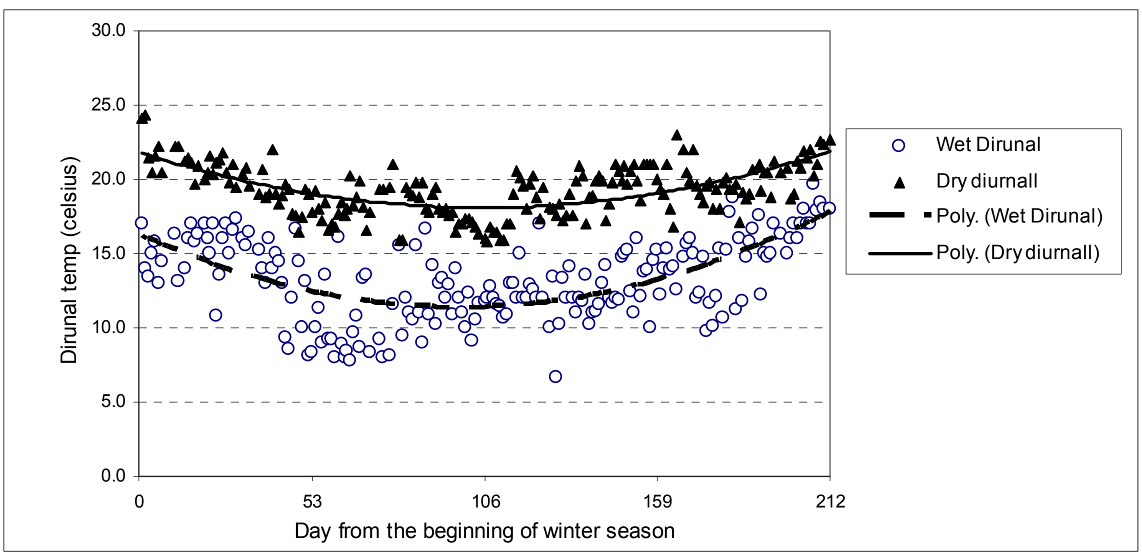

Figure 2-30. Graph of average cold-season diurnal temperature variations for dry and wet days fit the second degree parabolic functions.

Warm-Season Temperature

Warm-season daily maximum temperature data for days when there was no precipitation (dry days) and for those with precipitation (wet days) were described using parabolic functions. Maximum temperatures were also regressed with respect to day of year to determine the equation that best fit the data. In constructing the regression equation, May 1st as set as day 1and September 30th as day 153, the last day of the summer season.

The regression equation for dry days maximum temperature with respect to the number of warm-season day count (DAY) is

$$T_{dry} = 17.648 + 0.2899(DAY) - 0.0017(DAY)^2 \quad (2\text{-}49)$$

$$r^2 = 0.91$$

Where T_{dry} (^{o} C) is the predicted daily maximum temperature for days with no rain and DAY is the number of days since the beginning of the warm season.

The RMSE of the regression equation is 1.01, it has an r^2 value of 0.91, and is significant with *p*-value less than 0.0001. Similarly, the regression equation for the wet days maximum temperature with respect the number of day count from the beginning of the warm season is

$$T_{wet} = 10.071 + 0.4005(DAY) - 0.0022(DAY)^2 \quad (2\text{-}50)$$

$$r^2 = 0.69$$

where T_{wet} (^{o} C) is the predicted daily maximum temperature in the presence of rain.

The RMSE for the regression equation is 3.12, while its r^2 value is 0.69 and it is significant at the 0.0001 level. Figure 2-31 shows the scatter plots of the twenty years of maximum average daily temperatures for both dry and wet days and their best fit parabolic curves.

In the case of warm-season diurnal variation in temperature, a third degree parabolic function is fitted to the twenty year data (see Figure 2-32). For dry-days data, the best fit regression equation for diurnal temperature variation with respect to the number of days since the beginning of the summer season is

$$DV_{dry} = 20.043 + 0.242(DAY) - 0.0041(DAY)^2 - 0.00002(DAY)^3 \qquad (2\text{-}51)$$

$$r^2 = 0.62$$

Where DV_{dry} (^{o} C) is the predicted diurnal variation in temperature during dry days. The RMSE for the regression equation is 1.27, while its r^2 value is 0.62 and it is significant at the 0.0001 level. For wet days the best-fit equation is

$$DV_{wet} = 17.849 + 0.1282(DAY) - 0.0027(DAY)^2 + 0.00001(DAY)^3 \qquad (2\text{-}52)$$

$$r^2 = 0.39$$

where DV_{wet} (^{o}C) is the diurnal variation in temperature during wet days. The RMSE of the equation is 1.45 and has an r^2 value of 0.39 with 0.0001 significance level.

The autocorrelation coefficient of maximum daily temperatures for consecutive dry days is 0.96, while that for consecutive wet days is 0.735. In the case of diurnal temperature variations, the autocorrelation coefficients for consecutive dry and wet days are respectively, 0.85 and 0.27. The diurnal temperature variations for dry and wet days are simulated using the Markov equations of 2-25, 2-26, 2-31 and 2-32 respectively. In the warm season, precipitation comes in the form of rain, so the simulated maximum and minimum temperatures are used to determine the average daily temperatures during day and night times when calculating the various water balance output components described in the next chapter.

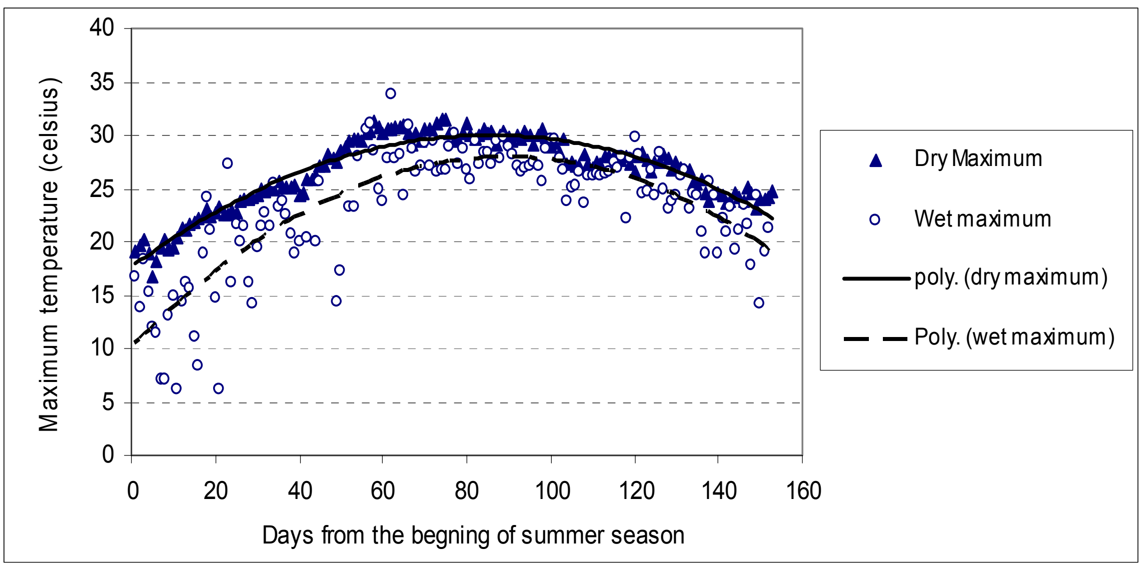

Figure 2-31. Graph of average warm-season maximum temperatures for dry and wet days fitted with second degree parabolic functions.

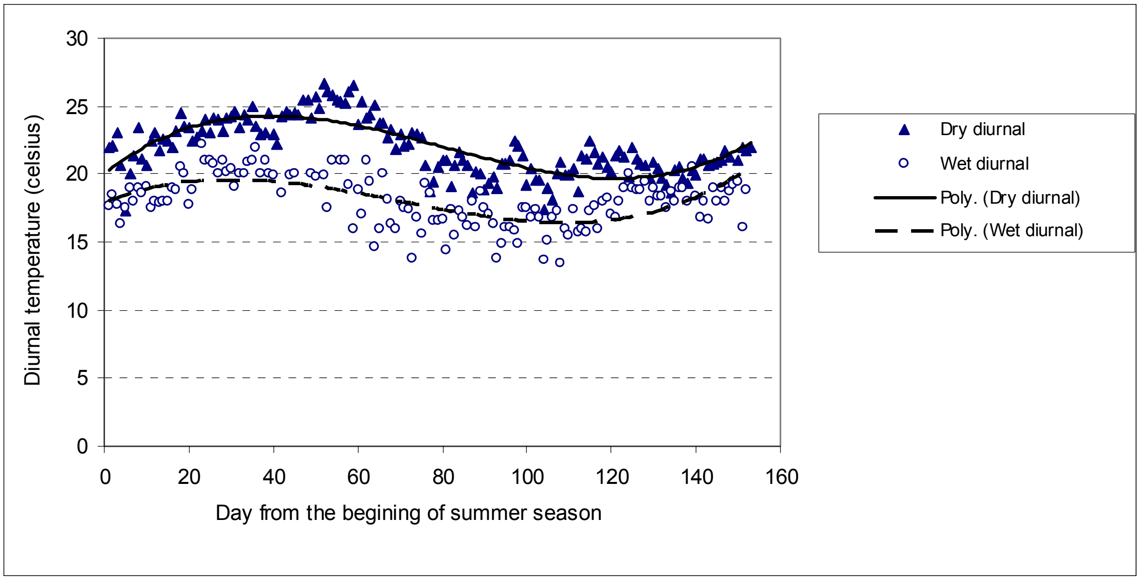

Figure 2-32. Graph of average warm-season diurnal temperatures variation for dry and wet days fitted with three degree parabolic functions

Summary and Conclusions

A stochastic, event based approach is used to describe and simulate the temporal distribution of both cold and warm-seasons precipitation events in a particular ponderosa pine watershed in north-central Arizona. In addition, the spatial distribution of precipitation in the watershed is described in terms of various landscape variables such as latitude, longitude, elevation and aspect and displayed in a map form using GIS. Simulated variations in the daily temperature are used to determine the form of precipitation, snow, rain or mixed in the cold season, and to calculate the various output components of the water balance model in the next chapter. Daily maximum and minimum temperatures are also described as stochastic processes and simulated using lag-one Marko Model.

The nature, type and causes of precipitation during cold and warm seasons in the study area are different. Cold-season precipitation often comes in the form of snow resulting from frontal storms that move into the region from the Pacific Northwest. These storms have durations of more than one day with separate storms often being related to each other by large-scale weather patterns. In contrast, warm-season storms are convective storms that are highly-localized, often intensive and short lived rains coming from the Gulf of Mexico. Because of the nature of precipitation in the two seasons, different models are employed to describe the seasonal precipitation characteristics. Five variables are used to describe cold-season precipitation characteristics. They are time between sequences, number of events per sequence, event depth, event duration, and inter-arrival time between events. However, only the last three variables: event depth, event duration, and inter-arrival time between events are used to describe the summer precipitation characteristics.

In the case of cold-season precipitation, events having an inter-arrival time less than 3.5 days are grouped into sequences. The assumption behind this grouping of events is that those events that occur close together in time are not independent events, while those arriving apart are assumed to be independent. Therefore the time between events and the time between sequences are modeled independently. The time between sequences is described using a gamma probability distribution function while time between events is described using Weibull probability distribution function. The Weibull probability distribution function is also found to best describe number of precipitation events per sequence. The same model, weibull, fit the time between events of warm-season.

Simulating precipitation event depth and duration requires knowledge of a joint probability density function for the two characteristics due to their dependency on each other. The method first requires describing each one of them using a univariate probability distribution function, which in this case, is the gamma distribution function. The second step is to describe the conditional distribution of depth given duration. In this study, the conditional *pdf* for depth given duration was also determined to be the gamma distribution function with shape and scale parameters that vary with event duration. The same method is used to describe and simulate the warm-season event depth and duration.

An analysis of daily temperature versus days since the beginning of the cold and warm-seasons indicates that both seasons can be described by fitting the parabolic functions to the data. However, the analysis reveals the existence of too much variability in the daily changes in temperature to describe them sufficiently using a single function.

Therefore, the variability of daily temperature is also modeled in addition to the daily trend. The variation in temperature from the parabolic regression curve is simulated using a random-number generator to produce values for deviation from the regression curve, assuming a normal distribution for the error of the regression. In addition, the tendency for temperature to show persistence from one day to the next is described using a lag-one Markov process.

Though the temporal precipitation model performs well, there are several drawbacks that need further study. Two of these drawbacks are related to the fitness quality of the theoretical distribution functions to the observed data. In the cold-season precipitation model, only the time between sequences satisfied all the goodness-of-fitness test criteria. The other variables that describe the cold-season precipitation events as well as the warm-season precipitation events did not find probability distribution functions that fit well. This may be because of limited amount precipitation data, in this case, twenty years of data, which may not be adequate to describe the distributions of the variables with the selected theoretical distribution functions. The second problem may be that the model describing cold-season precipitation events over-estimates the number of short duration and low depth storms. The effect of this problem, however, may eventually be small because though these small storms make up the majority of events, their contribution to the total water yield is usually little. But situation with the warm-season precipitation model is different, the model seems over-estimate the average total seasonal precipitation amount which result in increased total warm-season water yield.

Another problem may come from the difference in time-scales between the precipitation generator and the temperature data used. Precipitation is described in minutes of time resolution, while temperature is simulated on a daily basis. A procedure can be developed in the future to describe all related variables with the same time resolution. This would help to simulate possible changes in the forms of precipitation events within a day, such as having snow in the morning and rain in the afternoon. In addition, reading temperature continuously throughout the day would be useful to better estimate the other hydrologic processes, such as evaporation and transpiration.

The spatial analysis of precipitation shows that the variations in the cold and warm-seasons precipitation depths and durations in the study can be partially explained by latitude, longitude, elevation, and aspect, though the effects of each variable is different from the other. A regression analysis results in a prediction equation that can estimate the spatial distribution of storm depth given latitude (in UTM coordinates) for cold-season with an r^2 value of 0.65. Also a linear regression has been developed to predict cold-season precipitation duration with respect to longitude and elevation and having the same r^2 value of 0.66. In the warm-season, elevation, latitude, and longitude seem to have more influence on the spatial distribution of depth and duration than the other variables. The r^2 values of the prediction equations for the warm-season precipitation event depth and duration are 0.45 and 0.55 respectively. The smaller r^2 values in both cold and warm-season precipitation distributions indicate that a significant portion of the spatial variability of precipitation depth and duration is left unexplained. Perhaps an analysis of individual storms may provide more information regarding the spatial distribution of precipitation events across the watershed.

There are many factors that may influence the spatial variability of precipitation event depth and duration. As a result, care must be taken when applying the findings of the spatial analysis to areas outside the study watershed. The Mogollon Rim is the dominant landscape feature that affects the spatial distribution of precipitation events in the area. The factors controlling the areal distribution of precipitation on watersheds along the Mogollon Rim will be different from those on the Bar M watershed.

Overall the cold and warm-seasons precipitation event models presented in this study are useful tools for describing the seasonal precipitation patterns that occurs over a mountainous forest system. In addition to this, it provides precipitation and temperature inputs to the water balance model for use in estimating water yield from upland ponderosa pine forest watersheds.

Literature Cited

Bacchi, B., G. Becciu, and N.T. Kottegoda, 1994. Bivariate exponential model applied to intensity and durations of extreme rainfall, Journal of Hydrology, 144, pp. 225-236

Baker, M.B. Jr., 1982. Hydrologic regimes of forested areas in the Beaver Creek watershed. USDA Forest Service, General Technical Report RM-90.

Baker, M.B. Jr., and Harry. E. Brown, 1974. Multiple use evaluations on ponderosa pine forest land, 18 Annual Arizona Watershed Symposium Proceedings, Phoenix, Arizona, September 25.

Baker, M.B. Jr., and P.F. Ffolliott, 1999. Interdisciplinary land use along the Mogollon Rim, Chapter 5. In: Baker, M.B. Jr., compiler, History of watershed research in the central Arizona highlands. USDA Forest Service, Research paper RMRS-GTR-29. pp. 27-33.

Barndorff-Nielsen, O.E., V.K. Gupta, V.Perez-Abreu, and E.Waymire, 1996. Stochastic method in hydrology, Rain landforms and flood Vol 7, Guanajuato, Mexico.

Barros, A.P., and D.P. Lettenmaier, 1994. Dynamic modeling of orographically induced precipitation, Review of Geophysics, American Geophysical Union 32 (3), pp. 265-284.

Beschta, R.L., 1976. Climatology of the ponderosa pine type in central Arizona. Technical Bulletin 228, College of Agriculture, Agricultural Experiment Station, The University of Arizona, Tucson, Arizona.

Bogardi, J.J., L. Duckstein, and O.H. Rumambo, 1988. Practical generation of synthetic rainfall event time series in a semi-arid climatic zone. Journal of Hydrology, 103, pp. 357-373.

Brath, A., A. Montanari, and E. Toth, 2004. Analysis of the effects of different scenarios of historical data availability on the calibration of a spatially-distributed hydrological model. Journal of Hydrology, 291(3), pp. 232-253.

Brook, N. K., P.F. Folliott, H. M. Gregersen, and J. L. Thames, 1991. Hydrology and the management of watershed. Iowa State University press, Iowa.

Brown, H.E., M.B. Baker. Jr., J.J. Rogers, W.P.Clary, J.L. Kovener, F.R. Larson, C.C. Avery, and R.E. Campbell, 1974. Opportunities for increasing water yields and other water yields and other multiple use values on ponderosa pine forest lands USDA Forest Service, Research Paper RM-129.

Campell, R.E., and M.G. Ryan, 1982. Precipitation and temperature characteristics of forested watersheds in central Arizona, USDA Forest Service General Technical Report RM-93, Rocky Mountain Forest and Range Experimental Station, Fort Collins, Colorado.

Cherian, K.C., 1941. A bivariate correlated gamma-type distribution function, Journal of the Indian Mathimatical society, 5, pp. 133-144.

Court, A., 1961. Area-depth rainfall formulas, Journal of Geophysics Research, 66, pp. 1823-1831.

Covington, W.W., D.B. Wood, D.L. Young, D.P. Dykstra, and L.D. Garrett, 1988. TEAMS: A decision support system for multiresource management. Journal of Forestry, 86(8), pp. 25-33.

Dingman, S.L, 1994. Physical Hydrology, Macmillan College Publishing Company, New York.

Duckstein, L., M.M. Fogel, and C. Kisiel, 1972. A stochastic model of runoff-producing rainfall for summer type storms, Water Resource Research, 8(2), pp. 410-421.

Duckstein, L., M.M. Fogel, and J.L. Thames, 1973. Elevation effects on rainfall: a stochastic model. Journal of Hydrology 18 pp. 21-35.

Duckstein, L., M.M. Fogel, and D.R. Davis, 1975. Mountainous winter precipitation: a stochastic event-based approach, in proceedings of the National Symposium on Precipitation Analysis for Hydrologic Modeling, America Geophysical Union, pp. 172-188.

Eagleson, P.S. 1972. Dynamics of flood frequency, Water Resources Research, (8) 4.

Etoh, T., and A. Murota, 1986. Probabilistic model of rainfall of a single storm, Journal of Hydroscience and Hydraulic Engineering, 4, pp. 65-77.

Fiering, M.B., and B.B. Jackson, 1971. Synthetic Stream flows, Water Resources Monography Series 1, American Geophysical Union, Washington D. C.

Fogel, M.M, and L. Duckstein, 1969. Point rainfall frequency in convective storms, Water Resources Research (5) 6, pp. 1229-1237.

Fogel, M.M, and L. Duckstein, 1981. Stochastic precipitation modeling for evaluation non-point source pollution. Proceeding of the International Symposium on Rainfall-runoff Modeling, Mississippi State University, Mississippi State, Mississippi, USA.

Fogel, M.M., L. Duckstein, and C.C. Kisiel, 1971. Space-time validation of a thunderstorm rainfall model, Water Resources Bulletin (7) 2 pp. 309-315.

Fox, K.M., P.F. Ffolliott, M.B.Baker, Jr., and L.F. DeBano, 2000. A history of the Arizona watershed program and the Arizona water resources committee, Phoenix, AZ: Prime publisher.

Grayman, W.M. and Eagleson, P., 1969. Stream flow record lengths for modeling catchment dynamics, Hydrodynamic Laboratory Report no. 114, Department of Civil Engineering, Massachusetts Institute of Technology, Cambridge, Massachusetts.

Gumbel, E.J., 1960. Bivariate exponential distributions, Journal of the American Statistical Association, 55 pp. 698-707.

Hanes, W.T., M.M. Fogel, and L. Duckstein, 1977. Forecasting snowmelt runoff probabilistic model, Journal of Irrigation and Drainage Division, 103(IR3), pp. 345-355.

Hibbert, A.R., 1979. Managing vegetation to increase flow in the Colorado River Basin. USDA Forest Service General Technical Report, RM-66, pp. 27.

Kokkonen, S.T., and A.J. Jakeman, 2001. A comparison of metric and conceptual approaches in rainfall-runoff modeling and its implications. Water Resource Research, 37 (9), pp. 2345-2352.

Kottas, J.F., and H.S. Lau, 1978. On handling dependent random variables in risk analysis, Journal of the Operational Research Society, 29, pp.1209-1217

Law, A.M., and W.D. Kelton, 1982. Simulation modeling and analysis, McGraw-Hill, Inc., New York.

Leaf, C.F., and G.E. Brink, 1973. Computer simulation of snow melt within a Colorado subalpine watershed, USDA Forest Service Research Paper RM-

99, Rocky Mountain Forest and Range Experiment Station, Fort Collins, Colorado.
Loukas, A., and M.C. Quick, 1996. Spatial and temporal distribution of storm precipitation in southwestern British Columbia, Journal of Hydrology, 174(2), pp. 37-56.
Marquinez, J., J. Lastra, and P. Garcia, 2003. Estimation models for precipitation in mountainous regions: The use of GIS and multivariate analysis. Journal of Hydrology, 270(2), pp.1-11.
Maskey, S., V. Guinot, and R.K. Price, 2004. Treatment of precipitation uncertainty in rainfall-runoff modeling, A fuzzy set approach. Advances in Water Resources Research, 27(9), pp. 889-898.
Morris, C.D., 1984. A stochastic model for a small-time-interval intermittent hydrologic processes. Journal of Hydrology, 68(1) pp. 247-272
Oki, T., and K. Musiake, 1991. Spatial rainfall distribution at a storm event in mountainious regions, estimated by orography and wind direction, Water Resource Research, 27 (3), pp. 359-369.
Robinson, J.S., and M. Sivapalan, 1995. Catchment-scale runoff generation model by aggregation and similarity analysis, In: J.D. Kalma and M. Sivapalan (eds.), Scale issues in Hydrological Modeling, John Wiley & Sons, New York, NY. pp. 311-330.
Rogers, J.J., J.M. Prosser, L.D. Garrett, and M.G. Ryan, 1984. ECOSIM: A system for projecting multiresource outputs under alternative forest management regimes. USDA Forest Service Administrative Report, Rocky Mountain Forest and Range Experiment Station, Fort Collins, CO. pp. 167.
Rupp, D.E., 1995. Stochastic, event-based modeling of upland watershed precipitation-runoff relationships, Master's thesis, Northern Arizona University, Flagstaff, Arizona.
SAS Statistical software, 2004. SAS institute inc., Cary, NC, USA.
Schmeiser, B.W., and R. Lal, 1982. Bivariate gamma random vectors, Operation Research , 30, pp. 355-374.
Sellers, W.D., R.H. Hill, and M.S. Rae, 1985. Arizona Climate: The Hundred years, The University of Arizona Press, Tucson.
Singh, K., and V.P. Singh, 1991. Derivation of bivariate probability density functions with exponential marginal, Stochastic Hydrology and Hydraulics, 5, pp. 55-68
Smith, R.E. and H.A. Schreiber, 1973. Point process of seasonal thunderstorm rainfall, Water Resources Research, 9 (4).
Solomon, R.M, P.F. Ffolliott, M.B. Baker Jr., and J.R. Thomson, 1976. Computer simulation of snowmelt, USDA Forest Service Research Paper RM-174, Rocky Mountain Forest and Range Experiment Station, Fort Collins, Colorado.
Stephens, M.A., 1977. Goodness-of-Fit for the extreme value distribution, Bimetrica, 64 pp. 583-588.
Tayler, M.H, and S. Karlin, 1984. An introduction to stochastic modeling, Acadamic Press, Inc. Orlando, Florida.
Tecle, A, 1991. Hydrology and watershed management in southwestern ponderosa pine forests, Chapter 5. In: Tecle and Covington (eds.), Multiresource

Management of Southwestern Ponderosa Pine Forests: The Status-of-our-Knowledge. USDA Forest Service, Southwestern Region, Albuquerque, NM. pp.160-163.

Tecle, A, L. Duckstein, and P. Korhonen, 1994. Interactive, multiobjective programming for forest resources management. Applied mathematics and Computation, pp. 75-93.

Tecle, A, M.N Fogel, J. Long, and K.H. Kim, 1988. A reference manual for steps simulating the spatial and temporal distribution of storm rainfall in the Santa Cruz river basin. Report submitted to Pima County Department of Transportation and Flood Control. School of renewable natural resources, University of Arizona, Tucson, Arizona.

Tecle, A, and D.E. Rupp, 1996. Stochastic, event-based, and spatial modeling of cold-season precipitation. In: Mountain Hydrology: peaks and Valleys in Research and applications, Canadian Society for Hydrological Sciences, Vancouver, B.C. pp.183-186.

Tecle. A, and D.E. Rupp, 2002. Stochastic precipitation-runoff modeling for water yield from a semi-arid forested watershed. In: Risk, Reliability, Uncertainty, and Robustness of Water Resources Systems. Cambridge University press: London. Pp. 56-63.

Viessman, J.W, G.L. Lewis, and J.W. Knapp, 2003. Introduction to hydrology. 3rd ed.: Harper and Row. New York.

Ward, D.A, and W.J. Elliot, 1995. Environmental Hydrology, Lewis publisher, New York.

Chapter 3

Determination of Water Yield Through Precipitation-Runoff Relationship

Abstract

Event-based and spatially-varied cold and warm-seasons water yield models for the ponderosa pine type forest of Arizona are developed in this part of the thesis. The study area is Bar M watershed, located in the north-central Arizona 42 km south of Flagstaff with an area of 6,678 ha. Surface runoff is estimated by means of a water balance approach that accounts for all important hydrological processes such as canopy interception, evaporation, transpiration, snow accumulation and melt, infiltration, and soil water storage. A geographic information system (GIS) is used to divide the study watershed into 90 by 90 m cells on the basis of watershed characteristics such as elevation, slope, aspect, canopy cover, and soil type. Radiation balance and water balance are computed for each cell, to estimate surface runoff from the cell. Surface runoff is routed from cell to cell in the direction of flow as determined by GIS, and the total water yield is the surface runoff generated in a cell located at the outlet of the watershed. The estimated water yield for cold-season is 105 mm, which is 22 percent of the total seasonal precipitation falling in the area. The water yield estimated in the warm-season is 4.3 mm, which is 1.9 percent of the total seasonal precipitation. Due to the spatial variation of the various landscape characteristics such as latitude, longitude, elevation, and aspect, the water yield in both seasons is variable in the watershed.

Introduction

Ponderosa pine forests, which occupy 20 percent of the Salt-Verde Basin in Arizona, used to supply over 50 percent of the total amount of the water for Phoenix before the completion of the Central Arizona Project (Baker, 1982). In the study area, the cold season (which roughly runs from October to April) precipitation accounts for over 65 percent of the annual precipitation. The remaining one third of the annual precipitation comes during July, August, and September (Beschta; 1976). Nearly 90 percent of the water yield is generated during the cold-season primarily from snow melt (Baker, 1986).

The purpose of this research is to develop event-based precipitation-runoff relationship models for both cold and warm-seasons that take into account the temporal and spatial distribution of precipitation, and other important climatic and watershed characteristics. The latter includes elevation, slope, aspect, vegetation cover, and soil. The reason for developing models that are event-based is that, cold and warm-seasons water yields are hypothesized to be dependent on depth, duration and arrival time of precipitation events. Cold-season precipitation, in addition to the above factors, depends on the form in which precipitation comes, and the characteristics of the snowpack. For example, a spring rain storm on an existing snowpack is expected to produce more runoff than an early winter snowfall even though the amounts of the water equivalent of the two events are similar. This occurs because of the higher amount of water losses through evaporation and sublimation from an early cold season snowpack. An event-based model can account for variations in water yield caused by different combination of storm depths, durations, inter-arrival time, form of precipitation, and evaporation and snowmelt. A Geographical Information System (GIS) is used to analyze the effect of the spatial distribution of watershed characteristics and other climatic variable affecting runoff. Variables important to determine runoff such as precipitation, temperature, elevation, slope, aspect, vegetation cover and soil type will not be averaged over a watershed as has been done in many previous studies.

The developed models are deterministic water yield models. The method uses GIS to subdivide the study watershed into 90 by 90 m cells assumed to be homogenous with respect to the previously mentioned physical and biological watershed characteristics. A grid of other dynamic variables such as solar radiation and temperature are also generated using GIS. Water yield is estimated using a water balance approach that accounts for important hydrologic processes such as canopy interception, evaporation, transpiration, snow accumulation, infiltration and subsurface storage. The water balance model is applied to each cell to compute surface runoff from that particular cell. The precipitation simulated in the previous chapter of this study is the input for the runoff model. Appropriate mathematical equations are used to estimate the other outputs such as evaporation, transpiration, and infiltration. The output from each cell is then routed down stream in a cascading fashion to estimate the total amount of water coming out of the entire watershed.

Literature Review

Snowmelt from a cold-season precipitation in the ponderosa pine type forest in north-central Arizona is the major sources of water yield. Therefore, previous studies on water yield from the ponderosa pine type forests of Arizona and New Mexico have focused on snow accumulation and melt and not rainfall. Further, more attention was given to enhancing runoff from winter snowmelt using various forest treatment techniques

(Barr, 1956; Ffolliiot et al., 1989; Rupp, 1995). These studies range from simple local observations of snow dynamics to attempts to present models that describe the amount of regional water yield from snow fall.

Water Yield Studies

Watershed management practices from the early 1940s through the beginning of the 1980s focused largely on increasing water yield through vegetation management on upland watersheds. Water yield improvement tests were conducted on experimental watersheds located mostly in Arizona (Ffolliott, et al., 2000). Various silvicultural treatments including clear cutting and conversions ffrom high water-consuming vegetation to low water-consuming types were tested.

Studies demonstrated that the average long-term increase in water yield depends on a number of factors, such as amount of precipitation, species being treated, site characteristics, intensity of treatment, size of area receiving treatment, re-growth rate and length of time between treatments (Stephens, 2003). In areas of higher elevation where precipitation is higher, the potential for increased yield is greater (Baker, 1982). In a precipitation-limited area such as ponderosa pine forest system, the possibility of increasing water yield through vegetation management is limited (Ffolliott and Thourd, 1974; Stednick, 1996). Soil depth and composition influence the potential for increased water yield after forest treatment. The majority of watershed studies in the ponderosa pine type have showed changes in water yield on shallow, volcanic- derived soil types (Baker, 1986; Baker, 1999). Moreover, the intensity of vegetation treatment has an impact on the water yield from the watersheds. The result of 85 watershed studies in the

U.S. reviewed by Stednick (1996) showed that the changes in annual water yield that may occur due to harvesting of less than 20 percent of watershed area or forest cover was not significant. On the other hand, watershed research conducted in the Beaver Creek of Arizona showed that clear cutting of a watershed showed significant increase in water yield (Baker, 1982). Another factor to consider in predicting water yield after treatment is the rate of recovery of the vegetation (Desta and Telce, 2005), which will affect the amount of water flow. In the Beaver Creek watersheds, any increase in stream flow due to treatment disappears within seven years after the treatment mainly due to regeneration of understory vegetation (Tecle, 1991).

Local Water Yield Studies

The amount of snow converted to runoff depends in part on the amount of loss due to evaporation and sublimation (evapo-sublimation) processes. Interception loss refers to the amount of rainfall intercepted, stored, and subsequently lost by evaporation from a canopy. It is a significant and sometimes dominant component of evapotranspiration and can sometimes play a large part in the water budget of a watershed (Deguchi et al., 2006). However, time-lapse photography of intercepted snow in the ponderosa pine type forests of east-central Arizona shows that most intercepted snow eventually reaches the ground by mechanical processes such as snowslide and wind action or by stemflow and dripping of meltwater (Tennyson et al., 1974). However, forest cover does have an important influence on the rates of evapo-sublimation and melt of snow on the ground by reducing wind speed and by affecting short and long wave radiation. A forest canopy prevents some solar radiation and atmospheric long-wave radiation from reaching a snowpack, and also prevents some short and long-wave radiation reflected and emitted from the snow pack from escaping the forest system. In addition, forest canopy serves nearly as a black-body, emitting long-wave radiation in the direction of the snowpack (Dingman, 1994, Rupp, 1995).

The net result of the presence of forest cover is a reduction in evapo-sublimation rates (Ffolliott and Thorud, 1975). In eastern Arizona, Ashton (1966) found the average daytime evaporation rate from December to early May from an opening to be twice as large as from a ponderosa pine stand. In the case of snowmelt, empirical evidence suggests denser forest canopies result in lower melt rates. In an Arizona study on mixed conifer forest, snow melt rates were lower under dense canopies than under sparse or moderate canopies (Gottfried and Ffolliott, 1980). In the ponderosa pine forest of Arizona, Brown et al. (1974) and Baker (1986) noted an increase in water yield following a reduction in overstory.

Another element which affects snowpack characteristics is the combined factor of slope and aspect. In the northern hemisphere, south-facing slopes typically receive more solar radiation than north-facing slopes. Studies in forested areas in Arizona found snow accumulation to be greater and snowmelt to be slower on “cool” sites than on “warm” sites (Ffolliott and Hansen, 1968; Hansen and Ffolliott, 1968: Ffolliott and Thorud, 1969, 1972), where a site is defined as “cool” or “warm” depending on its slope, aspect, forest cover, and ambient temperature.

A number of models have been developed to predict water yield from the ponderosa pine type forests of Arizona and New Mexico. All models had the aim of determining the effects of forest management using a paired of treated and control watersheds. Some of the models are regression equations (Ffolliott and Thorud, 1972; Brown et al., 1974; Rogers et al., 1984; Baker, 1986), while others are combined physically /empirical models of water yield (Rogers, 1973; Solomon et al., 1976; Rogers and Baker, 1977; Ffolliott and Guertin, 1988). Other models which are worth nothing but are not designed specifically for the particular regions are those of Leaf and Brink (1973b), Leavesly (1973), and Combs et al. (1988).

Baker-Kovner model (Brown et al., 1974) was the first regression equation for the Beaver Creek area used to directly estimate annual water yield from a forested watershed. The regression equation used four predicting variables including total winter precipitation, tree basal area, a slope/aspect index, and the potential direct-beam solar radiation at 1200h on February 23 (Brown et al., 1974). The Baker-Kovner model took only the winter precipitation while assuming insignificant contribution of runoff from summer precipitation.

A modified form of the Baker-Kovner model is the water yield model in ECOSIM (Rogers et al., 1984). Both models, the Baker-Kovner and ECOSIM, have the same inputs such as total winter precipitation, tree basal area, a slope/aspect index, and potential insolation. In addition, the ECOSIM model includes a threshold precipitation level, below which water yield is zero, and a basal area threshold, above which no changes in tree density significantly affect water yield. The model assumes that water yield can be expressed as the yield from an untreated watershed plus the additional water yield resulting from basal area below a threshold value (Rogers et al., 1984).

The model of Baker (1986) consists of regression equations which are watershed-specific. The equations describe changes in annual water yield on a watershed following a certain forest treatment. The model variables are annual flow from untreated or control watershed, and time in years since treatment.

Ffolliott and Thorud (1972) developed regression equations for predicting snowpack accumulation from knowledge of basal area, timber volume and potential direct-beam solar radiation. Knowledge of snowmelt runoff efficiency of the watershed would then, in theory, allow for estimating the portion of snowpack that becomes stream water. Solomon et al. (1975a, 1975b) derived snowmelt-runoff efficiencies for small, upland watersheds characterized by mixed conifer forests, mountain grass lands, and ponderosa pine forests. The study was carried out in fourteen experimental watersheds located in “snow-zone" areas in Arizona. A regression equation relating the snowmelt runoff efficiency with ten inventory prediction variables was set up. They found out that snowmelt runoff efficiency is related significantly with timing of precipitation, total seasonal precipitation, and forest cover.

Other models which simulate the effects of forest management on water yield but are not simply regression equations are Yield II (Ffolliott and Guertin, 1988), the model in Rogers (1973), ECOWAT (Rogers and Baker, 1977), SNOWMELT (Solomon et al., 1976), the models in Leavesly (1973) and Leaf and Brink (1973b), and WTRYLD (Combs et al., 1988). The first three were specifically designed for the forests of Arizona and New Mexico, while the latter three were not.

YIELD II is a computer based water yield model designed in terms of water budget scheme and integrating many important hydrological processes (Ffolliott and Guertin, 1988). The model was used for both winter and summer seasons and predicts daily values of hydrologic processes including runoff, interception, evapotranspiration, infiltration, change in soil moisture storage, and deep seepage. To analyze the effects of forest management on water yield, YIELD II describes evapotranspiration and interception as a function of basal area. Snowmelt is simulated with a degree-day method, though the amount of snowmelt that appears at the watershed outlet requires knowledge of the snowmelt runoff efficiency for that specific watershed.

Rogers (1973) designed a water yield model to be sensitive to vegetation management. The model design consists of a procedure for energy and water balance computation that accounts for hydrologic processes such as canopy interception, snowpack water and energy balance, litter layer water balance, surface water and soil water balance, and the routing of overland flow, interflow and channel flow. A study by Brown et al., (1974) which tested the model on two of the Beaver Creek experimental watersheds found that this model often failed to accurately predict the volume of flow though it was able to predict the time of snowmelt and the timing of peak flows relatively well. The same study concluded that likely sources of error were in the way the model estimated some climatic inputs that could not be measured directly and in its method of describing treatment effects.

Similar to the earlier model developed by Rogers (1973), ECOWAT is a water yield model design to consider all important hydrologic processes (Rogers and Baker, 1977). The model uses a water balance approach and incorporates many validated previous models. ECOWAT contains sub-models for snow accumulation and melt, interception by vegetation and forest floor, transpiration, infiltration, overland flow, soil water and sub surface flow, and channel flow. A problem with the model is that it required 32 input parameters, which made it both difficult to use and test.

SNOWMELT is the snowmelt component of the water yield model (WTRYLD) (Solomon et al., 1976). It is an adaptation to southwestern conditions of the snowmelt model called MELTMOD that was created by Leaf and Brink (1973a) for Colorado subalpine forests. The original model assumed a continuous snowpack (Leaf and Brink, 1973b), but this becomes a major constraint when applied in areas such as Arizona, where the snowpack is intermittent. A modified snow component called SNOWMELT, developed by Solomon et al. (1976), provides for modeling intermittent snowpack conditions in Arizona and New Mexico. SNOWMELT requires daily inputs of maximum and minimum temperatures, precipitation, and solar radiation. Even though a separate testing of model was found satisfactory, it was never incorporated into a full water yield model. Though several other water yield models were tried in the ponderosa pine type forest, they were not implemented.

Hansen et al. (1977) attempted to determine the applicability of the runoff model developed by the US Geologic Survey (Leavesly, 1973) to the ponderosa pine type forest of Arizona. The results of the study, however, were inconclusive. Generally, the US Geologic Survey model and the MELTMOD seemed to have a problem of keeping the snowpack too cold during the mid-winter months and failed to predict any significant snowmelt during this period.

WATBAL which was developed by Leaf and Brink (1973b) and applied by Troendle (1979) used to develop procedures for predicting selected hydrologic impacts of silvicultural activities in snow dominated regions. WTRYLD (Combs et al., 1988) was tested in the Colorado subalpine forests and the Sierra Nevada of California. Both models require some modification to be used in the ponderosa pine type forests of Arizona and

New Mexico. An attempt was made to do so for the snowmelt component of WATBAL (Solomon et al., 1976). However, there has never been a real effort to use WTRYLD in the southwest. The problems of WTRYLD are: the model requires variables that are difficult to obtain, it uses a trial and error model fitting procedure, which makes it difficult to reliably test its transportability to other areas (Tecle, 1991).

As it was discussed previously, the main objective of most of the models described above is to know the impact of vegetation management on water yield. Studies such as those of Brown et al. (1974), Baker (1982, 1986) and Rupp (1995) in the ponderosa pine type suggested that the two major hydrologic processes influencing the timing and volume of the cold-season stream flow, which are most sensitive to vegetation manipulation, are evapotranspiration and snowmelt. Because of this, recent advances in the modeling of these processes are discussed below. For a review of the modeling of other processes involved in runoff generation in forests, with particular attention given to infiltration and subsurface flow, see Bonell (1993).

Evapotranspiration Modeling

Evapotranspiration is the major component of water balance in a forested watershed and accurately quantifying it is critical to predict the effects of forest management and global change on water and nutrient yield (Jianbiao et al., 2003). Evapotranspiration has always been difficult to measure, especially on an ecosystem or watershed spatial scale. Methods have been developed to measure evapotranspiration at a leaf level, the tree level and the stand level (Fisher et al., 2005). Evapotranspiration is one of the most difficult processes to evaluate in a hydrologic analysis. Estimates are generally considered to be a significant source of error in stream flow simulation (Kolka and Wolf, 1998; Fisher et al., 2005). Hence potential evapotranspiration at a watershed level in most cases is estimated using empirical or physical approaches that take into account the different climatic variables. Some temperature based methods are: Thornthwaite (Thornthwaite and Mather, 1955), Hamon (1963), and Hargraves-Samani (1985). Others energy, or radiation-based methods such as Penman-Monteith (1948), Turc (1961), Makkink (1957), and Priestley and Taylor (1972). Many recent evapotranspiration models use an energy balance that accounts for the effects of environmental conditions on stomatal resistance to molecular diffusion of water. Such models are those of Dickinson et al. (1986), Sellers et al. (1986), Running and Caughlan (1988), Stewart (1988), Famiglietti (1992), Famiglietti and Wood (1994), Wigmosta et al. (1994), Fisher et al., (2005).

Typically, the energy sources involved are net radiation flux, latent heat flux, and sensible heat flux, while more compressive models include soil heat flux and change in energy storage in the vegetation. When only the first three energy sources are accounted for, the Penman-Monteith approach provides a convenient and well-tested method of estimating evapotranspiration (Dickinson et al., 1991; Dingman, 1994). Two examples of studies which successfully include the Penman-Monteith equation in water balance scheme for vegetated surface are those of Running and Coughian (1988) and Wigmosta et al (1994).

Despite the different models used by various researchers mentioned above, all of these models incorporate canopy conductance (often referred to the reciprocal of canopy resistance). Canopy conductance is a measure of stomatal resistance of a canopy to transpiration and it has the effect of reducing the rate of evapotranspiration from the potential rate (Rupp, 1995). What the models of Dickinson et al. (1986), Sellers et al. (1986), Running and Caughlan (1988), Famiglietti and Wood (1994), and Wigmosta et al. (1994) all share in common is that when the vegetation surface is wet, they set the canopy conductance to be infinity (resistance to zero). Shuttleworth (1975) gives theoretical support for this practice, while Stewart (1977) provides empirical evidence that the canopy resistance of a completely wet pine forest is near zero.

Though conceptually similar, all the above models differ in specifics in how they determine the canopy conductance when the vegetation surface is dry. For all the models, and the general equation for canopy conductance, C_{can}, can be represented by

$$C_{can} = LAI_t\, C_{leaf}\, f(T)\ f(H)\ f(PAR)\ f(S_w)\ f(CO_2)\ f(Nut) \tag{3-1}$$

Where C_{leaf} is the species specific maximum leaf conductance, LAI_t, is the leaf area index, and the f's represents functions of environmental variables that limit the canopy conductance from its maximum value (Dicknson et al., 1991). The environmental variables that can affect the canopy conductance include temperature (T), absolute humidity deficit (H), photosynthetically active radiation flux (PAR), water stress (S_w), and carbon dioxide (CO_2) and nutrient (Nut) availability (Dickinson et al., 1991).

Each one of the models mentioned above uses different expressions for each of the first four limiting functions in equation (3-1), while carbon dioxide and nutrient availability are ignored. However, Jarvis (1976) found that stomatal conductance is affected primarily by quantum flux density, ambient carbon dioxide, specific humidity deficit, leaf temperature, and leaf water status. Using the finding of Jarvis (1976) as a basis, Stewart (1988) successfully simulated evapotranspiration rates in a pine forest using the Penman-Monteith approach with the canopy conductance dependent up on air temperature, absolutely humidity deficit, solar radiation, and soil moisture deficit. Carbon dioxide was excluded because there was very little change in available carbon dioxide during the study.

Snowmelt Modeling

Modeling of snowmelt typically involves the use of either an energy-balance approach, or an index method, where the index is most commonly air temperature (Gray and Prowse, 1992). Ohmura (2001) favored the temperature-index method rather than energy method due to three reasons: 1) simple and good performance in accuracy, 2) availability of air temperature data, and 3) easy spatial interpolation of air temperature. However, some studies have shown that the two approaches can be combined to successfully estimate daily snowmelt (Martinec, 1989; Kustas et al., 1994).

The energy-balance approach is constructed to describe the sources of energy flux into a snowpack. The net energy flux is taken to be the sum off the energy due to radiation, convection, conduction, advection, and the change in internal energy of the snowpack. The general formula of the energy balance equation (all in $kJm^{-2}hr^{-1}$) is:

$$\frac{dU}{dt} = Q_{sn} + Q_{li} + Q_p + Q_g - Q_{le} + Q_h + Q_e - Q_m \tag{3-2}$$

Where $\frac{dU}{dt}$ = the amount of energy available for snowmelt

Q_{sn} = net shortwave radiation,

Q_{li} = incoming longwave radiation,

Q_p = advected heat from precipitation,

Q_g = ground heat flux

Q_{le} = outgoing longwave radiation

Q_h = sensible heat flux

Q_e = latent heat flux

Q_m = advected heat removal by melt water (Tarboton et al., 1995)

In many cases the energy balance approach is not justified due to time, input, or computational restrictions and desired accuracy (Tarbotonet al., 1995). The data requirements become practically impossible to fulfill especially when simulating snowmelt over an entire watershed (Dingman, 1994).

A much simpler approach is the temperature-index, or degree-day method. The temperature index snowmelt model has been the most popular for most basin modeling approaches (Ward and Elliot, 1995). It is commonly expressed as

$$M = K (T_a - T_b) \tag{3-3}$$

Where M is melt for the day (in units of depth), K is the degree-day conversion factor (units of depth divided by temperature), T_a is the average air temperature, and T_b, is the base temperature, usually taken as the melting point of snow, 0 ^oC (32 ^oF) (Ward and

Elliot, 1995). One drawback to the temperature-index is that the degree-day convertion factor, K, is highly variable both temporarily and spatially and in practice the degree-day factor must be empirically calculated for different sites and times of the year (Rupp, 1995).

To deal with the spatial and temporal variability in snowmelt which is not accounted for by temperature alone, the use of a combination of the degree-day method and radiation budget approach has been proposed (Martinec and de Quervain, 1975; Ambach, 1988; Martinec, 1989: Kustas et al., 1994). Kustas et al. (1994) selected net radiation because previous studies have shown it to explain for most of the variation in snowmelt (Zuzel and Cox, 1975; Granger and Male, 1978; Marks and Dozier, 1992). The form of the combined equation as shown in Kustas et al. (1994) is

$$M = k_r T_a + m_q R_n \tag{3-4}$$

Where = k_r is called the restricted degree-day factor, Rn is the net radiation at the surface of the snowpack, and the other terms are as described above. Martinec (1989) finds the variability in k_r to be much less than that of the degree-day conversion factor, k, in equation (3-3). Kustas et al. (1994) find that equation (3-4) provides improved results over the simple degree-day method when compare to lysimeter outflow measurements. And the results are in good agreement with those of an energy-balance model.

Methods

Water Balance

One of the best ways of characterizing the hydrology and water resources of an area is using a water balance approach. This is because the approach includes all aspects of hydrology and other important factors that affect the system. The water balance is expressed in the form of a continuity equation that describes the relationship between inputs, outputs and any change in storage. Furthermore, the input and output parts are expressed in terms of many variables representing the different factors contributing to each part. The components of the water balance model consist of hydrologic processes such as precipitation, canopy interception, evaporation, transpiration, snow accumulation and melt, infiltration and soil water storage. The general expression for the water balance model used in this study is

$$\frac{\Delta S}{\Delta t} = P - R - E - T \tag{3-5}$$

Where $\frac{\Delta S}{\Delta t}$ is the change in storage with time in the soil or vegetation system, P is the rate of precipitation, R is net runoff rate, E is evaporation rate, and T is transpiration rate all in units of cm hr^{-1}. In this equation precipitation represents the input while the other terms on the right hand-side of the equation are the hydrologic outputs from the watershed system. Any loss of water from the watershed system as groundwater flow to distant water table below is assumed to be negligible and is not included in the water balance analysis. Before analyzing the various components of the water balance model, the different physical and vegetative characteristics that influence the behavior of the above water balance model components will be discussed.

Describing watershed characteristics

The spatial distributions of the physical and biological characteristics of the study watershed are described using GIS. The watershed is divided into 24,733 cells of size 90 by 90 m, on the basis of the different watershed characteristics, using the raster-based component of the ARC/INFO GIS called GRID. An individual cell is assumed to be homogeneous over its 8,100 m^2 with respect to the different watershed characteristics.

For the purpose of analysis, watershed characteristics may be considered as either static or dynamic. The static characteristics are elevation, slope, aspect, soil, and vegetation cover. Though vegetation cover is not static, it is assumed to be the same throughout the seasons. On the other hand, the dynamic watershed characteristics are precipitation, temperature, net radiation, evapotranspiration, soil moisture content, infiltration, snow accumulation and melt, and runoff.

The boundary of the watershed is taken from the Beaver Creek watersheds map data archive (http://ag.arizona.edu/OALS/watershed/beaver/geology.html, April 2, 2005). The elevation data were obtained from the 7.5' USGS DEM (digital elevation model) that represents the areal images for Arizona (http://landsat.ece.arizona.edu/, accessed May 10, 2005). The elevation data for the watershed are then created by clipping out the watershed boundary from the surrounding quad maps. The original data have a horizontal resolution of 30 m but were converted to 90 m to fit with other watershed data. In the elevation map, it is assumed that the elevation value of a particular cell will be representative of the entire cell having, all points in the cell has the same elevation value as the center point.

The distribution of soil types is obtained from the vector data set of the Terrestrial Ecosystem Survey (TES) for the Coconino National Forest (USFS, 1992). The soil information for the study area only is acquired by clipping out Bar M watershed using the watershed boundary. The soil vector layer was then converted to grids of soil types.

The other static watershed data, which include slope, aspect, overstory cover, and stand height are generated using the same method from Forest ERA (Ecosystem Restoration Analysis) GIS map database for the Western Mogollon Rim area (http://www.forestera.nau.edu., 2005). Dynamic watershed characteristics such as precipitation and temperature are taken from the simulated results in the previous chapter.

Construction of Water Balance Model

A water balance model is developed for both the cold and warm seasons to estimate runoff from the watershed by determine the various inputs and outputs. The individual components of the cold and warm seasons water balance models described in this section include the processes of precipitation, interception, evaporation, transpiration, infiltration, and runoff. Besides these components, snow melt is calculated for winter season. In addition to these hydrologic processes, a radiation balance is also discussed because it plays an important role in the estimation of evaporation, transpiration, and snowmelt.

Radiation

The model computes a daily radiation balance for each cell in the watershed for the cold and warm seasons. The net radiation balance consists of both long-wave and short-wave components, which are computed separately. Also, net radiation is determined for both the overstory and the ground. The first step in the process consists of determining the net short-wave radiation to estimate the incoming solar radiation (insolation) for each cell in the watershed. The model requires as input a value of the daily insolation striking a horizontal surface. This insolation value is multiplied by a slope factor to obtain an estimate of the daily insolation received by a non-horizontal surface. The slope factor is a function of the day of the year, the slope, aspect, and latitude of a given cell in the watershed. The slope factor is computed using the algorithm in Swift (1976) and adopted by Rupp (1995). The average total daily solar radiation received on a horizontal surface at 34^{o} 55' N latitude, 111^{o} 38' W longitude and elevation 1,977 m 32 km south of Flagstaff near the study site is taken as insolation values from Campbell and Stevenson, (1977) (See Table 3A-2 in Appendix 3A).

The net short-wave radiation at the surface is calculated in a way similar to that in Wigmosta et al. (1994), in which a radiation balance is determined for both the overstory and ground. One difference is that Wigmosta et al. (1994) computes the net radiation for both an understory and a ground surface, while in this study the understory and the ground surface are lumped together as ground. This is done because the sparse understory is assumed to not significantly affect the radiation balance, nor contribute significantly to the evapotranspiration, thus the added complexity of an extra layer is not necessary. The net short-wave radiation for the overstory is determined using

$$R_{so} = R_s[(1-\alpha_o) - \tau_o(1-\alpha_g)]F \tag{3-6}$$

Where R_{so} = net short-wave overstory radiation (cal cm^{-2} s^{-1})

R_s = insolation (cal cm^{-2} s^{-1})

α_o = albedo of overstory,

τ_o = fraction of short-wave transmittance through overstory,

α_g = albedo of ground and

F = overstory cover as a fraction of total surface area.

The albedo for snow α_s is used in place of the albedo of the overstory or the ground when either is covered with snow (Wigmosta et al., 1994). The albedo for ground is assumed to be 0.15, and for the overstory 0.18 while snow is assumed to have an average value of 0.63 (Burman and Pochop, 1994). As in Wigmosta et al. (1994), short wave radiation is attenuated through the overstory using Beer's law (Monteith and Unsworth, 1990) to obtain the short wave transmittance fraction (τ_o):

$$\tau_o = e^{-kLAI_p} \tag{3-7}$$

Where k is the overstory attenuation coefficient (0.5) and LAI_p is the projected leaf area index of the overstory, in this case ponderosa pine which as the leaf area index value of 6.5 (Barnes et al., 1998). According to Wigmosta et al. (1994), the net short-wave radiation at the ground R_{sg} is determined using

$$R_{sg} = R_s(1-\alpha_g)[\tau_o F + (1-F)] \tag{3-8}$$

Where all the terms are as described in equation (3-6).

Computation of the long-wave radiation balance is also done similar to that in Wigmosta et al. (1994). At the overstory, the net-long wave radiation is calculated as:

$$R_{lo} = (L_d + L_g - 2L_o)F \tag{3-9}$$

Where R_{lo} is the net overstory long-wave radiation, L_d is the downward long-wave radiation (from the sky), L_g is the long-wave radiation emitted from the ground, and L_o is the long-wave radiation emitted from the overstory. At the ground, the net long-wave radiation is computed using:

$$R_{\mathrm{lg}} = L_o F + L_d (1 - F) - L_g \tag{3-10}$$

Where R_{lg} is the net long-wave radiation at the ground and the remaining terms are as described in equation (3-9).

It is assumed that the ground and the overstory emit radiation as black bodies. Therefore, according to Wigmosta et al. (1994), the radiation emitted from the ground and the overstory are calculated using equations (3-11) and (3-12)

$$L_g = \sigma (T_g + 273.3)^4 \tag{3-11}$$

and

$$L_o = \sigma (T_o + 273.3)^4 \tag{3-12}$$

Where σ is the Stefan-Boltzman constant, which is equal to $1.355 X 10^{-12}$ ca cm^{-2} s^{-1} $^{o}C^{-4}$ and T_g and T_o are the ground and overstory temperatures respectively. The temperature of the overstory is assumed to be equal to the air temperature. The air temperature was simulated in the second chapter. However, the ground temperature is determined by creating a relationship between the measured air temperature and ground temperature from 1995 to 2005 data and using this relationship to estimate the simulated ground temperature..

Downward long-wave radiation (L_d) is estimated according to Brutsaert (1975) and Sugita and Brutsaert (1993). For the model in this study, clear-sky conditions are assumed for days when there is no precipitation. Therefore, on days of no precipitation, the downward long-wave radiation (L_{dc}) is determined using:

$$L_{dc} = \varepsilon\sigma(T_a + 273.3)^4 \tag{3-13}$$

Where ε is the atmospheric emissivity and T_a is the air temperature. As in Brutsaert (1975), the atmospheric emissivity is estimated by

$$\varepsilon = a[0.01e/(T_a + 273.3)]^b \tag{3-14}$$

Where e is the atmospheric vapor pressure, and a and b are constants. On the day in which precipitation occurs, the sky is assumed to be completely overcast. According to

Sugita and Brutsaert (1993), the downward long-wave radiation during a completely overcast day (L_{do}) can be approximated by $L_{do} = 1.1 L_{dc}$.

Interception

The overstory is assumed to intercept all precipitation until the maximum interception storage capacity is reached (Wigmosta et al., 1994). Accordingly, the change in interception storage, ΔS, under this condition is estimated by

$$\Delta S = P - EP \tag{3-15}$$

Where P is the interception rate (cm s^{-1}), and EP is the potential evaporation rate (cm s^{-1}). During the period before maximum interception storage capacity, $S_{\max}$, is reached, the rate of precipitation reaching the ground, P_g, is zero. After maximum interception storage capacity is reached, the precipitation rate reaching the ground is determined by

$$P_g = P - EP \tag{3-16}$$

As in Dickinson et al. (1991) and Wigmosta et al. (1994), the maximum interception storage capacity, $S_{\max}$ (cm), is estimated using

$$S_{\max} = 0.01 LAI_p F \tag{3-17}$$

for both rain and snow.

Evaporation

Evaporation can occur from either the water stored as interception on the overstory canopy, or from the water stored in the snow pack. In either case, a potential evaporation rate is assumed. The Penman-Monteith equation is used to determine the potential evaporation rate (Dingman , 1994). The Penman-Monteith equation is expressed as

$$EP = \frac{\Delta R_n + \rho_a C_a C_{at} \Delta e}{\rho_w \lambda_v (\Delta + \gamma)} \tag{3-18}$$

Where EP = potential evaporation rate (cm s^{-1}),

Δ = slope of saturation vapor pressure vs. air temperature (mb ^{o}C $^{-1}$),

R_n = net radiation (cal cm^{-2} s^{-1}),

ρ_a = density of air (g cm^{-3}),

C_a = heat capacity of air (cal g ^{o}C^{-1}),

C_{at} = atmospheric conductance (cm s^{-1}),

Δe = vapor pressure deficit (mb), which is equal to the saturated vapor pressure defecit (e_s) minus actual vapor pressure (e)

ρ_w = density of water (g cm^{-3}),

λ_v = latent heat of vaporization (ca g^{-1}), and

γ = Psychrometric constant (cal g $^{-1}$)

The atmospheric conductance (C_{at}) is a function of the prevailing wind speed and the height of the vegetation in the area. As in Dingman (1994), the canopy conductance is computed using:

$$C_{at} = \frac{V_a}{6.25(\ln[Z_m - Z_d) / Z_o)^2} \qquad (3\text{-}19)$$

Where- V_a = wind speed (cm s^{-1}),

$Z_d = 0.7\,Z_{veg}$ (m),

$Z_o = 0.1\,Z_{veg}$ (m),

Z_m = height of wind speed measurement (m), and

Z_{veg} = height of vegetation (m).

The net radiation (R_n) is the sum of the short-wave and long-wave components of radiation for either the overstory or ground, which are given in equation (3-6), (3-8), (3-9) and (3-10). The description of the remaining variables in equation (3-18) is found in appendix 3A.

Transpiration

Transpiration can occur when there is no water stored in the canopy. In this case, it is assumed that, during winter only the evergreen species of the canopy (i.e. ponderosa pine) transpire. Transpiration rates are determined using the Penman-Monteith equation with the inclusion of a canopy resistance term (C_{can}) (Dingman, 1994). In this case the Penman-Monteith equation for transpiration rate (Tr) is expressed as

$$Tr = \frac{\Delta R_n + \rho_a C_a C_{at} \Delta e}{\rho_w \lambda_v [\Delta + \gamma(1 + C_{at} / C_{can})]} \tag{3-20}$$

Where all the terms except the canopy conductance (C_{can}) are described in equations (3-18) and (3-19).

The canopy conductance can be expressed as a function of environmental characteristics, as well as characteristics of the transpiring species (Jarvis, 1976; Stewart, 1988; Dingman, 1994). As in Stewart (1988) and Dingman (1994), the canopy conductance is considered to be a function of the maximum leaf conductance of the tree species, the total leaf area index, the net short-wave radiation, the absolute humidity deficit of the air, the air temperature, and the soil moisture. In terms of these variables, the equation for canopy takes the following form:

$$C_{can} = LAI_t C_{leaf} f(R_{so}) f(\Delta\rho_v) f(T_a) f(\theta) \tag{3-21}$$

Where LAI_t is the total leaf area index, C_{leaf} is the maximum leaf area conductance, and the last four terms, in order, are functions describing the relationship between canopy conductance and the net short-wave radiation (R_{so}), absolute humidity deficit ($\Delta\rho_v$), air temperature (T_a), and soil moisture content (θ) (Dingman, 1994).

The short-wave radiation function in equation (3-21) is expressed as

$$f(R_{so}) = \frac{46225 R_{so}}{41870 R_{so} + 104.4} \tag{3-22}$$

for $0 < R_{so} < 0.0239$ cal cm^{-2} s^{-1}, $f(R_{so})$ equals 1 for $R_{so} > 0.0239$ cal cm^{-2} s^{-1} (Stewart, 1988). The absolute humidity deficit function in equation (3-21) can be written as

$$f(\Delta\rho_v) = 1 - 0.0666\Delta\rho_v \tag{3-23}$$

for $0 < \Delta\rho_v < 11.52$ g m^{-3} and $f(\Delta\rho_v)$ equals 0.233 for $\Delta\rho_v > 11.52$ g m^{-3} (Stewart, 1988). The temperature function in equation (3-20) is expressed as

$$f(T_a) = \frac{T_a(40 - T_a)^{1.18}}{691} \tag{3-24}$$

for $0 < T_a < 40$ ^{o}c and $f(T_a)$ equals 0 for $T_a > 40$ ^{o}C (Stewart, 1988).

The soil moisture function is expressed as

$$f(\theta) = \frac{\theta - \theta_{wp}}{\theta_{fc} - \theta_{wp}} \tag{3-25}$$

Where θ is the average soil moisture content in the soil column, θ_{wp} is the wilting point, and θ_{fc} is the soil moisture content above which transpiration is not soil-moisture limited, and under this condition $f(\theta)$ equals unity. For this study, this value is assumed to be equal to the field capacity of the soil. When the soil moisture content falls below the wilting point, however, $f(\theta)$ is set to zero. The soil moisture content in equation (3-25) is given as ratio of the actual soil moisture to the maximum soil moisture capacity.

Infiltration

Infiltration is determined using the Green-Ampt equation developed by Green and Ampt (1911). The Green-Ampt model is also based on the assumption that during infiltration the soil column is saturated behind the wilting front and that soil moisture component ahead of the wetting front equal to the antecedent soil moisture content which is considered to be distributed uniformly throughout the profile. For the purpose of this study, transport of water is assumed to occur in the vertical direction only and the soil column is treated as a single layer resting atop an impervious boundary.

Infiltration into the soil column can occur during periods of rainfall, snowmelt, or a combination of the two. Dingman (1994) describes three different cases for determining the rate of infiltration. These three cases depend upon the rate at which water is reaching from above, the time it takes for ponding to begin on the soil surface, and the time taken for the entire soil column to become completely saturated.

Case 1 occurs when the rate at which water is reaching the soil surface from above , (w) (cm hr^{-1}) is less than the saturated hydraulic conductivity of the soil, K_{sat} (cm hr^{-1}). In this case no ponding of water on the soil surface occurs. Under this condition the rate of infiltration (i) is assumed to be w while the time it takes (in hours) for the entire soil column to become saturated (t_{sat}) can be determined using

$$t_{sat} = Z_{sc}(\phi - \theta_o)/w \qquad (3\text{-}26)$$

Where Z_{sc} is the depth of the soil column (cm), ϕ is the saturated water content of the soil, and θ_o is the initial water content of the soil (Dingman, 1994). If t_{sat} is less than the duration of the event in hours that brings water to the soil surface from above (t_f), then the water content (θ) of the soil becomes the saturated water content (ϕ) at time t_{sat}, after which infiltration ceases. If the soil column does not become saturated, or t_{sat} is greater than t_f, then all the water infiltrates and the final water content of the soil is estimated using

$$\theta(t_f) = \theta_o + (wt_f / Z_{sc}) \tag{3-27}$$

Where $\theta(t_f)$ is the final water content of the soil and the other terms are as described above.

Case 2 refers to the condition in which the rate at which the water is reaching the soil surface from above (w) is greater than the saturated hydraulic conductivity of the soil (K_{sat}), and when the time it takes for the soil column to become saturated (t_{sat}), is less than the time to ponding (t_p). The time to saturation is found from equation (3-26) above, while the time to ponding can be calculated using

$$t_p = \frac{K_{sat}|\psi_f|(\phi - \theta_o)}{w(w - K_{sat})} \tag{3-28}$$

Where ψ_f is the effective tension at the wetting front (cm) (Dingman, 1994), all other terms are as described previously.

The determination of the infiltration rate for case 2 turns out to be the same as for case 1. When the duration of the event (t_f) is greater than the time it takes for the entire soil column to become saturated (see equation 3-26), the final soil water content is the saturated water content (ϕ). Under this condition, the infiltration rate, i (cm hr^{-1}) equals w before saturation and becomes zero when the soil is saturated. However, when the entire soil column does not reach saturation, or t_f is less than t_{sat}, then the final soil water content is determined using equation (3-27) and the infiltration rate remains at w throughout.

Case 3 occurs when the rate of precipitation (w) is greater than the saturated hydraulic conductivity (K_{sat}) and when the time it takes for the entire soil column to become saturated (t_{sat}) is greater than the time to ponding (t_p). The time to ponding is determined using equation (3-28). The time to saturation in this case is dependent on a rate of infiltration that decreases with time following ponding. This time to saturation is represented by

$$t_{sat} = \frac{I(t_{sat}) - I(t_p)}{K_{sat}} + \frac{|\psi_f|(\phi - \theta_o)}{K_{sat}} \ln\left[\frac{I(t_p) + |\psi_f|(\phi - \theta_o)}{I(t_{sat}) + |\psi_f|(\phi - \theta_o)}\right] + t_p \qquad (3\text{-}29)$$

Where $I(t_{sat})$ is the total amount of infiltration (cm) at the time of saturation and $I(t_p)$ is the total amount of infiltration (cm) at the time of ponding (Dingman, 1994). The total amount of infiltration at the time of ponding is wt_p and the total amount of infiltration at the time of saturation is $Z_{sc}(\phi - \theta_o)$.

When the precipitation event lasts longer than the time to saturation, or t_f is greater than t_{sat}, then the final soil moisture content is the saturated soil moisture content (ϕ). When the event duration (t_f) is less than the time of ponding (t_p), the final moisture content is calculated using equation (3-27). In this case, the infiltration rate before the time of ponding (t_p) equals w, and the rate becomes zero after the time of saturation.

When the precipitation even duration is greater than the time of ponding (t_p) and less than the time of saturation (t_{sat}), then the final soil moisture content is calculated using equation (3-30) which is

$$\theta(t_f) = \theta_o + I(t_f) / Z_{sc} \tag{3-30}$$

where $I(t_f)$ is the total amount of infiltration at the end of the event. The solution of the total amount of infiltration, I, requires the integration of the Green-Ampt equation, which can be expressed as

$$i = \frac{dI}{dt} = K_{sat}\left[1 + \frac{|\psi_f|(\phi - \theta_o)}{I}\right] \tag{3-31}$$

This is valid for t grater than t_p (Dingman, 1994).

The solutions for the infiltration rate (i) and the total infiltration rate (I) are determined using a series of approximations to equation (3-31) developed by Salvucci and Entekhabi

(1994). In this manner, equation (3-32) is constructed to approximate the infiltration rate (i') at time t.

$$i'(t) = K_{sat}\left[\frac{\sqrt{2}}{2}\left[t/(t+x)\right]^{-1/2} + \frac{2}{3} - \frac{\sqrt{2}}{6}\left[t/(t+x)\right]^{-1/2} + \frac{1-\sqrt{2}}{3}\left[t/(t+x)\right]\right] \tag{3-32}$$

Where x equals $\left|\psi_f\right|(\phi-\theta_o)/K_{sat}$ (Salvucci and Entekhabi, 1994), and all other variables are as explained previously.

Thus the approximate total infiltration ($I^{'}$) at time t can be estimated using equation (3-33), which is the result of integrating equation (3-32) with respect to time.

$$I'(t) = K_{sat}\left[\begin{array}{l}\frac{(3-\sqrt{2})}{3}t + \frac{\sqrt{2}}{3}(xt+t^2)^{1/2} + \frac{\sqrt{2}-1}{3}x\left[\ln(t+x)-\ln(x)\right] + \\ \frac{\sqrt{2}}{3}x\left\{\ln\left[t+x/2+(xt+t^2)^{1/2}\right]-\ln(x/2)\right\}\end{array}\right] \tag{3-33}$$

Equation (3-32) and (3-33) are valid only for ponded conditions. Considering for the period befor ponding, the total amount of infiltration at the end of the precipitation event is expressed as

$$I(t_f) = I'(t_f) - I'(t_p) + wt_p \tag{3-34}$$

Table 3.1 summarizes the three cases in which infiltration occurs discussed above. The table shows the different infiltration rates and the different final soil moisture contents for various combinations of precipitation rates, precipitation durations and antecedent soil moisture conditions.

Table 3.1 Three cases of infiltration

Case	Condition	Soil moisture	Infiltration
1.	$w < K_{sat}$		See equation 3-26 for t_{sat}
a.	$t_f > t_{sat}$	$\theta(t_f) = \phi$	When $t < t_{sat}, i = w$; When $t > t_{sat}, i = 0$;
b.	$t_f < t_{sat}$	$\theta(t_f) = \theta_o + wt_f / Z_{sc}$	$i = w$
2.	$w > K_{sat}$; $t_{sat} < t_p$		(See equ. (3-26) for t_{sat})
a.	$t_f > t_{sat}$	$\theta(t_f) = \phi$	When $t < t_{sat}, i = w$; When $t > t_{sat}, i = 0$;
b.	$t_f < t_{sat}$	$\theta(t_f) = \theta_o + wt_f / Z_{sc}$	$i = w$
3.	$w > K_{sat}$ $t_{sat} > t_p$		(See equ. (3-29) for t_{sat})
a.	$t_f > t_{sat}$	$\theta(t_f) = \phi$	When $t < t_p, i = w$; When $t_p < t < t_{sat}, i =$ decreasing When $t > t_{sat}, i = 0$;
b.	$t_p < t_f > t_{sat}$	$\theta(t_f) = \theta_o + I(t_f) / Z_{sc}$ (see equation (3-34) for $I(t_f)$)	When $t < t_p, i = w$; When $t > t_p, i =$ decreasing
c.	$t_f < t_p$	$\theta(t_f) = \theta_o + wt_f / Z_{sc}$	$i = w$

Snow melt

The expression for snowmelt is constructed by combining the commonly-used temperature index, or degree-day method with a limited surface energy budget. The limited surface energy budget includes the surface radiation budget and the energy advected to the snowpack by precipitation. During days of no rainfall, a computation of snowmelt employs the equation used by Kustas et al. (1994), which takes the form

$$M = a_r T_{avg} + m_q R_n \tag{3-35}$$

Where M = daily snow melt depth (cm)

a_r = restricted degree day factor (cm d^{-1} ^{o}C^{-1}),

T_{avg} = daily average temperature (^{o}C)

m_q = the convertion factor for energy flux density to snowmelt depth (cm d^{-1}(cal cm^{-2} d^{-1})$^{-1}$), and

R_n = daily net radiation (cal cm^{-2} d^{-1})

In the current study, rain-on-snow events are accounted for by adding the energy advected by the rain (Q_r) to the right hand side of equation (3-35) to get

$$M = a_r T_{avg} + m_q (R_n + Q_r) \tag{3-36}$$

The energy advected by rain (Q_r) in units of cal cm^{-2} is calculated using

$$Q_r = \rho_w C_w T_r P_r \tag{3-37}$$

Where ρ_w is the density of water (g cm-3), C_w is the heat capacity of water (cal g^{-1} ^{o}C^{-1}), T_r is the rain temperature (^{o}C), and P_r is the depth of rain (cm). The rain temperature is assumed to be equal to the air temperature.

Runoff

The surface runoff consists of the rainfall reaching the ground (P_g) and/or the snowmelt (M) that neither evaporates (EP) nor infiltrates (I) into the soil. The net surface runoff (R_i) in unit of centimeters from a cell i is determined using

$$R_i = P_{gi} + M_i - I_i - EP_i \tag{3-38}$$

The values for the right-hand side components of equation (3-38) are determined separately using the different modules discussed above.

Surface runoff can enter a cell from any of eight possible adjacent cells, though no cell can be fed by more than seven adjoining cells at once because one cell must remain as the outflow cell. With restrictions like these imposed on surface flows into and out of a cell, each cell can be thought of as the outlet cell of a sub-basin, where the sub-basin is composed of as little as one cell or up to as many cells as there are in the entire watershed. Therefore, the total runoff in a cell is an accumulation of the runoff generated from that cell plus the runoff generated from all the contributing sub-basin cells upstream. If a sub-basin is composed of n cells, then the runoff leaving the n^{th} cell or outlet cell, can be expressed as

$$R_n = P_{gn} + M_n - I_n - EP_n + \sum_{i=1}^{n-1} R_i \tag{3-39}$$

This assumes that the components of the water budget (i. e. evapotranspiration, infiltration etc.) on any given cell are independent of the processes operating on any other cell. Surface runoff is routed downstream from cell to cell in a cascading fashion. The surface water yield from the entire watershed is considered to be the cumulative total runoff at the watershed outlet cell.

Results

The water balance model was developed on a daily basis to estimate the amount of seasonal surface water yield produced from the ponderosa pine forest watershed for both cold and warm seasons. The daily precipitation simulated in the previous chapter and snowmelt are the main inputs for the cold-season but only the former constitutes the input for warm-season. Evaporation, transpiration and infiltration are considered the main outputs of the water balance model. Because intercepted water is eventually either evaporated or reaching the ground through stemflow or drip, we have not considered it in the water balance analysis.

The most important biophysical characteristics that affect the amount and rate of water yield are described in detail using GIS. The developed GIS layers are used in calculating the various outputs such as evapotranspiration, infiltration and runoff and to show their spatial distributions. The model generated water yields are compared with twenty years of actual stream flow measured at the outlet of the Bar M watershed to verify the reliability of the model.

Description of Watershed Characteristics

The spatial distribution of the static watershed characteristics are represented as raster layers of 90 by 90 m resolution for use in the water yield model. Figures 3-1 through 3-4 are the grid maps of elevation, slope, aspect, and soil type of the Bar M watershed. The spatial distributions of elevation, slope, aspect, and soil type are summarized in the form of relative frequency histograms in Figures 3-5 through 3-5. Figure 3-5 shows that 60 percent of the area has elevations ranging from 2100 to 2300 m mostly located in the eastern half of the watershed (see also Figure 3-1).

The histogram of the relative frequency distribution for slope data shows that more than 75 percent of the area has less than 10 percent slopes (see Figure 3-6). Spatially, the different slopes are fairly distributed throughout the watershed with the steepest slopes occurring on the sides of hills, ridges, and valleys. However, Figure 3-2 shows the largest concentration of steep slopes occurs in the transition zone between the eastern and the western halves of the watershed.

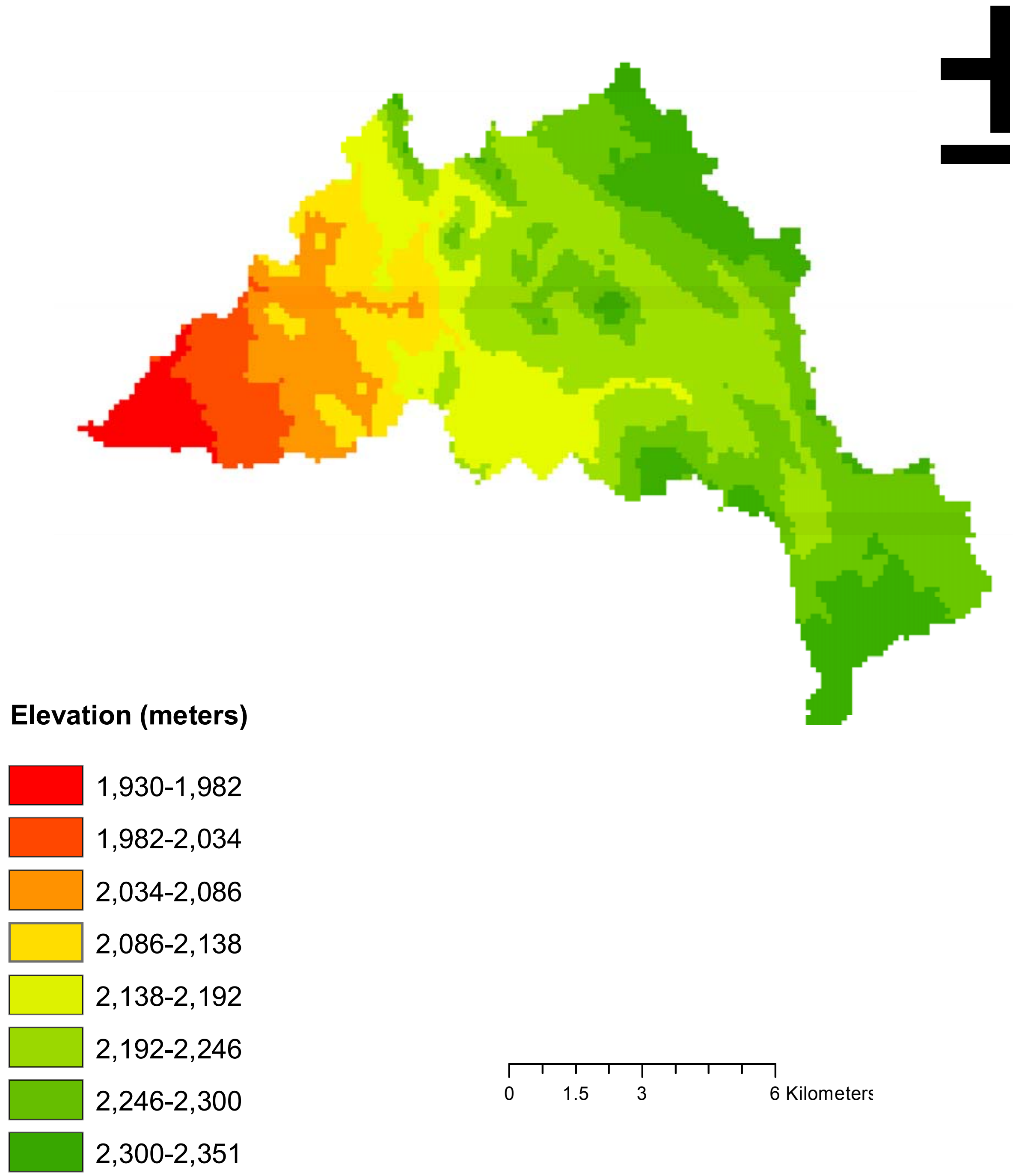

Figure 3-1. Elevation map of the Bar M watershed.

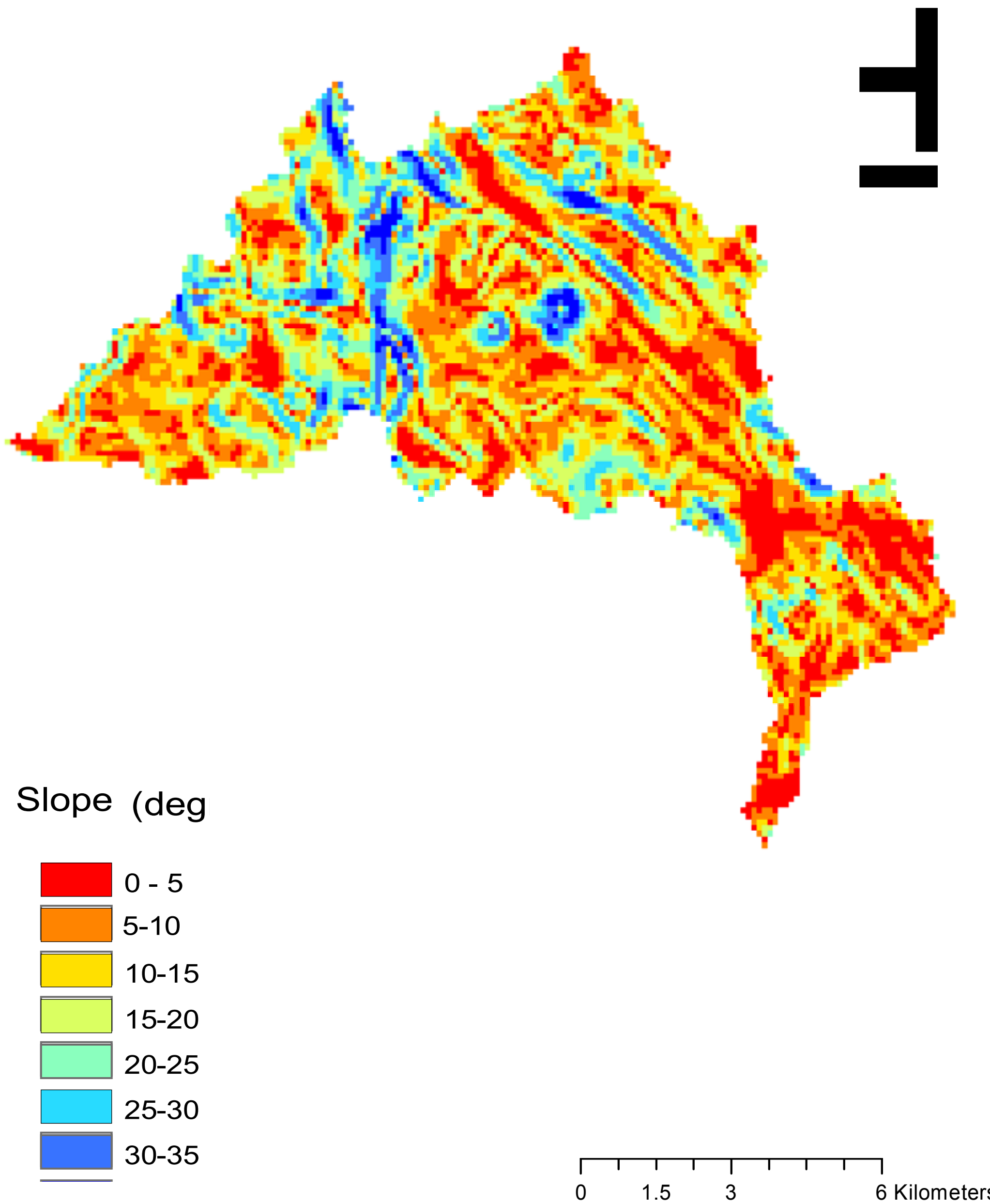

Figure 3-2. Slope map of the Bar M watershed.

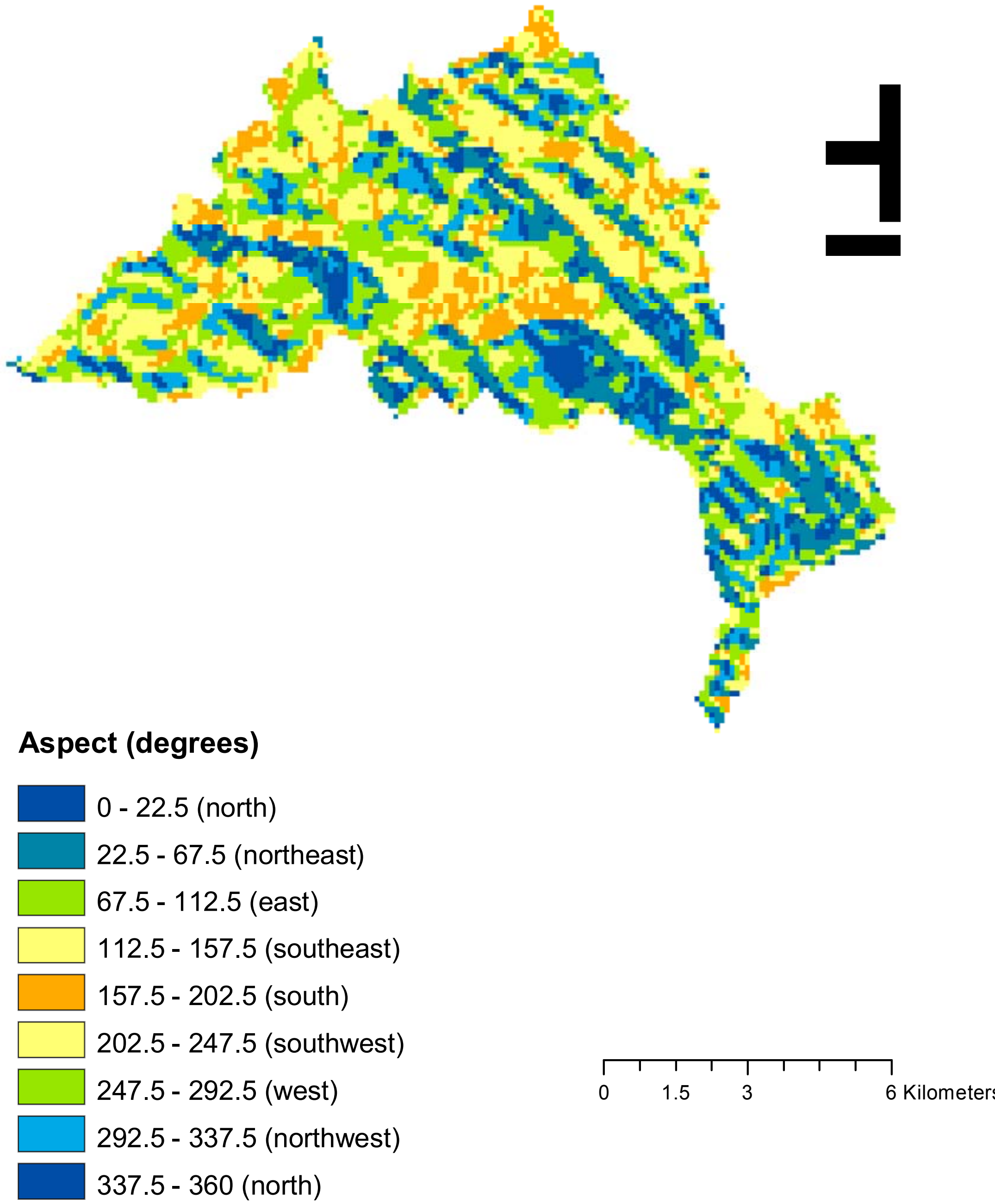

Figure 3-3 Aspect map of the Bar M watershed.

Analysis of the Bar M watershed aspect characteristics shown in Figure 3-7 reveals that the majority of the watershed is facing southwest, with its east and south east facing surfaces contributing the least space to the total surface area of the watershed. The GIS map in Figure 3-3 shows the spatial distribution of the aspect of the different parts of the Bar M watershed area.

The soil types and their distributions are derived from the Coconino National Forest Terrestrial Ecosystem Survey (TES) data (USFS, 1992). Figures 3-4 and 3-8 illustrate the spatial distributions of the different soil types by TES code and the proportion of the watershed covered by each of the soil type respectively. In addition the keys for the TES code are given in Table 3-2 and Appendex 3B.   Most of the soil textures on the Bar M watershed are of the loam or clay loam type (see Figure 3-8), and their depths in the watershed vary from approximately 50 to 124 centimeters (Williams and Anderson, 1967; USFS, 1992).

The values of the most important hydrologic parameters for the various TES soil units are given in Table 3-2. These parameters estimated from soil texture characteristics and used in the Green-Ampt infiltration equation. Rawls et al. (1983) and Rawls and Brakensiek (1985) computed the values for the effective porosity (ϕ), the wetting front suction ($|\psi|$), and the hydraulic conductivity (K_{sat}), using soil texture samples taken from approximately five thousand soil horizons. The values of the hydraulic parameters for the TES soils calculated by Rawls et al. (1983) are consistent with the range of values given to these soil parameters in the Beaver Creek watershed by Williams and Anderson (1967).

Table 3-2 Estimated hydrologic soil parameters for various TES soil units.

TES CODE (1)	Texture (2)	Depth (cm) (3)	Φ(cm) (4)	ψ (cm) (5)	Ksat(cm/s) (6)
50	clay	98	0.385	31.63	1.66667E-05
55	loam/clay loam	124	0.409	11.28	0.000152222
520	loam	80	0.434	8.89	0.000188889
565	loam	72	0.434	8.89	0.000188889
575	loam	50	0.434	8.89	0.000188889
579	clayloam/loam	61	0.365	15.49	8.80556E-05
582	loam/clay loam	109	0.415	10.69	0.000161389
584	loam	102	0.434	8.89	0.000188889
585	loam	61	0.434	8.89	0.000188889
586	loam	72	0.434	8.89	0.000188889

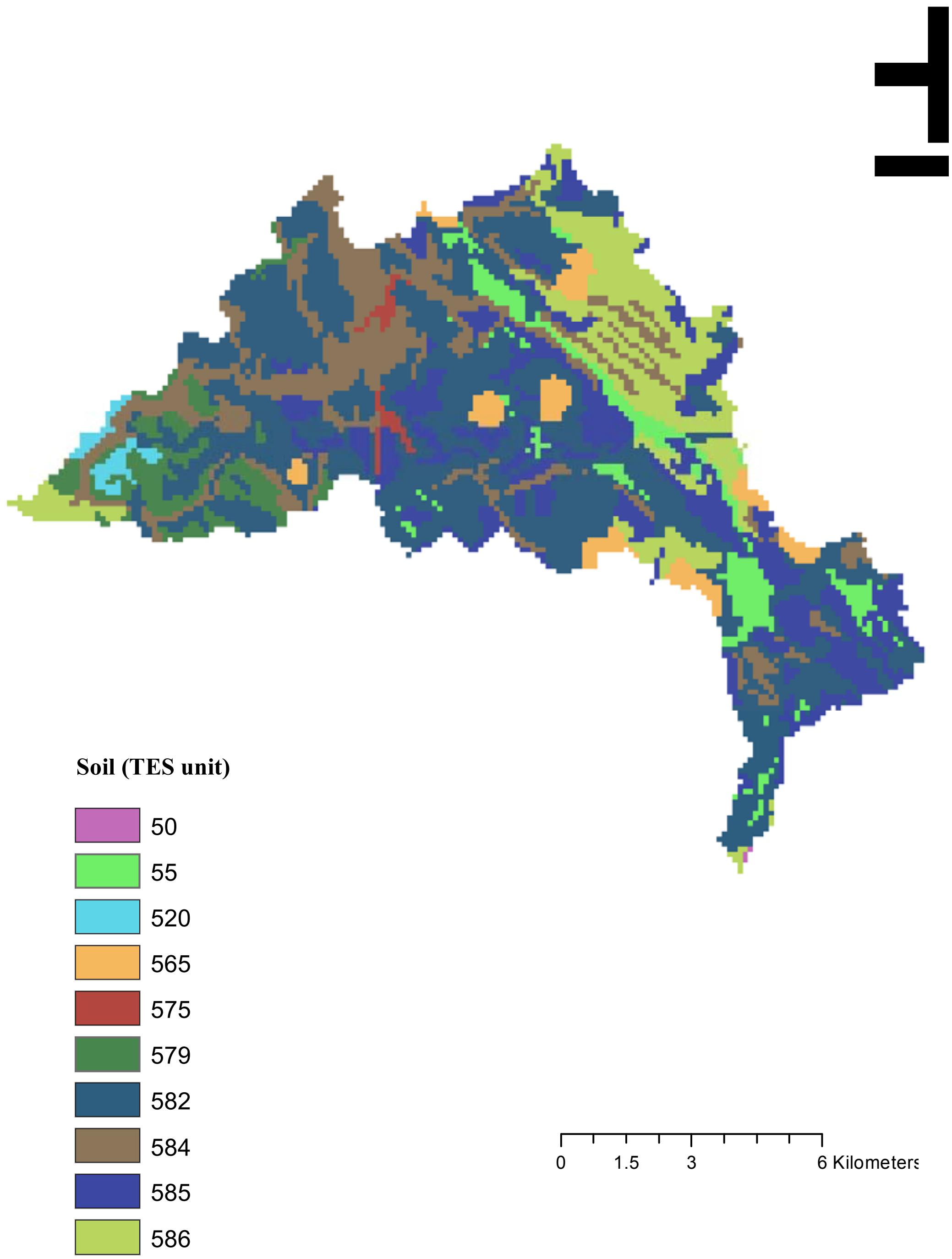

Figure 3-4 Soil (TES) map of the Bar M watershed.

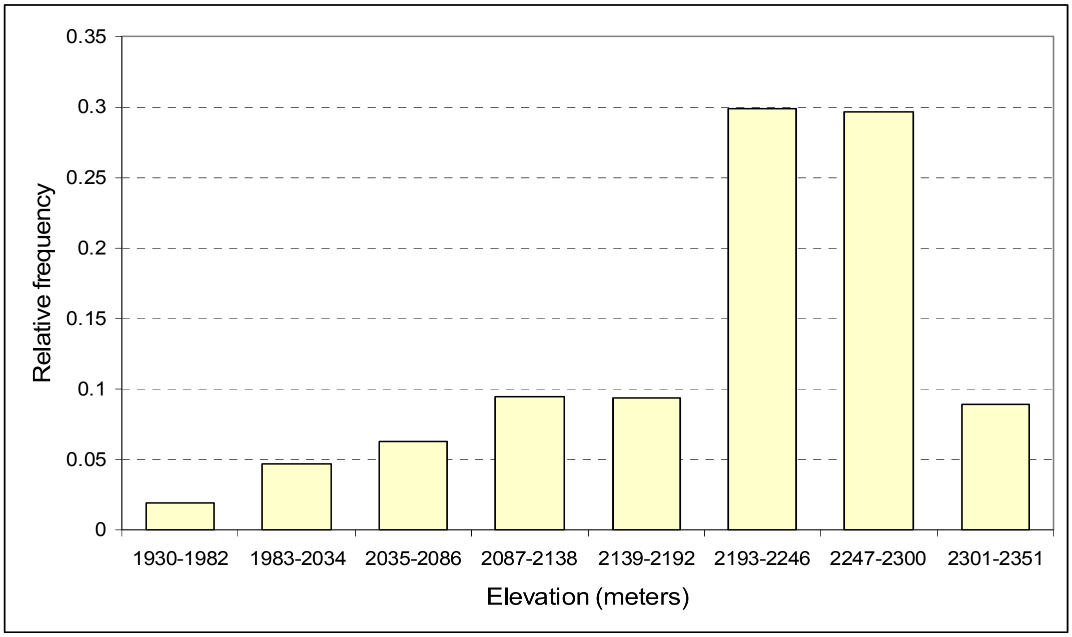

Figure 3-5. Relative frequency histogram of elevation.

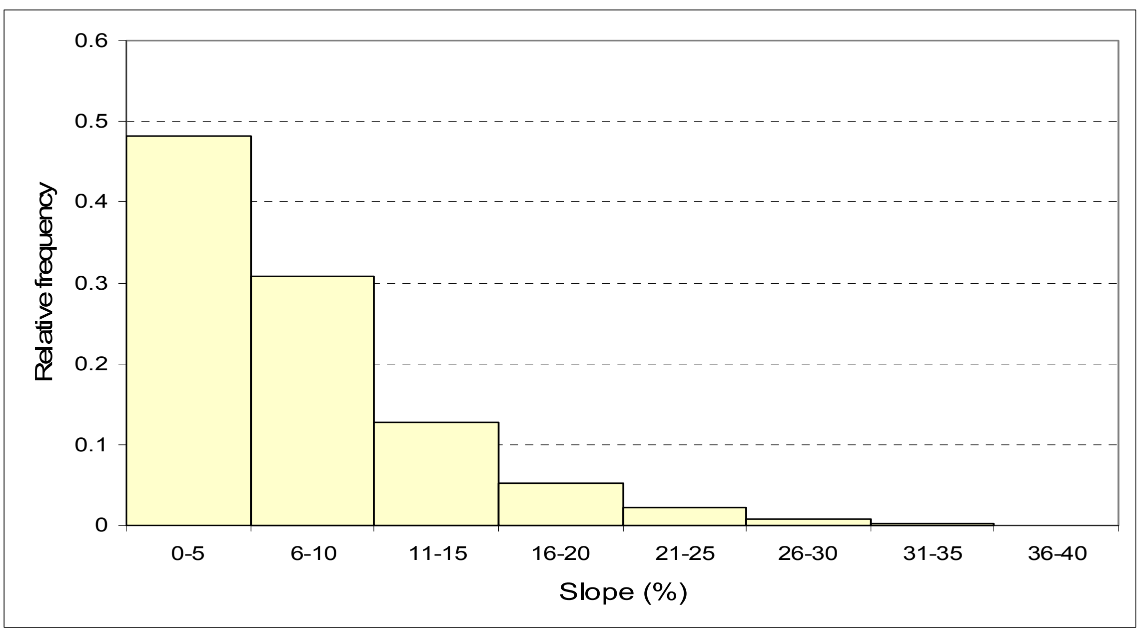

Figure 3-6. Relative frequency histogram of slope.

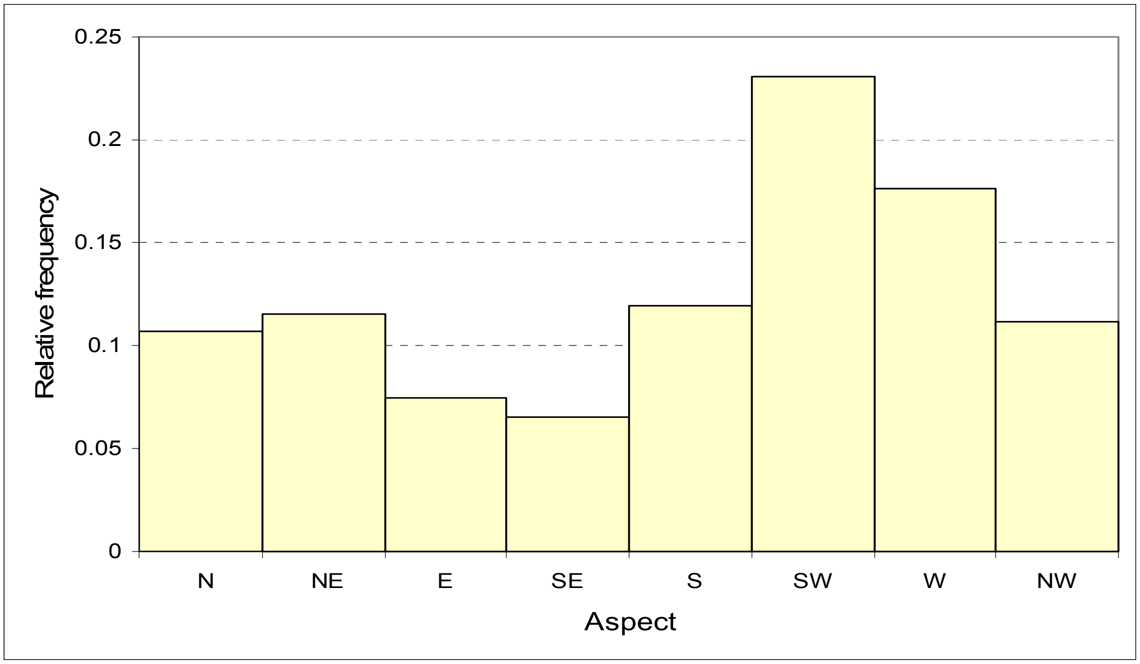

Figure 3-7. Relative frequency histogram of aspect.

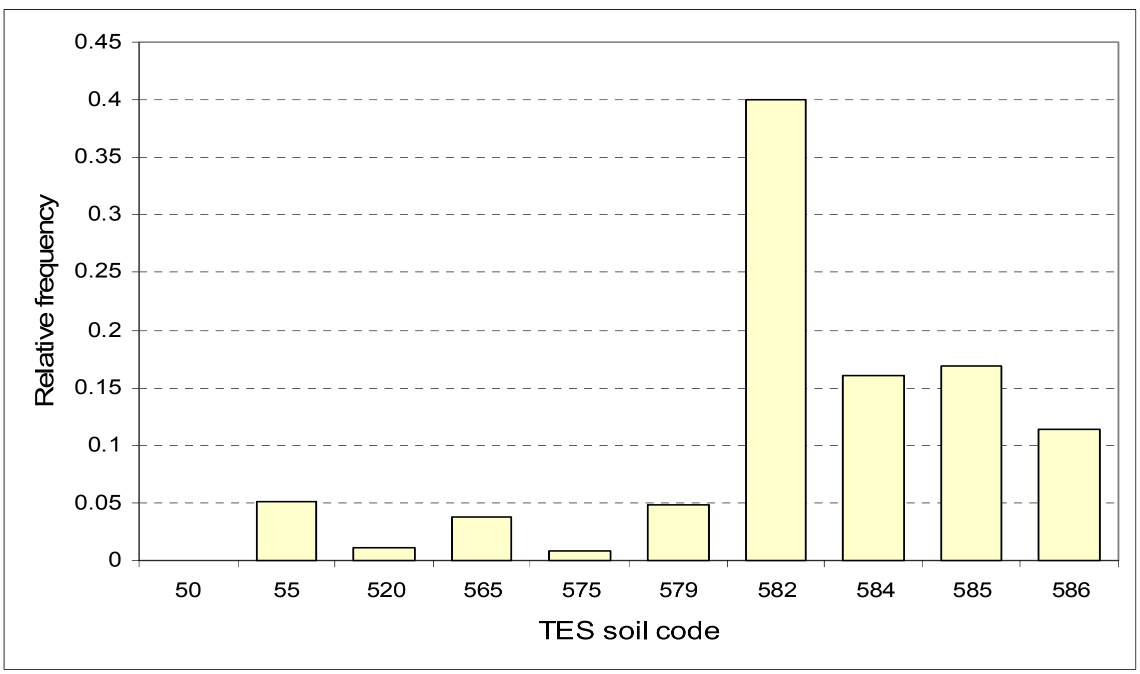

Figure 3-8. Relative frequency histogram of soil type.

The GIS map of the overstory cover and stand height of Bar M watershed are generated from a Forest ERA GIS map database of the Western Mogollon Rim study area. The spatial distribution of various overstory cover density levels is illustrated in Figure 3-10. The relative frequency distribution of the percent canopy cover density classes over the watershed is given in Figures 3-11. The cover density on most of the watershed ranges from thirty one to seventy percent. Two percent of the watershed has park-like openings with no overstory at all. Overall the watershed has the average canopy cover of forty six percent.

Figures 3-11 and 2-12 show a spatial distribution map and the relative frequency distribution histogram of the stand height in Bar M watershed, respectively. The stand height map of the watershed revels that more than 95 percent of the stands consist of trees with height that range from 12 to 18 m. The average stand height in the watershed is 14 m.

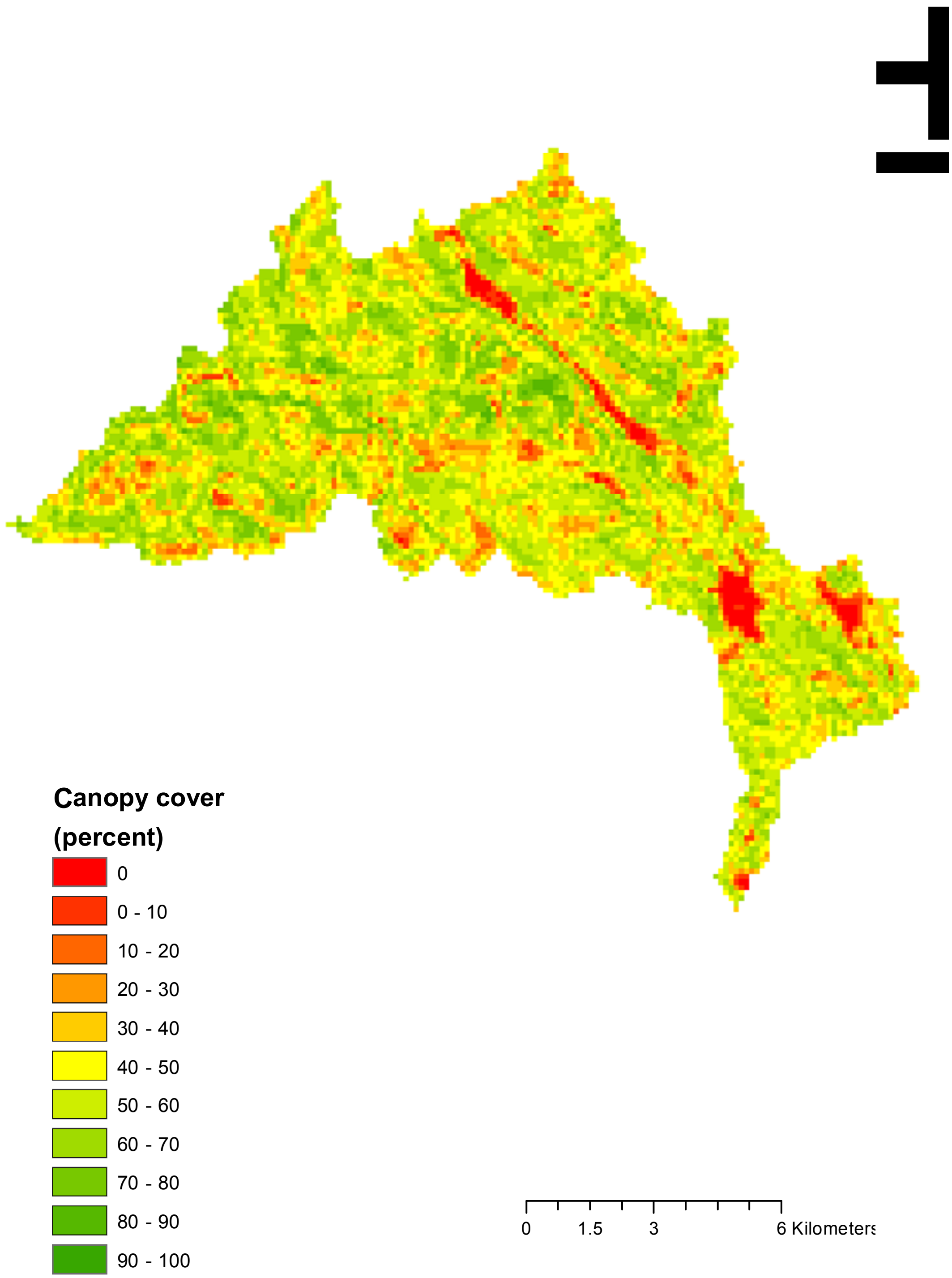

Figure 3-9. Overstory cover map of the Bar M watershed.

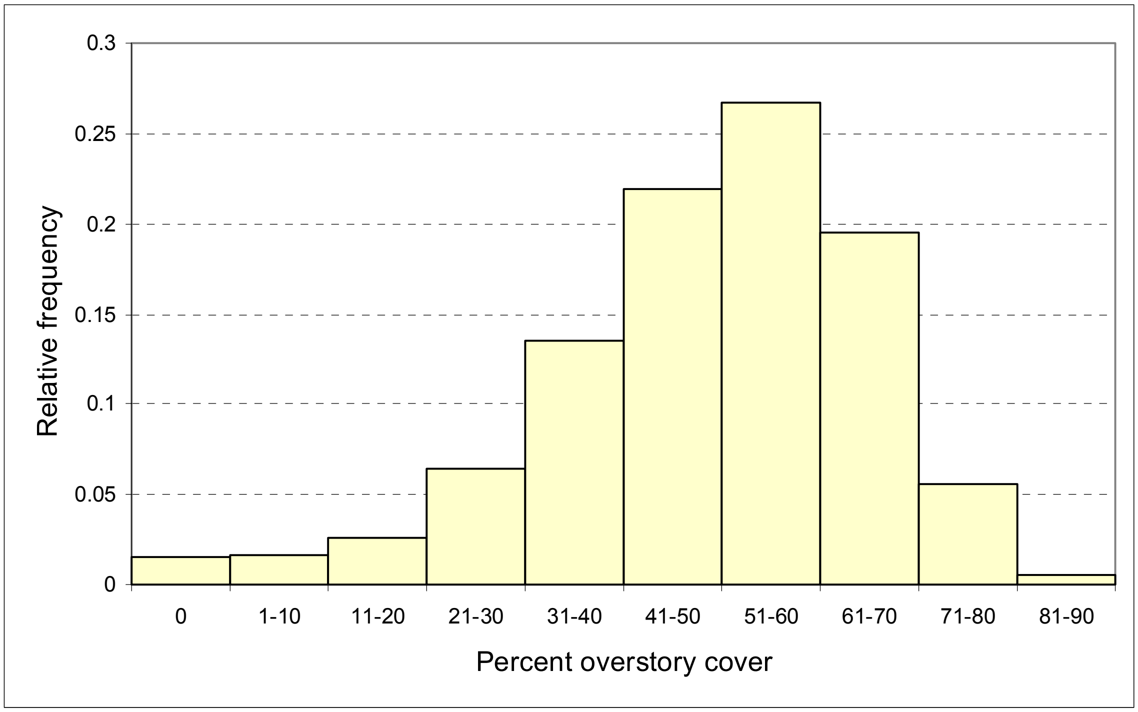

Figure 3-10. Relative frequency histogram of the overstory cover

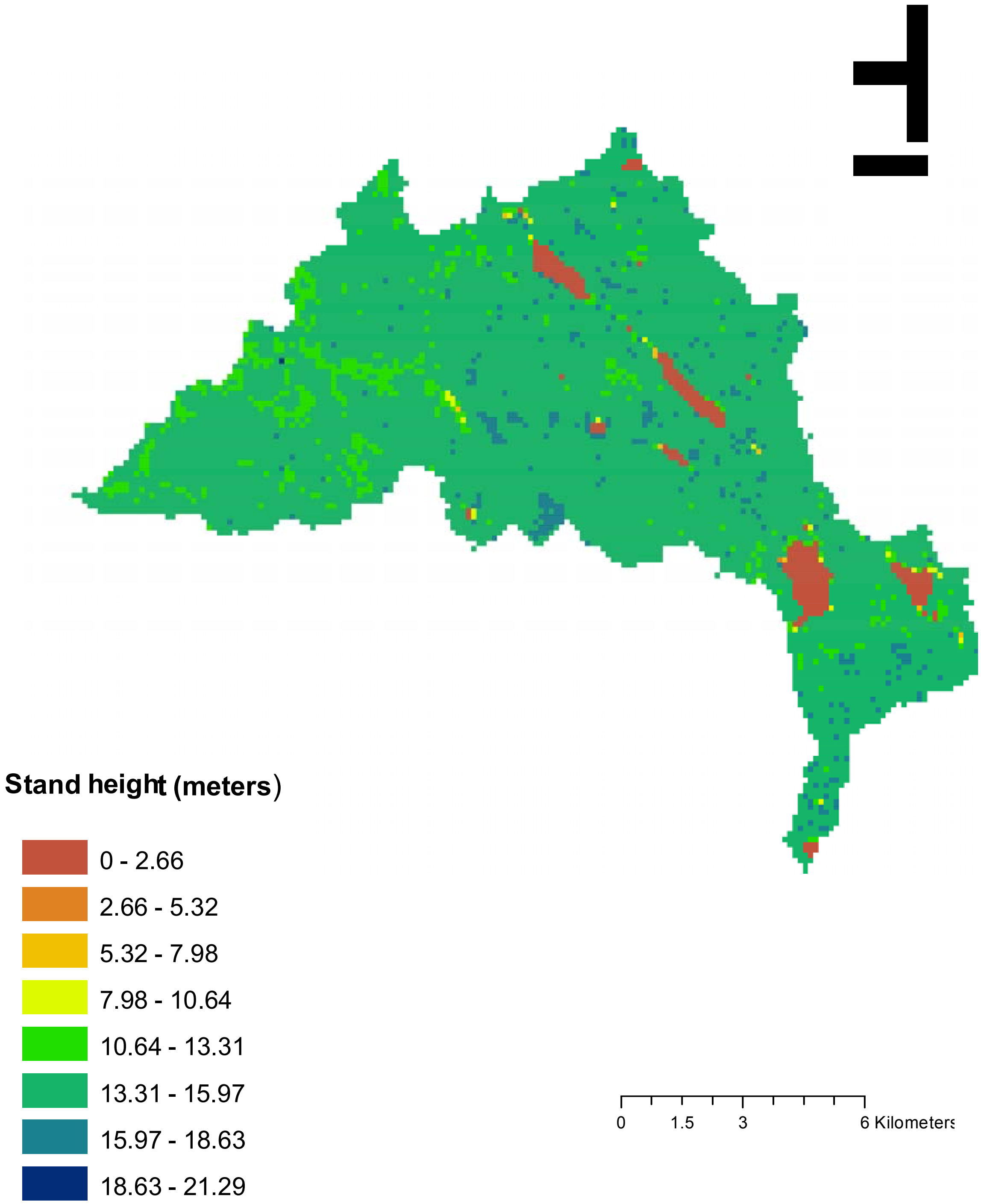

Figure 3-11. Stand height map of the Bar M watershed.

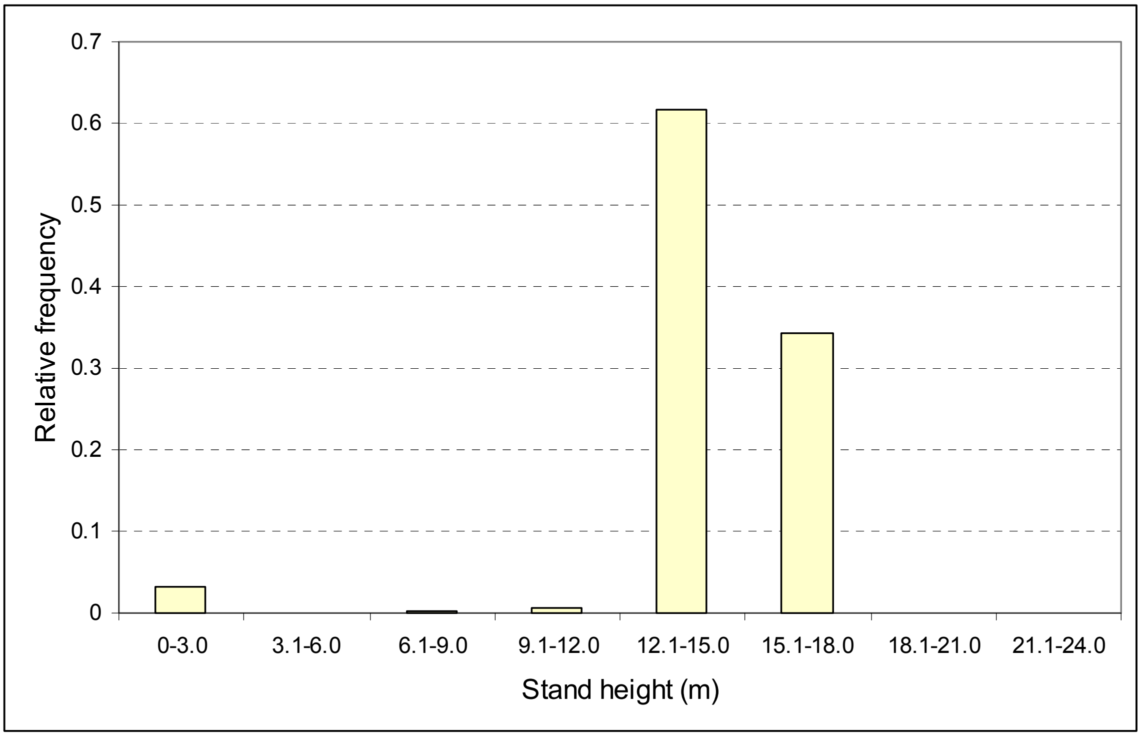

Figure 3-12. Relative frequency histogram of stand height.

Water Yield Model Result

The amount of water yield is estimated using a water balance model which takes the precipitation simulated in chapter two as its main input. The biophysical characteristics of the watershed that are important to calculate the various outputs of the water balance model, were discussed earlier in this chapter. Evaporation, transpiration, and infiltration are considered the main outputs of the water balance model for both cold and warm seasons.

We calculated the values of potential evapotranspiration using the Penman-Monteith approach but actual evapotranspiration must be used to accurately estimate water yield. During the cold-season, potential evapotranspiration compares reasonably well with the actual one while, in the warm-season, potential evapotranspiration is much higher than the actual evapotranspiration. This is because potential evapotranspiration models represent water loss from well-watered soil conditions where there is no restriction on the rate of evapotranspiration from the watershed (Ward and Elliot, 1995). Fisher et al. (2005) estimated the potential evapotransporation from the ponderosa pine watersheds in the Sierra Nevada Mountains of northern California using five models that include the Penman-Monteith. They compared the estimated potential evapotranspiration with the measured values. The result found using the Penman-Monteith approach showed that on the average the actual evapotranspiration is equal to 80 percent of the potential. For our study, we multiplied the potential values by 80 percent to estimate the actual values.

Since canopy interception values make up only a small portion of the amount of water stored in the watershed system, they are not considered in the water balance analysis. This is because most of the water or snow intercepted by plants is either evaporated while it is in the canopy or infiltrated after it falls to the ground.

The amount of water yield was estimated one time for each season on a daily basis by subtracting the outputs from the inputs of the water balance equation, and a GIS map was constructed to show the spatial distribution of the water yield values across the watershed. In addition, the efficiency of the Bar M watershed to convert precipitation into surface runoff was determined by comparing the simulated precipitation with the estimated water yield. Finally, to verify the reliability of the model, the total seasonal amount of the simulated water yield was compare with the average measured stream flow at the outlet of the watershed.

Cold- season

For the cold-season, the precipitation on the particular day, when the water balance is calculated, and the snowmelt from the snow in the previous days are considered as the inputs into the water balance models. The simulated precipitation for one season and the resulting amount of water yield are shown in Figures 3-13 and 3-14, respectively. In the figures, day zero corresponds to the day before the beginning of the season, September 30 and day 212 is the last day of the season, April 30. As shown in the figures, there are large amounts of water yield during days of high amount of precipitation. Runoff was observed in days right after the precipitation days due to snowmelt. The total seasonal amount of simulated precipitation is 472 mm while the amount of water yield produced from this precipitation is only 105 mm, which is 22.22 percent of the total precipitation. On the other hand, the measured seasonal average amount of cold-season stream flow is 37 percent. According to Baker (1982) the average amount of precipitation converted to runoff in the Beaver Creek watersheds is 22 percent which is similar to the results of the simulation in this research. The distribution of the simulated daily water yield over the season also compared well with the twenty year average observed one shown in Figure 3-15. There is a difference between the water yields estimated using this model and the actual measured stream flow at the out let of the watershed. There are many factors that contribute to this discrepancy. Error in measuring the actual evapotranspiration accurately, lack of soil water content, and use of measured hydrologic variables to simulate outputs are some of the factors.

Since the model simulates precipitation events as random, the events seem to be distributed evenly during the season. But in the actual case, most of the runoff producing cold-season precipitation events in the study area fall from December to March. Because of this, large amounts of runoff were measured during these months. In addition, winter season snow stays in the ground for many days and thus producing runoff from snowmelt sometimes till April and May.

The spatial distribution of the total cold-season water yield is shown in Figure 3-16, which seems to indicate that the runoff produced by each cell in the watershed is highly variable. There are many reasons for the variability in the amount of runoff such as density of forest, soil type, precipitation distribution, aspect, and elevation. In general, open areas located farther north, at higher elevation and on south facing slopes produce more runoff (see Figure 3-16).

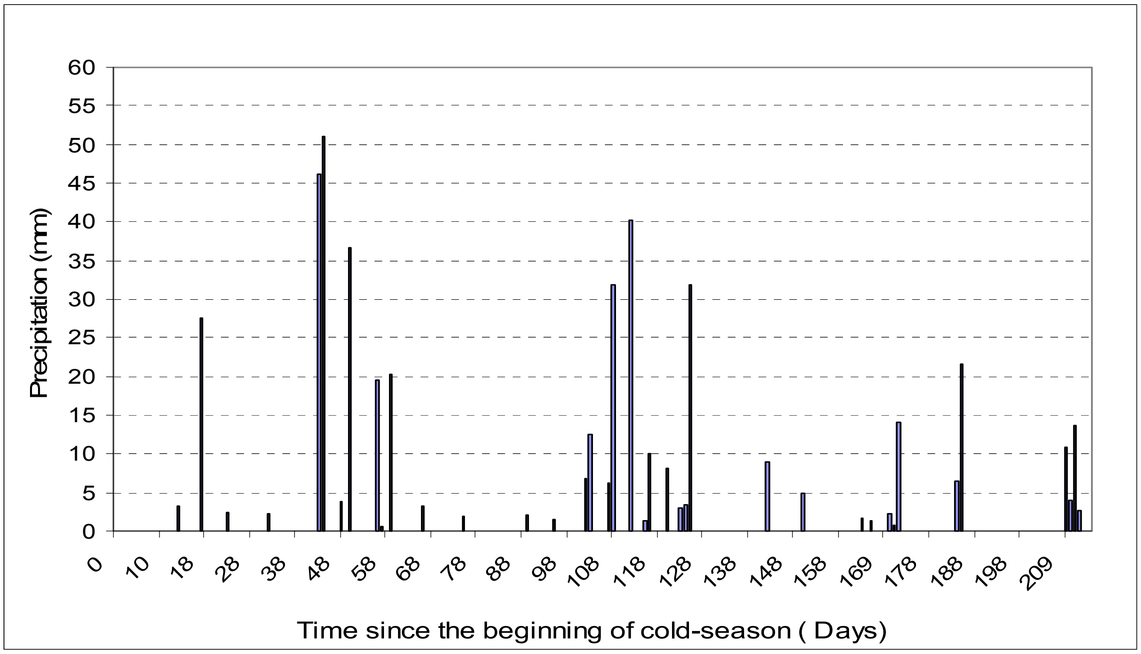

Figure 3-13. Simulated daily precipitation vs. time for one cold-season.

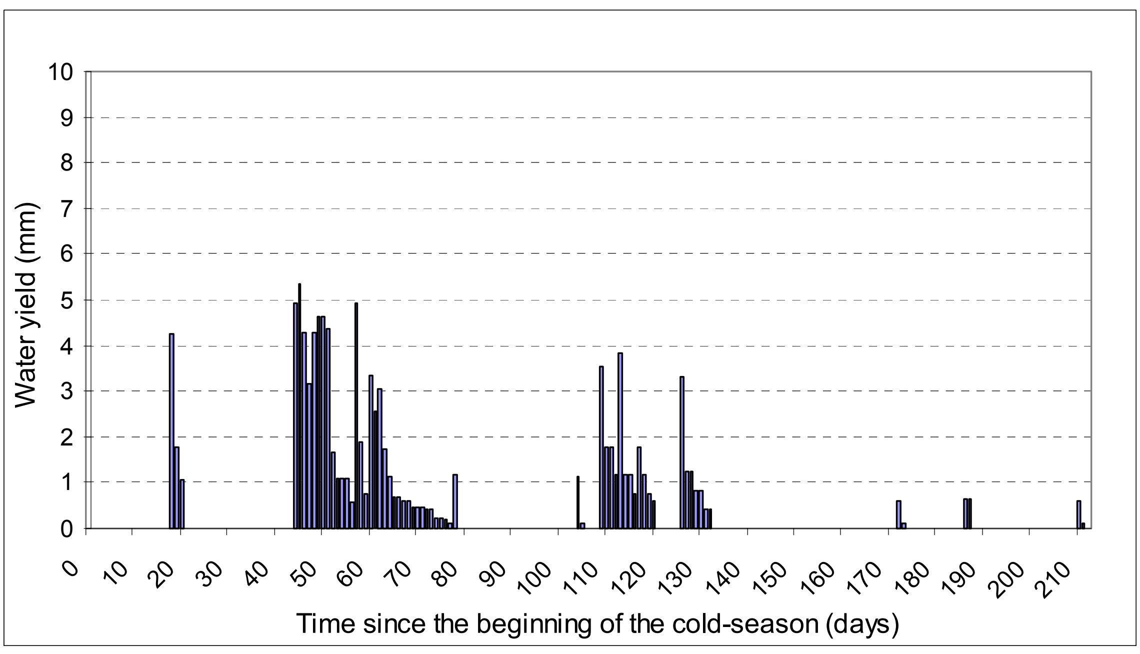

Figure 3-14. Simulated daily water yield vs. time for one cold-season.

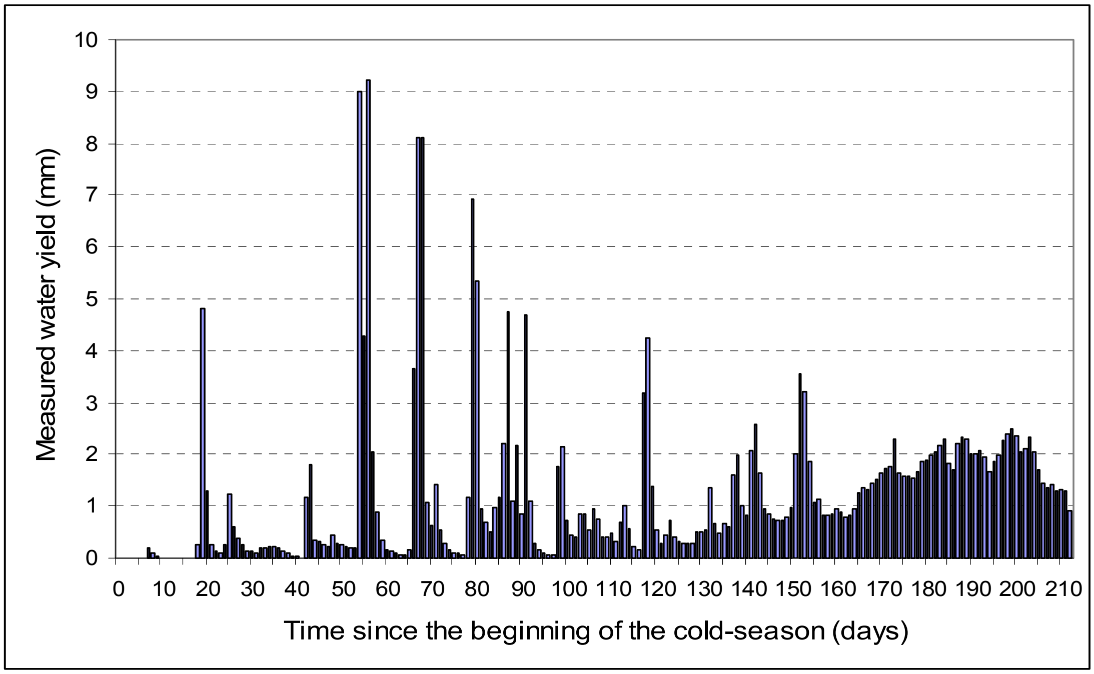

Figure 3-15. Twenty year average measured daily stream flow for the cold-season.

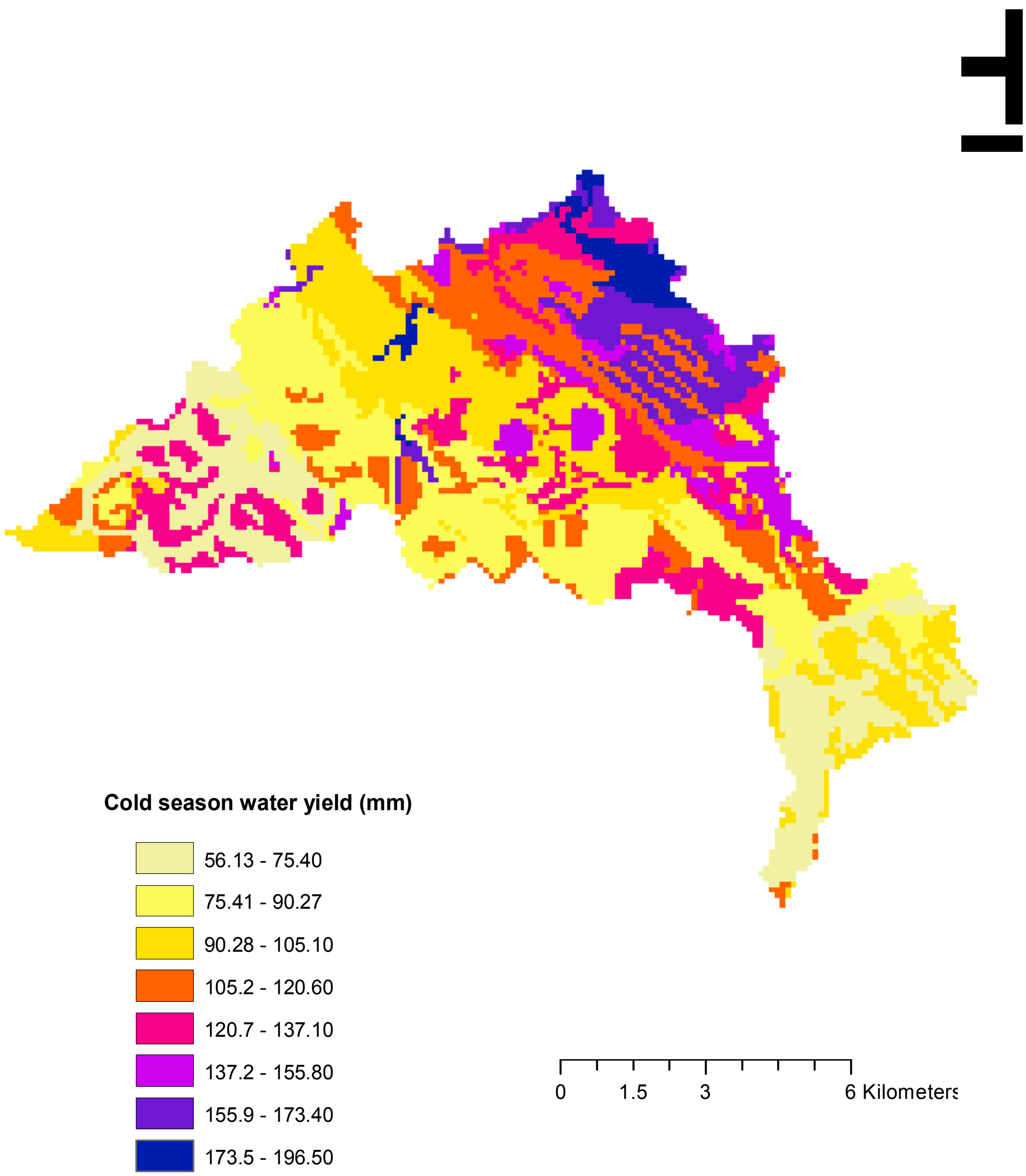

Figure 3-16. Spatial distribution of cold-season water yield in the Bar M watershed.

Warm- season

Unlike the cold-season, the input into the warm-season water balance model is only daily precipitation. The daily simulated precipitation amounts for one season and the resulting amounts of water yield are shown in Figures 3-17 and 3-18, respectively. In the figures, day zero corresponds to April 30, one day before the beginning of the warm-season and day 153 is September 30, the end of the summer season. As shown in the figures, there was runoff produced only for four days during the entire season where there were larger precipitation amounts. The reason for the very small number of days with runoff is mainly because of the absence of days with large amounts of precipitation events and higher loss of water through evapotranspiration. The total simulated warm-season precipitation amount is 226 mm while the water yield produced from this precipitation is 4.3 mm which is 1.9 percent of the total precipitation, while the recorded average seasonal amount of warm-season stream flow is 2.38 percent.

According to Baker (1982) the average amount of precipitation converted to runoff in the Beaver Creek watersheds is 2 percent which approximately equal to the results obtained in this research. But there is a large difference between the water yield estimated using this model and the actually measured stream flow at the outlet of the watershed.

Warm-season precipitation is also considered and analyzed as a random process. Due to this, precipitation events seem to be distributed randomly through out the season and only precipitation events of larger magnitudes produce significant amounts of runoff. But in the actual case, most of the summer runoff comes mainly from the residual snow melt from the previous cold season snow (see Figure 3-19). Because of this, large amounts of runoff in the warm-season are measured during the first months of the season.

The spatial distribution of the total warm-season water yield is shown in Figure 3-20, which shows that the runoff produced by each cell in the watershed is highly variable. There are many reasons for the variability of runoff such as density of forest, soil type, precipitation distribution, aspect, and elevation. In general, open areas located further east , at higher elevation, in south facing slopes produce more runoff than others.

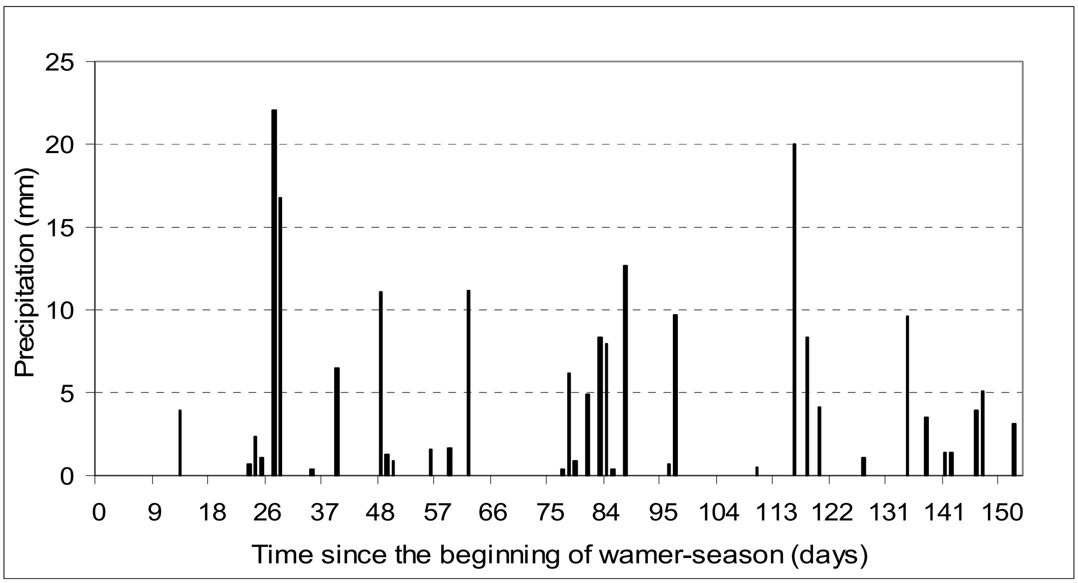

Figure 3-17. Simulated daily precipitation vs. time for one warm-season.

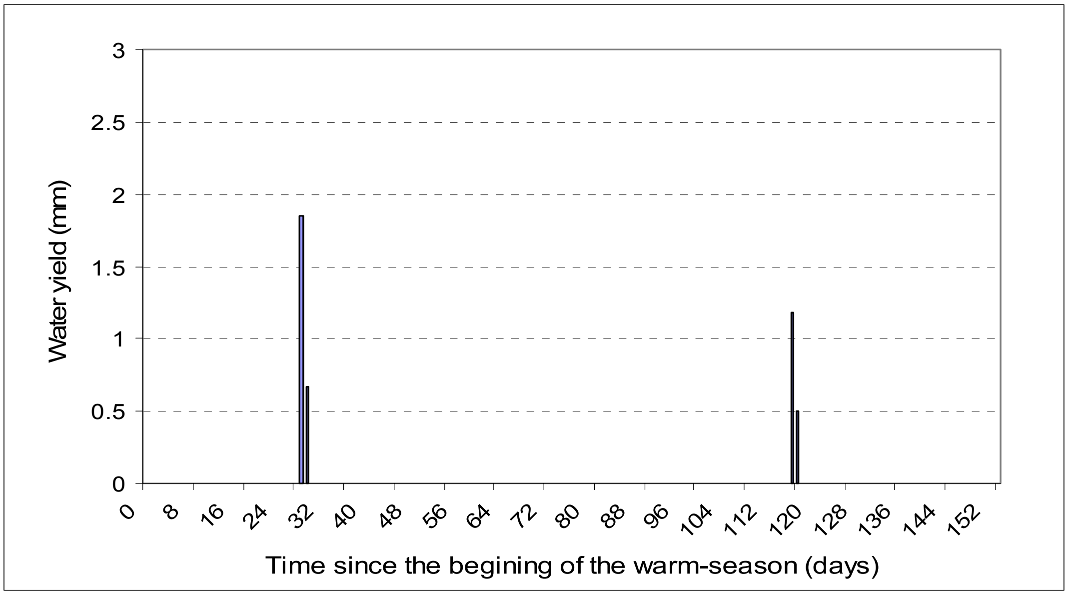

Figure 3-18. Simulated daily water yield vs. time for one warm-season.

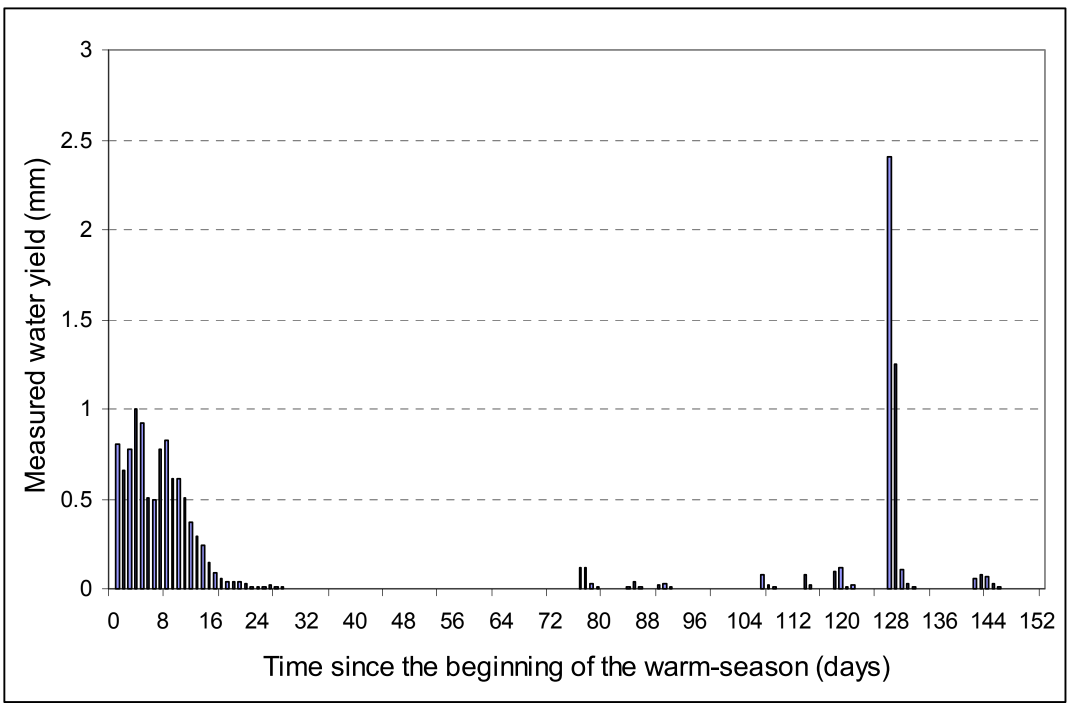

Figure 3-19. Twenty year average measured daily stream flow for the warm-season.

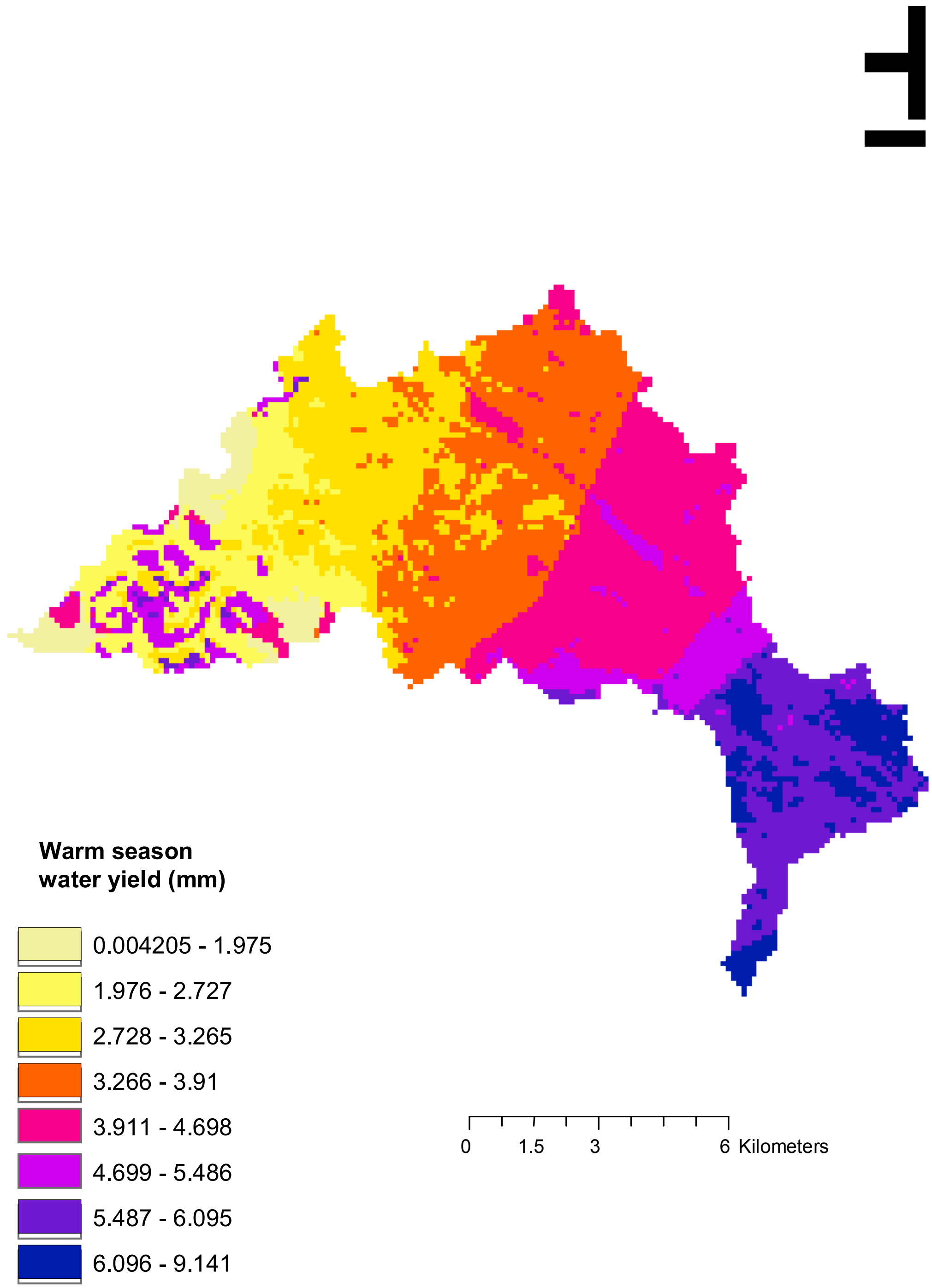

Figure 3-20. Spatial distribution of simulated warm-season water yield

Summary and conclusions

Deterministic daily water yield models are developed for cold and warm seasons for use on an upland ponderosa pine type watershed in north-central Arizona. The models use a GIS software to illustrate the spatial distribution of watershed characteristics. The use of GIS enables description of the study watershed as a grid composed of thousands of microwatersheds, or cells. Watershed characteristics, such as elevation, slope, aspect, soil type, and canopy cover, are defined for each individual cell and each characteristic is assumed to be spatially homogeneous across a cell.

A water balance approach is used to determine the water yield and to account for the inputs, outputs, and changes in soil storage of water in each cell. The most important hydrological processes considered in developing the model are canopy interception, evaporation, transpiration, infiltration and snow accumulation and melt. Various reliable equations were tested and used by others to determine these processes. The amount of water yield generated from the entire watershed is determined by first computing the runoff for each cell on a daily basis. Then the runoff from each cell is routed downstream in a cascading fashion until it reaches the watershed outlet. Finally, the daily runoffs produced from each cell are summed over the entire cold and warm-seasons to determine the total seasonal amount of water yield in each season from the watershed.

Though the models enable us estimate the amounts of water yield reasonable well, they have some problems. One of the main problems of the models is length of time required to run the models. The reasons for the long time requirement are first the water yield is synthetically generated at the cell level and there are thousands of cells in the watershed, second the models require estimation of the various input and output components of the water balance model individually, and their spatial description of the various watershed, climatic, and hydrologic characteristics involved in the water yield estimation.

The second problem in this modeling process is availability of data. For example solar radiation data are found by taking the average daily amount that was collected for two years near the study area. The solar radiation in a particular day is then estimated by taking the two year average amount for that day. This results in underestimating the amount of insolation during clear sky days, while over estimating the amount of insolation on wet and cloudy days. The soil moisture data consists of the nine month data collected by the School of Forestry in the Centennial Forest, near Flagstaff and differentiating values for wet and dry days was not easy. Some constant parameters used to calculate the various outputs component of the water balance model are adopted from other books and research papers.

In a forested watershed system, evapotranspiration is one of the main components of a water balance model. Hence, proper assessment of both evaporation and transpiration is important to accurately estimate the water yield. In this study, The potential evapotranspiration from the watershed was calculated using the Penman-Monteith equation and multiplied the result by 0.8 to estimate the actual evapotranspiration from the watershed. But the ratio of the actual to the potential evapotranspiration is variable form day to day depending on the moisture, temperature and other climatic conditions. Hence, there should be some way to accurately estimate the actual evapoteanspiration in order to get better water yield values.

Also estimation of water yield on a daily basis has some problems related to estimating the daily values of the inputs and outputs of the models and these problems are prominent in the warm-season water yield. The input, in this case the precipitation occurs within a short time period while the movement of the water produced from the system takes a much longer time through evaporation, transpiration, infiltration, and runoff. For example, if the rain falls at 5 pm., the output from that day should be only all the losses that occure after 5 pm. However, in this modeling all the losses before and after 5 pm. are considered as the losses for that day. This underestimates the water yield by deducting outputs from non existing input.

Generally the amount of water yield from a watershed in a particular season is affected by the climatic conditions in the previous seasons. This model, however, estimates the seasonal water yield independent from conditions in previous seasons. This should be acceptable because there are permanent flows in the study area.

Though the study examines the ability of the models to predict the total amount of cold and warm-seasons water yield at the watershed outlet, the problem of model performance on a daily basis is not yet fully explored. Because the different model components are difficult to test on a daily basis due to lack of data availability such as daily soil moisture content, snowpack depth and evapotranspiration. Furthermore, complete verification of the spatial distribution of the model generated results are difficult because of lack of adequate spatial data such as soil moisture, radiation, vegetation characteristics.

Overall, this study has resulted in a physically-based and spatially-varied, water yield model that accounts for the majority hydrologic processes involved in estimating the amount of water yield from an upland ponderosa pine type watershed with out being over complex. However, there still remains some work that needs to be done as described above before the water yield model developed in this study can be made fully operational.

Literature cited

Ambach, W., 1988. Interpretation of the positive degree-days factor by heat balance characteristics-West Greenland, Nordic Hydrology, 19, pp 623-625.

Anderson, E.A., 1976. A point energy and mass balance model of a snow cover, NOAA Technical Report NWS 19.

Arizona Image Archive, http://landsat.ece.arizona.edu/, Accessed May 10, 2005.

Ashton, P.G., 1966. Factor affecting snow evaporation in the white mountain Arizona, Master's thesis, University of Arizona, Tucson, Arizona.

Baker, M.B. Jr., 1982. Hydrologic regimes of forested areas in the Beaver Creek Watershed, USDA Forest Service General Technical Report Rm-90, Rocky Mountain Forest and Range Experiment Station , Fort Collins, Colorado.

Baker, M.B. Jr., 1986. Effects of ponderosa pine treatment on water yield in Arizona, Water Resource Research, 22(1), pp. 67-73.

Baker, M.B. Jr., 1999. History of watershed research in the central Arizona Highlands, USDA Forest Service General Technical Report, RMRS-GTR-29. Fort Collins, CO: Rocky Mountain Forest and Range Experiment Station.

Baker, M.B. Jr., and H.E. Brown, 1974. Multiple use evaluations on ponderosa pine forest land, 18th Arizona Watershed Symposium, Report No 6.

Barnes, V.B., D.R. Zak, S.R. Denton and S.H. Spurr, 1998. Forest Ecology, Forth edition, John Wiley and Sons, Inc., USA.

Barr, G.W., 1956. Recovering rainfall, Department of Agricultural Economics, University of Arizona, Tucson, Arizona.

Beschta, R.L., 1976. Climatology of the ponderosa pine type in central Arizona, Technical Bulletin 228, Agricultural Experimental Station, College of Agriculture, University of Arizona, Tucson, Arizona.

Bonell, M., 1993. Progress in the understanding of the runoff generation dynamics in forest, Journal of Hydrology, 150, pp. 217-275.

Brown, H.E., M.B. Baker Jr., J.J. Rogers, W.P. Clary, J.L. Kovener, F.R. Larson, C.C. Avery, and R.E. Campbell, 1974. Opportunities for increasing water yiel and other multiple use values on ponderosa pine forest lands, USDA Forest Service General Technical Report Rm-129, Rocky Mountain Forest and Range Experiment Station , Fort Collins, Colorado.

Brutsaert W., 1975. On a derivable formula for long wave radiation from clear skies, Water Resource Research, 11, pp. 742-744.

Burman, R., and L.O. Pochop, 1994. Evaporation, Evapotranspiration and climatic data, University of Wyoming, Laramie, Wyoming, USA.

Campbell, R.E., and M.G. Ryan, 1982. Precipitation and temperature characteristics of forested watershed in central Arizona, USDA Forest Service General Technical Report Rm-93, Rocky Mountain Forest and Range Experiment Station , Fort Collins, Colorado.

Campbell, R.E., and O.G. Stevenson, 1977. Solar radiation measurement in northern Arizona, USDA Forest Service Research note Rm-339, Rocky Mountain Forest and Range Experiment Station , Fort Collins, Colorado.

Combs, S.T., L.Y. Bowie, and J.C. Tello, 1988. Investigation of the response of a large watershed to changes in vegetation: Development of the WTRYLD simulation model, in Proceedings of the ASAE International Symposium on modeling Agriculture, forest, and rangeland hydrology, Chicago, Illinois.

Deguchi, A., S. Hattori, and H.T. Park, 2006. The influence of seasonal changes in canopy structure on interception loss: Application of the revised Gash model, Journal of Hydrology, 318 pp. 80-102.

Desta A., and A. Tecle, 2005. Restoration capability of the former Beaver Creek watershed. Hydrology and Water Resources in Arizona and the Southwest. Vol.35. pp.1-6

Dickinson, R.E., A.H. Sellers, P.J. Kennedy, and M.F. Wilson, 1986. Biosphere/atmosphere transfer scheme (BATS) for the NCAR community climate model, NCAR Technical Note, TN275, National Center for Atmospheric Research, Boulder, Colorado.

Dickinson, R.E., A.H. Sellers, C. Rosenzewig, and P.J. Sellers, 1991. Evapotranspitration model with canopy resistance for use in climate models, Agriculture and Forest Meteorology, 54, pp. 373-388.

Dingman, S.L., 1994. Physical hydrology, Macmillan College publishing Company, New York.

Famiglitti, J.S., 1992. Aggregation and scaling of spatially-variable hydrological processes: Local, catchment-scale and macro scale models of water energy balance, Ph.D dissertation, Princeton University, Princeton, New Jersey.

Famiglietti, J.S., and E.F. Wood, 1994. Multiple modeling of spatially variable water and energy balance processes, Water Resource Research, 30 (11), pp 361-3078.

Ffolliott, P.F., M.B. Baker, Jr., and V.L. Lopes, 2000. Watershed management perspectives in the Southwest: past, present, and future. Pp. 30-36 in: Land Stewardship in the 21st Century: the contributions of watershed management; March 13-16, 2000, Tucson, AZ; USDS Forest Service Proceedings RMRS-P-13. Fort Collins, CO: Rocky Mountain Research Station.

Ffolliott, P.F., and G.J. Gottfried, and M.B. Baker, Jr., 1989. Water yield from forest snowpack management: research findings in Arizona and New Mexico, Water Resources Research , 25(9), pp. 1999-2007.

Ffolliott, P.F., and P. Guertin, 1988. Yield II: an interactive computer model to simulate water yield from southwestern ecosystems , in proccedings of the ASAE International symposium on modeling agriculture, forest, and rangeland hydrology, Chicago Illinois.

Ffolliott, P.F., and E.A. Hansen, 1968. Observations of snowpack accumulation, melt, and runoff on small Arizona watershed. USDA Forest Service Research Note Rm-124, Rocky Mountain Forest and Range Experiment Station , Fort Collins, Colorado.

Ffolliott, P.F., and D.B. Thorud, 1969. Snowpack density water content and runoff on a small Arizona watershed, in proccedings of the western snow conference, 37 pp 12-18.

Ffolliot, P.F., and D.B. Thorud, 1972. Use of forest attributes in snowpack inventory-prediction relationships for Arizona ponderosa pine, Journal of Soil and Water Conservation, 27, pp. 109-111.

Ffolliott, P.F., and D.B. Thorud, 1974. Vegetation management for increased water yield in Arizona. Technical Bulletin 215, Agricultural Experiment Station, University of Arizona, Tuscon, pp. 38-45.

Ffolliott, P.F., and D.B. Thorud, 1975. Water yield improvement by vegetation management: focus on Arizona, Paper PB-246 005, U.S. Department of Commerce, National Technical Information Service , Washington D.C.

Fisher, J.B., A.D. Terry, Y. Qi, M. Xu, and H.G. Alen., 2005. Evapotranspiration models compared on a Serra Nevada forest ecosystem, Environmental modeling and software 20, pp. 783-796.

Forest ERA, Forest Ecosystem Restoration Analysis http://www.forestera.nau.edu/data_foundational.htm, Last update May, 2005.

Gottfried, G. J., and P.F. Ffolliott, 1980. An evaluation of snowmelt lysimeters in an Arizona mixied conifer stand, hydrology and water resources in Arizona and the southwest, 10, pp. 221-229.

Granger, R.J., and D.H. Male, 1978. Melting of a prairie snowpack, Journal of Applied Meteorology, 17, pp. 1833-1842.

Gray, D.M., and T.D. Prowse, 1992. Snow and floating ice, in Handbook of hydrology, edited by David R. Maidement, Mc-Graw Hill, Inc., New York.

Green, W.H., G.A. Ampt, 1911. Ampt Studies in soil physics, I, Flow of air and water through soils, Journal of Agricultural Science, 4(1) pp. 1-24.

Hanson, W.T., and P.F. Ffolliott, 1968. Observations of snow accumulation and melt in demonstration cuttings of ponderosa pine in central Arizona, USDA Forest Service Research Note Rm-111, Rocky Mountain Forest and Range Experiment Station , Fort Collins, Colorado.

Hanes, W.T., M.M. Fogel, and L. Duckstein, 1977. Forecasting snowmelt runoff: probabilistic model. Journal of the irrigation and drainage division, ASCE, 103 (IR3), pp. 343-355.

Hibbert, A.R., 1979. Vegetation management to increase flow in the Colorado River Basin, USDA Forest Service General Technical Report Rm-66, Rocky Mountain Forest and Range Experiment Station , Fort Collins, Colorado.

Hodgman, C.D., R.C. Weast, and S.M. Selby (eds.), 1958. Handbook of Chemistry and Physics, Chemical Rubber Publishing Co., Cleveland, Ohio.

Jarvis, P.G., 1976. The interpretation of the variations in leaf water potential and stomata conductance found in canopies in the field, Phil. Trans. R. Soc. Lon., Ser. B, 273, pp. 593-610.

Jianbiao Lu, G. Sun, G. M. Steven, and M. A. Devendra, 2003. Modeling actual evapotranspiration from the forested watersheds across the southeastern United States, Journal of the American Water Resources Association.

Kolka, R.K., and A.T. Wolf, 1998. Estimating actual evapotranspiration for forested sites: Modifications to the Thornthwaite model, United States Department of AgricultureForest Service, Southern Research Station, Research note SRS-6.

Kustas, W.P., A. Rango, and R. Uijlenhoet, 1994. A simple energy budget algorithm for the snowmelt runoff model, Water Resources Research, 30(5) pp. 1515-1527.

Leaf, C.F., and G.E. Brink, 1973a. Computer simulation of snowmelt within a Colorado subalpine watershed, USDA Forest Service Research Paper Rm-99, Rocky Mountain Forest and Range Experiment Station, Fort Collins, Colorado.

Leaf, C.F., and G.E. Brink, 1973b. Hydrologic simulation model of Colorado subalpine forest, USDA Forest Service Research Paper Rm-107, Rocky Mountain Forest and Range Experiment Station, Fort Collins, Colorado.

Leavesly, G.H., 1973. A mountainous watershed simulation model Ph. D dissertation, Colorado State University, Fort Collins, Colorado.

Managing Arid and Semi Arid Watershed, Beaver Creek Watershed http://ag.arizona.edu/OALS/watershed/beaver/, Last updated January, 2002.

Marks, D., and J. Dozier, 1992. Climate and energy exchange at the snow surface in the alpine region of the Sierra Nevada, 2, Snow cover energy balance, Water Resource Research, 28, pp. 3043-3054.

Martinec, J., 1989. Hour-to-hour snowmelt rates and lysimeter outflow during an entire ablation period, in snow cover and glacier variations, proceedings of the Baltimore symposium, Maryland, May 1989, edited by A. Rango, IAHS publ., 183, pp. 19-28.

Martinec, J., and M.R. de Quervain, 1975. The effect of snow displacement by avalanches on snowmelt and runoff in snow and ice symposium, Proceeding of the Moscow symposium, August 1971, IAHS publ., 104, pp. 364-377.

Monteith, J.L., and M.H., Unsworth, 1990. Principles of Environmental Physics, pp 291, Routledge Chapman and Hall, New York.

Ohmura A., 2001. Physical basis for the temperature based melt-index method, Institute of Climate Research, Swiss Federal Institute of Technology, Zurich, Switzerland.

Parton, W.J., and J.E. Logan, 1981. A model for diurnal variation in soil and temperature, Agricultural Meteorology, 23, pp 205-216.

Rawls, W.J., and Brakensiek, 1985. Prediction of soil water properties for hydrologic modeling, In watershed management in the 80's, Edited by E. B. Jones and T. J. Ward ASCE, pp. 293-299, New York.

Rawls, W.J., Brakensiek, and N. Miller, 1983. Green-Ampt infiltration parameters from soil data, Journal of Hydraulic Engineering, 109(1) pp. 62-70.

Rogers, J.J., 1973. Design of a system for predicting effects of vegetation manipulation on water yield in the Salt-Verde Basin, Ph.D. dissertation, University of Arizona, Tucson, Arizona.

Rogers, J.J., and M.B. Baker, 1977. Progress Report on simulation of hydrology and water relations of managed forest ecosystems, unpublished report, Rocky Mountain Forest and Range Experiment Station, Flagstaff, Arizona.

Rogers, J.J., J.M. Posser, L.D. Garrett, and M.G. Ryan, 1984. ECOSIM: a system for projecting multiresource outputs under alternative forest management regimes, USDA Forest Service Administrative, Rocky Mountain Forest and Range Experiment Station, Fort Collins, Colorado.

Running, S.W., and J.C. Caughlan, 1988. A general model of forest ecosystem processes for regional applications I. Hydrologic balance, canopy gas exchange, and primary production processes, Ecological modeling 42, pp. 125-154.

Running, S.W., R.R. Nemania, and R.D. Hungerford, 1987. Extrapolation of synoptic meteorological data in mountainous terrain and its use for simulating forest evapotranspiration and photosynthesis, Canadian Journal of Forest Research, 17(6), pp. 472-483.

Rupp, D.E., 1995. Stochastic, event-based modeling of upland watershed precipitation-runoff relationships, master's thesis, Northern Arizona University, Flagstaff, Arizona.
Salvucci, G.D., and D. Entekhabi, 1994. Explicit expressions for Green-Ampt (delta function diffusivity) infiltration rate and cumulative storage, Water Resource Research 30 (9). Pp. 2661-2663.
Sellers, P.J., Y. Mintz, Y.C. Sud, and A. Dalcher, 1986. The designs of a sample biosphere model (SIB) for use within general circulation models, Journal of Atmospheric science, 43, pp. 505-531.
Shuttleworth, W.J., 1975. The concept of intrinsic surface resistance: Energy budgets at partially wet surface, Boundary-Layer Meteorology, 8, pp. 81-99.
Solomon, R.M., P.F. Ffolliott, M.B. Baker Jr., and G.J. Gottfried, 1975a. Snowmelt runoff efficiencies in Arizona watershed, Research Report 274, Agricultural Experiment Station, University of Arizona, Tucson, Arizona.
Solomon, R.M., P.F. Ffolliott, and D.B. Throud, 1975b. Characterization of snowmelt runoff efficiencies. Paper presented at symposium on Watershed Management, American Society of Civil Engineers, Logan, Utah.
Solomon, R.M., P.F. Ffolliott, M. B. Baker Jr., and J. R. Thomson, 1976. Computer simulation of snowmelt, USDA Forest Service Research Paper Rm-174, Rocky Mountain Forest and Range Experiment Station, Fort Collins, Colorado.
Stednick, J.D., 1996. Monitoring the effects of timber harvest on annual water yield, Journal of Hydrology, 176, pp. 79-95.
Stephens, D.B. 2003. Alternative: restore and manage forests, pinon-juniper woodlands, and riparian systems. Appendix F, White Paper 1 in: Jemez y Sangre Regional Water Plan: Vol. 1. Report prepared for Jemez y Sangre Water Planning Council.
Stewart, J.B., 1977. Evaporation from the wet canopy of a pine forest, Water Resource Research, 13(6) pp. 915-921.
Stewart, J.B., 1988. Modeling surface conductance of a pine forest, Agriculture and Forest meteorology, 43, pp. 19-35.
Sugita, M, and W. Brutsaert, 1993. Cloud effect in the estimation of the instantaneous long wave radiation, Water Resources Research, 29(3), pp. 599-605.
Swift, L. W., Jr, 1976. Algorithm for solar radiation on mountain slopes, Water Resources Research, 12(1), pp. 108-112.
Tarboton, D.G., G.C. Tanveer, and H.J. Thomas, 1995. A spatially distributed energy balance snowmelt model, Submitted for IAHS proceedings of Symposium on Biochemistry of Seasonally Snow Cover Catchments, June 3-14, 1995, Boulder, CO.
Tecle, A, 1991.Hydrology and watershed management in southwestern ponderosa pine forests, in multiresoirce management of southwestern ponderosa pine forests: the status of knowledge, edited by Aregai Tecle and W. Wallace Convington, pp 162-272, School of Forestry, Northern Arizona University, Flagstaff, Arizona.
Tennyson, L.C. P.F. Ffolliott, and D.B. Thorud, 1974. Use of time-lapse photograpy to assesses potential interception in Arizona ponderosa pine, Water Resource Bulletin, 10, pp. 1246-1254.

Thornthwaite, C.W., and J.R. Mather, 1967. Instructions and tables for computing potential evapotranspiration and the water balance, Drexel Institute of Technology Laboratory of Climatology, volume X, 3, Centerton, New Jersey.

Troendle, C.A., 1979. Hydrologic impacts of silvicultural activities, Journal of Irrigation and Drainage Division, America Society of Civil Engineers, 105(IRI), pp 57-70.

Troendle, C.A., 1983. The potential for water yield augmentation from forest management in the Rocky Mountain Region, Water Resource Bulletin, 19, pp. 359-373.

USFS, Terrestrial Ecosystem Survey of the Coconino National Forest, 1992. Draft Report, USDA forest Service, 3.

Ward, A.D., and W.J. Elliot, 1995. Environmental Hydrology, CRC Press LLC, USA.

Wallace, J. M. and Peter V. Hobbs, 1977. Atmospheric Science: An Introductory Survey, Acadamic Press, Inc., Orlando, Florida.

Wigmosta, M.S., L.W. Vail, and D.P. Lettenmaier, 1994. A distributed hydrology-vegetation model for complex terrain, Water Resources Research, 30(6), pp. 1665-1697.

Williams, J.A., and T.C. Anderson, Jr., 1967. Soil Survey of Beaver Creek area, USDA Forest Service and Soil Conservation Service, and Arizona Agricultural Experiment Station, U.S. government printing office, Washington, D.C.

Zuzel, J.F., and L.M. Cox, 1975. Relative importance of meteorological variables in snowmelt, Water Resources Research, 11, pp. 174-176.

Appendix 3A

Description of Climate-Related Information

When daily temperature data is available in the form of daily maximum and daily minimum temperatures, average daytime and night time temperatures can be estimated by assuming that the change in temperature throughout a 24-hour period can be described by a sine function (Parton and Logan, 1981; Running et al., 1987). After integrating over daytime portion of the sine curve, the resulting equation for estimating the average daytime temperature according to Running et al., (1987) is

$$T_{davg} = 0.606T_{\max} + 0.39T_{\min} \tag{3A-1}$$

Where T_{davg} = average daytime temperature (^{o}C),

$T_{\max}$ = daily maximum temperature (^{o}C), and

$T_{\min}$ = daily minimum temperature (^{o}C)

The average nighttime temperature is estimated by

$$T_{navg} = 0.303T_{\max} + 0.697T_{\min} \tag{3A-2}$$

Where T_{navg} is the average nighttime temperature in ^{o}C (Running et al., 1987).

Atmospheric pressure at any elevation is determined as a function of the air temperature and the air pressure measured at a reference elevation and assumes that air temperature changes linearly with elevation. According to Wallace and Hobbes (1977) the equation used for computing atmospheric pressure is

$$P = P_o\{[T_o + \Gamma(Z - Z_o)]/T_o\}^{-g/R\Gamma} \qquad (3A\text{-}3)$$

Where P = atmospheric pressure (mb),

P_o = atmospheric pressure at reference elevation (mb),

T_o = air temperature at a reference elevation (°K)

Γ = lapse rate (°K m^{-1})

Z = elevation (m),

Z_o = reference elevation (m),

g = gravitational acceleration (m s^{-1}), and

R = gas constant for air (J °K^{-1} Kg^{-1}).

The gravitational acceleration (g) is assumed constant at 9.807 m s^{-1} and the gas constant for air (R), though a function of the amount of water vapor in the air, is set constant at 288 J °K^{-1} Kg^{-1}. The reference elevation (Z_o) is set 2132.38 m, which is the elevation of the Flagstaff WSO. The daily average pressure at Flagstaff is used as the pressure at the reference elevation. (P_o). Different lapse rates are used for different months, but within months the lapse rate (Γ) is assumed not to change.

Vapor pressure

According to Dingman (1994), the saturation vapor pressure can be estimated by

$$e_s = 6.11 \exp[17.3 T_a / (T_a + 237.2)] \quad \text{(3A-4)}$$

Where e_s is saturation vapor pressure (mb), and T_a is air temperature (^{o}C). The vapor pressure deficit (Δe), is determined by first calculating the actual vapor pressure deficit which is

$$e_a = e_s (RH) \quad \text{(3A-5)}$$

Where RH is the average daily relative humidity determined from the existing data in the Beaver Creek. Then the vapor pressure deficit is simply the saturated vapor pressure minus the actual vapor pressure which is

$$\Delta e = e_s - e_a \quad \text{(3A-6)}$$

The equation for converting vapor pressure deficit (Δe) to absolute humidity deficit ($\Delta \rho_v$) is

$$\Delta \rho_v = 217 \Delta e / T_a \quad \text{(3A-7)}$$

Where $\Delta \rho_v$ has units of gm^{-3} (Dingman, 1994).

Slope of Saturation vapor pressure vs. temperature

The slope of the relationship between saturation vapor pressure and temperature is calculated by taking the derivative of the equation for saturation vapor pressure, equation (3A-4), with respect to temperature. The resulting equation is (3A-8)

$$\Delta = \frac{de_s}{dT_a} = \frac{25083}{(T_a + 237.3)^2} \exp[17.3T_a + 237.3)] \tag{3A-8}$$

Where Δ is in mb $^oC^{-1}$ (Dingman, 1994).

Air density

Air density is a function of the prevailing air temperature, air pressure (Hodgman et al., 1958). The equation for air density is

$$\rho_a = 3.4853X10^{-4}[(P - 0.3783e)/(T_a + 273.2)] \tag{3A-9}$$

Where ρ_a is the air density in g cm^{-3} and the other terms are as described above (Hodgman et al., 1958).

Latent heat of vaporization

The latent heat of vaporization (λ_v) is calculated by

$$\lambda_v = 597.3 - .564T_a \tag{3A-10}$$

Where λ_v is in cal g^{-1} (Dingman, 1994).

Psychrometric constant

The psychrometric constant (γ) is defined as

$$\gamma = \frac{C_a P}{0.622 \lambda_v} \tag{3A-11}$$

Where γ has units of mb $^{o}C^{-1}$ and C_a, the heat capacity of air, equals 0.24 cal g^{-1} $^{o}C^{-1}$ (Dingman, 1994).

Table 3A-1. Daily sunshine hours for the study area, 35 latitude in the Northern Hemisphere (Thornthwaite and Marher, 1967).

day	January	Feburary	March	April	May	June	July	August	Septembei	October	November	December
1	9.96	10.56	11.4	12.48	13.56	14.28	14.4	13.8	12.84	11.88	10.8	10.08
2	9.96	10.56	11.52	12.48	13.56	14.28	14.4	13.8	12.84	11.88	10.8	10.08
3	9.96	10.56	11.52	12.6	13.56	14.28	14.4	13.8	12.84	11.76	10.8	10.08
4	9.96	10.56	11.52	12.6	13.56	14.28	14.4	13.8	12.84	11.76	10.68	10.08
5	9.96	10.68	11.64	12.6	13.56	14.28	14.4	13.68	12.72	11.76	10.68	10.08
6	9.96	10.68	11.64	12.72	13.68	14.28	14.28	13.68	12.72	11.64	10.68	9.96
7	9.96	10.68	11.64	12.72	13.68	14.28	14.28	13.68	12.72	11.64	10.56	9.96
8	10.08	10.68	11.64	12.72	13.68	14.28	14.28	13.68	12.6	11.64	10.56	9.96
9	10.08	10.8	11.76	12.84	13.68	14.28	14.28	13.56	12.6	11.52	10.56	9.96
10	10.08	10.8	11.76	12.84	13.68	14.28	14.28	13.56	12.6	11.52	10.56	9.96
11	10.08	10.8	11.76	12.84	13.8	14.4	14.28	13.56	12.48	11.52	10.56	9.96
12	10.08	10.8	11.76	12.96	13.8	14.4	14.28	13.56	12.48	11.52	10.44	9.96
13	10.08	10.92	11.88	12.96	13.8	14.4	14.28	13.56	12.48	11.4	10.44	9.96
14	10.08	10.92	11.88	12.96	13.8	14.4	14.28	13.44	12.48	11.4	10.44	9.96
15	10.08	10.92	11.88	12.96	13.92	14.4	14.16	13.44	12.36	11.4	10.44	9.96
16	10.2	10.92	12	13.08	13.92	14.4	14.16	13.44	12.36	11.4	10.44	9.96
17	10.2	11.04	12	13.08	13.92	14.4	14.16	13.32	12.36	11.28	10.32	9.96
18	10.2	11.04	12	13.08	13.92	14.4	14.16	13.32	12.36	11.28	10.32	9.96
19	10.2	11.04	12.12	13.2	13.92	14.4	14.16	13.32	12.24	11.28	10.32	9.96
20	10.2	11.04	12.12	13.2	14.04	14.4	14.16	13.32	12.24	11.16	10.32	9.96
21	10.2	11.16	12.12	13.2	14.04	14.4	14.04	13.2	12.24	11.16	10.32	9.96
22	10.32	11.16	12.12	13.2	14.04	14.4	14.04	13.2	12.12	11.16	10.32	9.96
23	10.32	11.16	12.24	13.32	14.04	14.4	14.04	13.2	12.12	11.16	10.2	9.96
24	10.32	11.28	12.24	13.32	14.04	14.4	14.04	13.2	12.12	11.04	10.2	9.96
25	10.32	11.28	12.24	13.32	14.16	14.4	14.04	13.08	12	11.04	10.2	9.96
26	10.32	11.28	12.24	13.32	14.16	14.4	13.92	13.08	12	11.04	10.2	9.96
27	10.44	11.4	12.36	13.44	14.16	14.4	13.92	13.08	12	11.04	10.2	9.96
28	10.44	11.4	12.36	13.44	14.16	14.4	13.92	12.96	12	10.92	10.2	9.96
29	10.44		12.36	13.44	14.16	14.4	13.92	12.96	11.88	10.92	10.08	9.96
30	10.44		12.48	13.44	14.16	14.4	13.92	12.96	11.88	10.92	10.08	9.96
31	10.44		12.48		14.16		13.92	12.96		10.92		9.96

Table 3A-2. Daily total solar radiation received on a horizontal surface in cal cm^{-2} s^{-1} 20 miles south of Flagstaff near the study site (Campbell and Stevenson, 1977).

day	January	February	March	April	May	June	July	August	September	October	November	December
1	0.0009	0.0046	0.0056	0.0042	0.0083	0.0089	0.0084	0.0063	0.0060	0.0060	0.0029	0.0031
2	0.0019	0.0042	0.0043	0.0061	0.0084	0.0086	0.0072	0.0064	0.0060	0.0060	0.0031	0.0037
3	0.0040	0.0043	0.0058	0.0077	0.0087	0.0085	0.0058	0.0062	0.0042	0.0047	0.0033	0.0035
4	0.0027	0.0037	0.0053	0.0079	0.0079	0.0081	0.0057	0.0061	0.0043	0.0059	0.0044	0.0027
5	0.0026	0.0038	0.0048	0.0079	0.0072	0.0085	0.0065	0.0057	0.0066	0.0058	0.0041	0.0028
6	0.0020	0.0047	0.0042	0.0061	0.0073	0.0087	0.0067	0.0072	0.0037	0.0034	0.0045	0.0034
7	0.0021	0.0045	0.0053	0.0046	0.0082	0.0083	0.0047	0.0072	0.0038	0.0040	0.0043	0.0034
8	0.0011	0.0050	0.0022	0.0056	0.0086	0.0088	0.0066	0.0060	0.0064	0.0048	0.0029	0.0036
9	0.0020	0.0038	0.0030	0.0065	0.0086	0.0086	0.0084	0.0068	0.0055	0.0057	0.0043	0.0036
10	0.0024	0.0036	0.0019	0.0056	0.0088	0.0091	0.0080	0.0072	0.0066	0.0053	0.0042	0.0036
11	0.0034	0.0051	0.0039	0.0060	0.0088	0.0088	0.0068	0.0070	0.0069	0.0057	0.0044	0.0035
12	0.0033	0.0046	0.0053	0.0055	0.0088	0.0079	0.0055	0.0073	0.0059	0.0030	0.0041	0.0026
13	0.0035	0.0025	0.0047	0.0078	0.0085	0.0082	0.0060	0.0081	0.0049	0.0044	0.0041	0.0022
14	0.0041	0.0035	0.0041	0.0077	0.0088	0.0086	0.0056	0.0072	0.0063	0.0056	0.0038	0.0034
15	0.0041	0.0030	0.0061	0.0077	0.0086	0.0083	0.0053	0.0070	0.0061	0.0055	0.0041	0.0033
16	0.0035	0.0034	0.0065	0.0075	0.0068	0.0087	0.0060	0.0071	0.0059	0.0054	0.0041	0.0036
17	0.0028	0.0029	0.0068	0.0060	0.0053	0.0087	0.0064	0.0076	0.0047	0.0053	0.0030	0.0035
18	0.0037	0.0051	0.0066	0.0067	0.0077	0.0076	0.0065	0.0073	0.0044	0.0050	0.0032	0.0034
19	0.0041	0.0054	0.0056	0.0084	0.0078	0.0086	0.0064	0.0073	0.0047	0.0040	0.0041	0.0035
20	0.0027	0.0056	0.0031	0.0077	0.0080	0.0088	0.0061	0.0063	0.0050	0.0035	0.0036	0.0027
21	0.0028	0.0044	0.0067	0.0080	0.0069	0.0088	0.0071	0.0074	0.0065	0.0039	0.0039	0.0018
22	0.0044	0.0056	0.0038	0.0073	0.0071	0.0080	0.0071	0.0069	0.0064	0.0027	0.0029	0.0035
23	0.0042	0.0056	0.0066	0.0071	0.0076	0.0086	0.0059	0.0071	0.0061	0.0044	0.0040	0.0027
24	0.0044	0.0059	0.0070	0.0054	0.0089	0.0086	0.0072	0.0067	0.0045	0.0050	0.0039	0.0037
25	0.0043	0.0055	0.0052	0.0065	0.0090	0.0082	0.0058	0.0069	0.0059	0.0047	0.0037	0.0029
26	0.0036	0.0058	0.0044	0.0073	0.0084	0.0088	0.0061	0.0060	0.0054	0.0037	0.0037	0.0025
27	0.0035	0.0048	0.0067	0.0086	0.0088	0.0088	0.0040	0.0060	0.0058	0.0038	0.0025	0.0032
28	0.0040	0.0055	0.0072	0.0086	0.0084	0.0084	0.0068	0.0074	0.0063	0.0025	0.0022	0.0029
29	0.0045		0.0072	0.0086	0.0086	0.0084	0.0056	0.0075	0.0055	0.0032	0.0028	0.0030
30	0.0026		0.0068	0.0085	0.0081	0.0087	0.0059	0.0075	0.0054	0.0034	0.0038	0.0036
31	0.0037		0.0072		0.0090		0.0072	0.0070		0.0025		0.0028

Appendix 3B

Description of TES soil types (USFS, 1992)

TES code	sub unit	soil name	soil texture class	% composition
50	0.1	Vertic Haplaquolls Fine, Montmorillonitic	clay	100
55	0.1	Pachick Argiborolls Fine, Montmorillonitic	Loam	65
	0.2	Vertic Argiborolls Fine, Montmorillonitic	Clay loam	20
	0.5	Typic Argiborolls Fine, Montmorillonitic	Loam	10
	0.6	Typic Argiborolls Clayey-skeletal, montmorillonitic	Loam	5
520	0.1	Udic Haplustalfs Fine, Montmorillonitic	Loam	60
	0.2	Lithic Haplustalfs Clayey-skeletal, montmorillonitic	Loam	30
	0.5	Udic Haplustalfs Clayey-skeletal, montmorillonitic	Loam	5
	0.6	Udic Argiborolls Fine, Montmorillonitic	Loam	5
565	0.1	Mollic Eutroboralfs Clayey-skeletal, mixed	Loam	70
	0.5	Mollic Eutroboralfs Loamy-skeletal, mixed	Loam	15
	0.6	Lithic Eutroboralfs Clayey-skeletal, mixed	Loam	15
575	0.1	Mollic Eutroboralfs	Loam	40
	0.2	Lithic Eutroboralfs	Loam	40
	0.3	Rock outcrop	Loam	20

Continued……..

579	0.1	Lithic Eutroboralfs Clayey-skeletal, montmorillonitic	Loam	45
	0.2	Mollic Eutroboralfs Fine, Montmorillonitic	Clay loam	35
	0.5	Typic Argiborolls Fine, Montmorillonitic	Clay loam	10
	0.6	Lithic Eutroboralfs Clayey, montmorillonitic	Clay loam	10
582	0.1	Typic Argiborolls Fine, Montmorillonitic	Loam	65
	0.2	Mollic Eutroboralfs Clayey-skeletal, montmorillonitic	Loam	20
	0.5	Typic Argiborolls Clayey-skeletal, montmorillonitic	Clay loam	5
	0.6	Mollic Eutroboralfs Fine, Montmorillonitic	Clay loam	10
584	0.1	Mollic Eutroboralfs Clayey-skeletal, montmorillonitic	Loam	40
	0.2	Typic Argiborolls Fine, Montmorillonitic	Loam	35
	0.5	Mollic Eutroboralfs Fine, Montmorillonitic	Loam	15
	0.6	Typic Argiborolls Clayey-skeletal, montmorillonitic	Loam	10
585	0.1	Lithic Eutroboralfs Clayey-skeletal, montmorillonitic	Loam	40
	0.2	Mollic Eutroboralfs Fine, Montmorillonitic	Loam	30
	0.5	Lithic Eutroboralfs Clayey-skeletal, montmorillonitic	Loam	15
	0.6	Mollic Eutroboralfs Clayey-skeletal, montmorillonitic	Loam	15
586	0.1	Mollic Eutroboralfs Fine, Montmorillonitic	Loam	45
	0.2	Mollic Eutroboralfs Clayey-skeletal, montmorillonitic	Loam	40
	0.5	Lithic Eutroboralfs	Loam	15

Chapter 4

Summary, conclusions and recommendations

Summary

The main objective of this study is to develop a model to estimate water yield from a ponderosa pine watershed in north-central Arizona by incorporating the various hydrologic processes and spatial watershed characteristics. Previous studies in this area considered the cold-season precipitation as the only source of runoff (Brown et al., 1974; Baker, 1982; Tecle and Rupp, 2002). Though the contribution of warm-season precipitation and water yield is minimal, they are estimated separately in this study. Hence, to achieve our objective, the modeling process in this study is pursued in two parts. The first part consists of developing an event-based, stochastic model to describe and simulate the cold and warm-season precipitation characteristics in the study area. In the second part, daily water yield models are developed for the cold and warm-seasons separately that consider the temporal and spatial distribution of precipitation depth and other important watershed characteristics such as elevation, aspect, slope, overstory density, and soil.

In the first part of the study, the characteristics of precipitation events are considered as random and time variant variables and modeled using stochastic processes. The probability distributions of the specific precipitation characteristics, such as event depth, event duration, and interarrival time between events, are described using appropriate theoretical distribution functions that best fit the observed data. In addition, temperatures are described and simulated as stochastic processes to account for their uncertain variability throughout the two seasons. The simulated temperature values are used to determine the form of precipitation during the cold-season. The precipitation may come in the form of rain, snow, or mixed, and used as an input variable to calculate water yield using the water balance models. The components of the water yield model are precipitation, evaporation, transpiration, and infiltration, and all of them are estimated in this study.

Conclusions

The precipitation models for both seasons perform well except that the cold-season precipitation model over-estimates the depth and duration of small precipitation events while the warm season precipitation model over-estimates the total seasonal precipitation amount. These may be due to the lack of best fit theoretical distribution functions to describe the precipitation characteristics in the study area. None of the theoretical distribution functions selected ware able to describe the precipitation characteristics well except time between sequences in the cold-season. Since there are inadequate observed data (20 years), it may be s difficult to correctly portray the temporal trend of the precipitation characteristics. In the future, acquiring additional data would be necessary to describe the characteristics well.

Another problem of with the stochastic precipitation modeling is simulating the arrival of events randomly throughout the seasons. However, in the study area, most cold-season precipitation events fall between December and March and the warm-season precipitation events fall between July-September. Due to random behavior of the model generated data, we may have larger or smaller number of precipitation events during the drier periods of the seasons and less or more number of events in the wet periods of the seasons. So we have to have many trials to see the validity of the models.

The spatial analysis of the precipitation events reveals that the variability of c old and warm seasons' precipitation depths and durations in the study area are partially explained by elevation, latitude, and longitude though the influence of aspect seems to be small when dealing with small are at the watershed scale. Four regression equations are developed in describing the spatial distribution of precipitation depth and duration. The cold-season precipitation depth is explained by only the latitude (UTM-Y) with a regression equation having an r^2 value of 0.74 while event duration is influenced by both elevation and latitude with an r^2 value of 0.66. In the warm-season, the distribution of precipitation depth is affected by latitude, longitude and elevation, while the duration of precipitation events is influenced by longitude and elevation. The warm-season regression equations for precipitation depth and duration have values r^2 values of 0.45 and 0.55 respectively. In all the regression equations the r^2 values are low which show that significant portions of the spatial variability of precipitation depth and duration in the watershed are unexplained.

The spatial distribution of the precipitation in north-central Arizona is highly influenced by orographic features such as the San Francisco Mountains, the Mogollon Rim and the White Mountains (Beschta, 1976; Tecle and Rupp, 2002). Since the precipitation gauges used to analyze the spatial distribution are located within a small area and far from these landscape features, care must be taken when applying the finding of the spatial analysis to sites outside the study watershed. The spatial factors controlling the areal distribution of precipitation on watersheds on these landscape features may be different from those on the Bar M watershed.

Overall, the cold and warm-season precipitation models presented in this study are useful tools for describing the seasonal precipitation patterns that occur over a mountainous ponderosa pine forested watersheds. In addition they serve to provide the precipitation and temperature inputs into the water balance models used to estimate water yield from upland forested watersheds of the type considered in this study.

The second part of the study, developed a precipitation event-based runoff model for estimating water yield for the cold and warm-seasons in the ponderosa pine forested watersheds of north-central Arizona. A GIS is used as a part of the modeling scheme to describe the spatial characteristics of the watershed. The GIS software enables to subdivide the watershed into thousands of cells or microwatersheds each having relatively the same (or homogeneous) spatial characteristics. These characteristics are elevation, slope, aspect, soil type, and canopy cover, and all of which are defined for each cell. The water yield from each cell is then estimated using a water balance model developed specifically for each season. The most important hydrological processes involved in developing the models are canopy interception, evaporation, transpiration, snow accumulation and melt, infiltration, and change in storage. The models use the simulated precipitation in the previous chapter as their primary input and the values of the output variables used are estimated using various empirical equations, which have been tested and used by others (Wigmosta, et al., 1994; Dingman, 1994).

The amount of water yield generated from the entire watershed is determined by first computing the runoff for each cell from each precipitation event. Then the runoff from each cell is routed to the adjacent downstream cell in a cascading fashion until it reaches the watershed outlet. Finally, the event-based runoffs produced are summed over the entire cold and warm-seasons to determine the total seasonal amounts of water yield from the entire watershed.

The results of the total seasonal water yield for the cold and the warm-seasons are 22 and 1.9 percent of their respective total seasonal amount of precipitation. However, the recorded stream flow data measured at the outlet of the watershed shows 37 and 2.3 percent of the recorded seasonal precipitation becoming runoff during the cold and warm seasons respectively. The most probable reasons for the major discrepancies in the cold-season results may be overestimation of the losses due to evaporation and transpiration, and possible errors in estimating soil water storage due to inadequate data. Other weakness in this modeling approach is the randomness of the precipitation events and inability to find a perfect theoretical distribution function to describe the data correctly.

Recommendations

Future work on water yield models should include developing them to provide better hydrologic responses to climatic and biotic changes. In addition, there should be some modification to reduce the time required to run the models, in order to make it a practical tool for watershed management purposes. Also since the models in this study are realistic that are based on actual data, efforts should be in the future to collect adequate data on all variables including solar radiation, soil moisture, and snow pack depth to make the model results more reliable.

Overall, this research is able to simulate precipitation events through the stochastic event-based approaches. Furthermore, it develops a spatially-varied physically-based water yield models that account for the major hydrologic processes and watershed characteristics that affect the amount of runoff. This is quite useful to estimate runoff and water yield from area which receive intermittent and spatially varied precipitation events such as the study area.

Literature Cited

Baker, M.B., Jr., 1982. Hydrologic regimes of forested areas in the Beaver Creek Watershed, USDA Forest Service General Technical Report Rm-90, Rocky Mountain Forest and Range Experiment Station , Fort Collins, Colorado.

Beschta, R.L., 1976. Climatology of the ponderosa pine type in central Arizona, Technical Bulletin 228, Agricultural Experimental Station, College of Agriculture, University of Arizona, Tucson, Arizona.

Brown, H.E., M.B. Baker Jr., J.J .Rogers, W.P. Clary, J.L. Kovener, F.R. Larson, C.C. Avery, and R.E. Campbell, 1974. Opportunities for increasing water yiel and other multiple use values on ponderosa pine forest lands, USDA Forest Service General Technical Report Rm-129, Rocky Mountain Forest and Range Experiment Station , Fort Collins, Colorado.

Dingman, S.L., 1994. Physical hydrology, Macmillan college publishing Company, New York.

Tecle. A, and D.E. Rupp, 2002. Stochastic precipitation-runoff modeling for water yield from a semi-arid forested watershed. In: Risk, Reliability, Uncertainty, and Robustness of Water Resources Systems. Cambridge University press: London. Pp. 56-63.

Wigmosta, M.S., L.W. Vail, and D.P. Lettenmaier, 1994. A distributed hydrology-vegetation model for complex terrain, Water Resources Research, 30(6), pp. 1665-1697.